Alma Mater Studiorum – Università di Bologna

DOTTORATO DI RICERCA IN

Scienze Chirurgiche

Ciclo XXX

Settore Concorsuale: o6/N1

Settore Scientifico Disciplinare: MED/46

Characterization of the Scarification and Neolymphangiogenesis in Experimental Mouse Model of Acute and Chronic Myocardial Infarction: the Dual Role of Podoplanin Expressing Cells

Presentata da: Maria Cimini

Coordinatore Dottorato — Supervisore

Prof.ssa Annalisa Patrizi — Prof. Gianandrea Pasquinelli

Esame finale anno 2018

Index

Chapter III

Chapter IV

The secret of change is to focus all of the energy, not on fighting the old, but on building the new.

Socrates

Legend	
Abbreviation	**Full description**
MI	**Myocardial Infarction**
SHAM	**Sham-operated mice**
NO	**Non Operated mice**
BZ	**Infarct Border Zone**
RA	**Infarct Remote Area**
CLVs	**Cardiac Lymphatic Vessels**
LVs	**Lymphatic vessels**
LECs	**Lymphatic Endothelial Cells**
BVs	**Blood vessels**
ECs	**Endothelial cells (blood)**
ECM	**Extra Cellular Matrix**
EMT	**Epithelial Mesenchymal Transition**
FRCs	**Fibroblastic Reticular Cells**
CAF	**Cancer Associated Fibroblast**

Abstract

Cardiovascular diseases, including myocardial infarction (MI) and heart failure, are the leading causes of death in the industrialized world. The epidemic problem of cardiomyopathies, together with the limitation of their management, constitutes the basis for the current interest in regenerative cardiology. Restoration of the cardiac function is one of the main aims of the cardiovascular research community. Although there are continuous news and scientific papers about clinical trials of cardio-protective drugs and new approaches with the stem cell-based therapies, the knowledge regarding the scar formation after MI or non-ischemic cardiomyopathies is confined to the discoveries from decades ago. Thus, there is still a question that has to be addressed: what happens during the healing process of scar formation?

The repair and regeneration of the injured tissue are inter-related. In some instances, a regenerative process of endogenous new cardiomyocyte formation and neo-vascularization occur concomitantly with the scar development. Unfortunately, physiologically the regeneration is much less pronounced than the replacement fibrosis. As said, cardiac scars are dynamic living structures, although, the blood vascular rarefaction and the poor neo-angiogenesis contribute to the deleterious effects of the cardiac inflammation and edema. However, the crucial role in the maintenance of tissue fluid balance and immune surveillance is played by the lymphatic system, suggesting that the lymphangiogenesis in the process of scarification is very important for the heart healing. The lymphatic system is present throughout the entire body in all vertebrates and regulates the tissue homeostasis, fluid balance and repair due to its function in the transport of molecules and cells. The unique structure of the lymphatic vessels (LVs) such as, discontinuous basal lamina, fenestrations, wide lumen and lack of pericyte and smooth muscle cell lining, are advantageous features for cell trans-migration and diapedesis. Hence, functional LVs are critical

for the circulation-trafficking of immune, cancer and other cell types. Cardiac lymphatic vasculature undergoes substantial expansion in response to MI; however, there is limited information on the cellular mechanisms mediating post-MI lymphangiogenesis and accompanying fibrosis. In the heart, the cardiac lymphatic system is crucial for the control of intra-myocardial pressure and prevention of swelling, lipid transport and balanced regulation of tissue inflammation and there is a documented link between lymphatic malfunction and cardiovascular diseases. Using a mouse model of permanent coronary artery ligation, we examined spatiotemporal changes in the expression of lymphendothelial and mesenchymal markers in the acutely and chronically infarcted myocardium. We found that at the time of wound granulation, a three-fold increase in the frequency of podoplanin-labeled cells occurred in the infarcted hearts compared to non-operated and sham-operated counterparts. Podoplanin is a very interesting protein; it is expressed in a variety of different type of cells and in different context; mostly orchestrates the lymphatic and the immune system but also the malignancy of tumors. It is known that a multitude of stimuli can drive podoplanin expression, including physiological differentiation factors in embryogenesis, potentially malignant factors such as pro-tumorigenic signaling pathways in cancer and pro-inflammatory cytokines in immune diseases. In our study podoplanin immunoreactivity detected LYVE-1-positive LVs, as well as masses of LYVE-1-negative cells dispersed between myocytes, predominantly in the vicinity of the infarcted region. Podoplanin-carrying populations displayed a mesenchymal progenitor marker PDGFRα, and intermittently expressed Prox-1, a master regulator of the lymphatic endothelial fate. At the stages of scar formation and maturation, concomitantly with the enlargement of lymphatic network in the injured myocardium, the podoplanin-rich LYVE-1-negative multicellular assemblies were apparent in the fibrotic area, aligned with extracellular matrix

deposits, or located in immediate proximity to activated blood vessels with high VEGFR-2 content. Of note, these podoplanin-containing cells acquired the expression of PDGFRβ or a hematoendothelial epitope CD34. Although Prox-1 labeling was abundant in the area affected by MI, the podoplanin-presenting cells were not consistently Prox-1-positive. The concordance of podoplanin with VEGFR-3 similarly varied. Based our observations, podoplanin is highly expressed not only by the lymphatic endothelial cells (LECs), but by different type of cells at the time of inflammation; this heterogeneous cell cohorts that express podoplanin contribute to scar tissue biology in early and advanced phases of scar maturation. Thus, our data reveal previously unknown phenotypic and structural heterogeneity within the podoplanin-positive cell compartment in the infarcted heart, and suggest an alternate ability of podoplanin-presenting cardiac cells to generate lymphatic endothelium and pro-fibrotic cells, contributing to scar development.

Riassunto

Le malattie cardiovascolari rappresentano una delle principali cause di morte nel mondo industrializzato. Oggigiorno l'insufficienza cardiaca secondaria a infarto del miocardio o altre patologie è trattata esclusivamente su base sintomatica; la medicina rigenerativa ha l'ambizione di curare le cause della insufficienza cardiaca ripristinando il tessuto cardiaco danneggiato e limitando l'estensione del tessuto cicatriziale non funzionante. Sebbene ci sia una solida letteratura, comprensiva di studi clinici, sui farmaci cardioprotettivi e sulle terapie a base di cellule staminali, le conoscenze riguardanti la formazione della cicatrice secondaria a infarto del miocardico o a cardiomiopatie non ischemiche sono limitate a osservazioni di alcune decadi fa. Oggi, grazie alle nuove tecnologie e all'utilizzo di sonde molecolari, è possibile studiare con precisione gli stadi infiammatori che esitano nella formazione della cicatrice e lo sviluppo temporale di quest'ultima; tali informazioni sono di grandissima utilità per migliorare sia la somministrazione che la tipologia delle terapie cardioprotettive o riparative.

Durante la formazione della cicatrice, la rigenerazione, ovvero la formazione di tessuto competente costituito da nuovi cardiomiociti e vasi sanguigni, è fisiologicamente molto meno pronunciata rispetto ai meccanismi che governano la fibrosi sostitutiva. Nelle fasi iniziali la rarefazione vascolare e la inefficiente neo-angiogenesi favoriscono gli eventi pro-fibrotici, quali infiammazione e l'edema interstiziale. L'omeostasi tessutale e la risoluzione dell'infiammazione, indispensabili per rallentare e contenere la formazione della cicatrice vengono modulati dal sistema linfatico. Il sistema linfatico ricopre un ruolo estremamente importante nella fisiologia della formazione della cicatrice e del processo rigenerativo. Il sistema linfatico è presente in tutto il corpo di tutti i vertebrati ove modula l'omeostasi tessutale grazie alla sua funzione di trasporto di molecole e cellule. I vasi linfatici sono caratterizzati da una struttura peculiare, presentano una

lamina basale discontinua, fenestrazioni tra le cellule dei vasi, un ampio lume e mancano del rivestimento pericitario e di cellule muscolari lisce, caratteristiche peculiari dei vasi ematici. Queste proprietà sono vantaggiose per la trans-migrazione cellulare e la diapedesi. Pertanto, i vasi linfatici sono fondamentali per la circolazione e distribuzione di cellule immunitarie, tumorali o di altro tipo.

Nel cuore, il sistema linfatico è cruciale per il controllo della pressione intra-miocardica ed il trasporto dei lipidi, primaria fonte di energia dei cardiomiociti e subisce una notevole espansione in risposta all'infarto del miocardio, anche se vi sono limitate informazioni sui meccanismi che mediano la linfangiogenesi e la formazione della cicatrice post ischemica. In letteratura, sono presenti alcuni studi che descrivono il legame tra il malfunzionamento dei linfatici e le malattie cardiovascolari.

Nel presente progetto di ricerca, usando un modello murino di legatura permanente dell'arteria coronaria discendente, abbiamo esaminato i cambiamenti spazio-temporali dell'espressione dei marcatori linfo-endoteliali e mesenchimali nel miocardio infartuato in fase acuta e cronica. Abbiamo osservato che nel tessuto di granulazione post ischemia vi è un notevole aumento dell'espressione della podoplanina, un marcatore linfatico che per la prima volta abbiamo trovato associato anche a cellule non linfatiche. La podoplanina è una proteina dalle sfaccettature molto interessanti; viene espressa da svariati tipi di cellule e in contesti diversi; per lo più governa il funzionamento del sistema linfatico e del sistema immunitario ma ha un ruolo importante nel predire la malignità dei tumori.

Come atteso, nel tessuto ischemico cardiaco la podoplanina viene co-espressa insieme a LYVE-1 dalle cellule endoteliali che formano i vasi linfatici; allo stesso tempo, abbiamo osservato numerose cellule podoplanina positive che co-esprimevano PDGFRα, marcatore di cellule

progenitrici mesenchimali, e, in maniera meno costante, Prox-1, fattore di trascrizione deputato a regolare il lineage linfo-endoteliale; queste cellule podoplanina^{+}, PDGFRα^{+}, Prox-1$^{+/-}$, non delimitavano strutture vascolari, ma risultavano distribuite in maniera dispersa nel tessuto fibro-infiammatorio post-infartuale.

Nelle fasi di formazione e maturazione della cicatrice, in concomitanza con l'espansione della rete linfatica del miocardio danneggiato, le cellule podoplanina^{+} sono state osservate nell'area fibrotica, allineate con depositi di matrice extracellulare o situate nelle immediate vicinanze di vasi sanguigni positivi al VEGFR-2. Nella fase acuta dell'infarto, anche le cellule positive al PDGFRβ o al CD34 esprimevano la podoplanina rimanendo distribuite in maniera dispersa nello stroma fibro-infiammatorio. La co-espressione della podoplanina con il VEGFR-3, altro marcatore degli endoteli linfatici, risultava invece variabile rispetto al LYVE 1.

Sulla base delle nostre osservazioni, nella cinetica post-ischemica del tessuto miocardico, la podoplanina viene espressa non solo dalle cellule endoteliali linfatiche, ma anche da altri tipi di cellule che partecipano alla fase acuta e cronica dell'infarto del miocardio, contribuendo in maniera importante alla modulazione del tessuto cicatriziale nelle varie fasi della riparazione del danno tessutale.

In conclusione, questo studio ha confermato come i linfatici prendano parte al rimodellamento del tessuto fibro-infiammatorio post-infarto, rivelando una intensa e inattesa distribuzione del marcatore linfatico, podoplanina; i nostri dati evidenziano come la podoplanina venga espressa da cellule di diversa natura, alcune delle quali possibilmente implicate nell'indirizzare la riparazione miocardica verso la fibrosi cicatriziale; queste nuove conoscenze consentiranno di studiare in maniera più approfondita i meccanismi endogeni di rigenerazione, e di attivare o sopprimere pathway molecolari che finora non erano stati presi in considerazione.

Introduction

How can we fix a broken heart?

Love heals broken hearts but not cardiac wounds.

Cardiovascular diseases, including myocardial infarction (MI) and heart failure, are the leading causes of death in the industrialized world. The epidemic problem of cardiomyopathies, together with the limitation of their management, constitutes the basis for the current interest in regenerative cardiology. Restoration of the cardiac function is one of the main aims of the cardiovascular research community. Although there are continuous news and scientific papers about clinical trials of cardio-protective drugs and new approaches with the stem cell-based therapies, the knowledge regarding the scar formation after MI or non-ischemic cardiomyopathies is confined to the discoveries from decades ago. Thus, there is still a question that has to be addressed: what happens during the healing process of scar formation?

MI may be the most common cause of ventricular scarring in humans, scars also occur in non-ischemic cardiomyopathies due to replacement fibrosis during both pressure/volume overload [1] and normal ageing [2], although aging is not necessarily associated with fibrosis *per se* [3]. In addition, scars result from clinical interventions such as ablation and surgical procedures [4].

'Fibrosis' is not synonymous with an elevated presence of interstitial cells: it is quantified through the presence of collagen – a key component of the acellular fraction of connective tissue. Fibrotic scars, such as in skin, are generally acellular and predominantly composed of fibrillar collage [5]. In the heart, however, scar tissue assumes a more proactive role than simply preserving ventricular integrity, facilitating force transmission, and preventing rupture. Nonetheless, myocardial scarring does share common mechanisms and morphological milestones with classic wound healing (reviewed in [6] [7]).

Briefly, injury is followed by spreading tissue necrosis, neutrophil infiltration, and macrophage-driven clean-up of cellular debris. Subsequently, granular tissue formation, neovascularization, and (partial) sympathetic re-innervation occur. Infiltration from intra- and extra-cardiac sources and proliferation of fibroblast-like cells occurs throughout, and is observed as early as a few hours post-injury [8] [9]. Large amounts of newly produced collagen act to reinforce the healing tissue, eventually establishing a steady state involving balanced extracellular matrix (ECM) production by fibroblasts and degradation *via* matrix metalloproteinases that are released by leukocytes, fibroblasts, and smooth muscle cells [10]. The traditional view of scar formation (based on observations in organs such as skin) suggests that healing is followed by apoptosis of the vast majority, if not all, of the cells (including fibroblasts), leaving a mature, fibrillar scar. This whole process takes several weeks post-injury, and – in the heart at least – takes place in an environment of rhythmically changing stress and strain.

Below (Fig 1) is shown a cross-section of an infarcted mouse heart at one month after the left ventricular descendent coronary artery ligation. The heart section is stained with the Masson trichrome staining; it is well recognizable the scar/fibrotic area colored in blue.

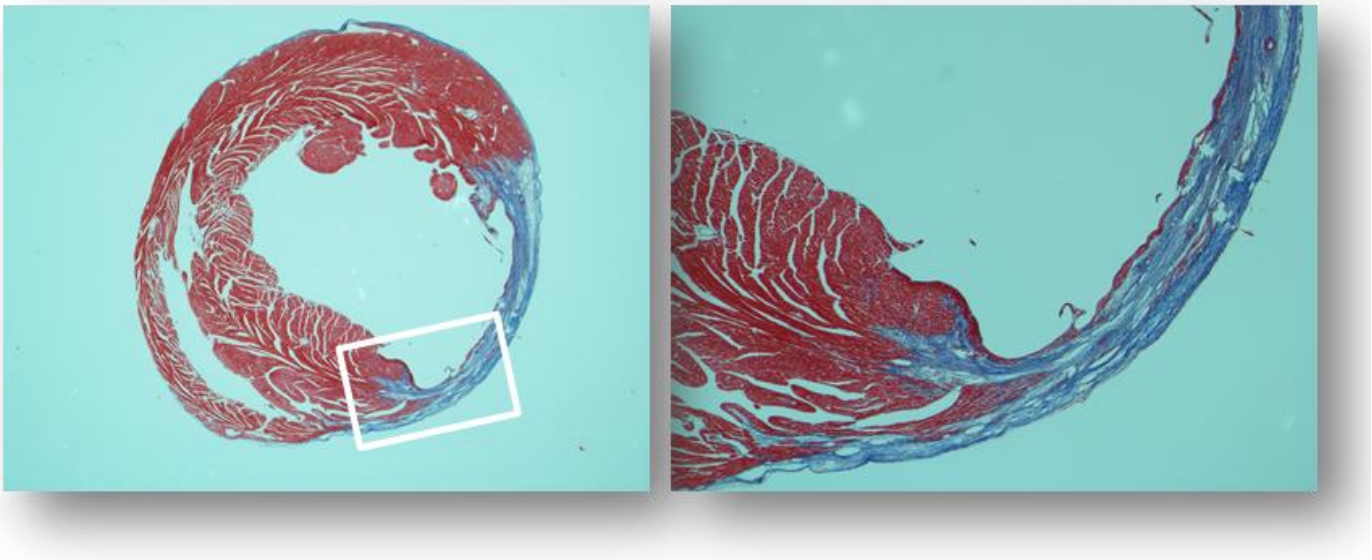

Fig 1. Scar formation after MI in a mouse hearth. Thin cardiac cross section of mouse heart at one month after MI was stained with Masson trichrome staing, the border zone of the MI and the newly formed fibrotic tissue is magnified on the left.

The Living Scar

Despite prevailing perceptions, cardiac scars are dynamic living structures [11]. The abundantly present ECM is interlaced with phenotypically diverse groups of cells: interstitial fibroblast-like cells, functionally and structurally heterogeneous, endothelial cells, vascular smooth muscle cells, surviving cardiomyocytes, immune cells, neurons, adipocytes and several type of progenitor cells such as endothelial progenitor cells (EPCs), pericytes, mesenchymal stem cells and cardiac progenitor cells (CPCs). The scar is a metabolically dynamic tissue which furthermore, exhibits non-linear passive and active mechanical properties; 'active' force-generation by non-myocytes over time occurs at scales that are orders of magnitude longer than the heartbeat [12]. Contractile properties of the scar rely on the presence of non-vascular, α-smooth muscle actin-expressing non-myocytes, which persist in cardiac scars for many years following injury, such as with MI [13]. Note that not all subsets of fibroblasts express contractile proteins [14]. They also depend on the presence of an extensive cytoplasmic fibrillar system of cell-to-cell and cell-to-ECM attachments [15].

The impact of scar tissue on cardiac electrical activity is a matter of debate [16]. Fibrosis can exhibit variable degrees of density, from focal and compact (in the case of scars) to patchy and diffuse. This can lead to the separation of strands of myocardium, forcing excitation waves to take anisotropic, circuitous paths [17] that may set the stage for re-entry of excitation [18]. Although fibrosis is strongly associated with an elevated risk of arrhythmogenesis, it is not well

understood how exactly it is involved in either the active generation or the passive maintenance of abnormal electrical conduction episodes.

In some instances, a regenerative process of endogenous new cardiomyocyte formation and neo-vascularization occur concomitantly with the scar development. The repair and regeneration of the injured tissue are inter-related. Unfortunately, physiologically the regeneration is much less pronounced than the replacement fibrosis [19].

The healthy scar formation

As said, cardiac scars are dynamic living structures [11] although, the blood vascular rarefaction and the poor neo-angiogenesis contribute to the deleterious effects of the cardiac inflammation and edema [20].

However, the crucial role in the maintenance of tissue fluid balance and immune surveillance is played by the lymphatic system, suggesting that the lymphangiogenesis in the process of scarification is very important for the heart healing [21].

The lymphatic system is present throughout the entire body in all vertebrates and regulates the tissue homeostasis, fluid balance and repair due to its function in the transport of molecules and cells [21].

The unique structure of the lymphatic vessels (LVs) such as, discontinuous basal lamina, fenestrations, wide lumen and lack of pericyte and smooth muscle cell lining, are advantageous features for cell trans-migration and diapedesis [21] . Hence, functional LVs are critical for the circulation-trafficking of immune, cancer and other cell types. . The lymphatic markers, function and features are summarized in the table below (Fig 2).

Lymphatic Markers	Lymphatic function	Lymphatic features
Lyve-1	Tissue homeostasis	Discontinuous basal lamina
Podoplanin	Tissue repair	Wide lumen
Prox-1	Cell trafficking (immune, cancer cells)	Lack of smooth muscle cell lining
VEGFR-3		

Fig 2. Characteristics of lymphatic vessels. In the table are summarized the major markers of the lymphatic endothelial cells and their role in the tissues all over the body.

The Lymphangiogenesis

The lymphatic vascular system is closely related to the blood vascular system in terms of origin, morphogenesis, and the regulatory molecules required for its development and growth. The lymphatic system develops in parallel and secondarily to the blood vascular system through lymphangiogenesis [22]. As revealed by lineage tracing, lymphatic endothelial cells (LECs) are differentiated entirely from venous endothelial cells in a process controlled by the transcription factor prospero homeobox-1 (Prox-1). Migrated LECs then form primary lymph sacs from which LECs germinate, proliferate, and migrate to give rise to the entire lymphatic vascular network. Vascular endothelial growthfactor-3 (VEGF-3) is a critical regulator for LVs growth, acting via its receptor, VEGFR-3, which is primarily found on LECs [23]. Initial differentiation of the LECs lineage begins from venous endothelial cells (ECs) [24]. Through yet-unknown mechanisms, a subset of venous ECs starts to become committed to the lymphatic endothelial fate at embryonic day (E) E8.5. These cells express the transcription factor Sox18, which directly activates Prox1 by binding to its proximal promoter. Transcription factor Prox-1 then serves as master regulator of LECs identity during embryonic development and postnatal remodeling [25]. Besides Prox-1, differentiating LECs at E9.5 also express lymphatic endothelial hyaluronan

receptor-1 (LYVE-1) and VEGFR-3. Starting at E10.5, podoplanin, a type-1 transmembrane sialomucin-type O-glycoprotein is expressed on the LECs surface. LECs, stimulated by vascular endothelial growth factor C (VEGF-C) secreted from adjacent tissue, migrate and proliferate to form primary lymph sacs around E11.5. During this step, the lymphatic and venous systems become separated via a process that involves podoplanin, [26]. Podoplanin activates C-Type lectin receptor 2 (CLEC-2), thus activating the hematopoietic protein Syk/Slp-76 signaling pathway and platelet aggregation. Aggregated platelets "seal off" the lymph sacs from cardinal veins [27]. Finally, LVs maturation and remodeling occur in a stepwise manner, leading to the formation of the complete lymphatic network.

In the cartoon below (Fig 3) are summarized the Steps of mouse lymphangiogenesis [28].

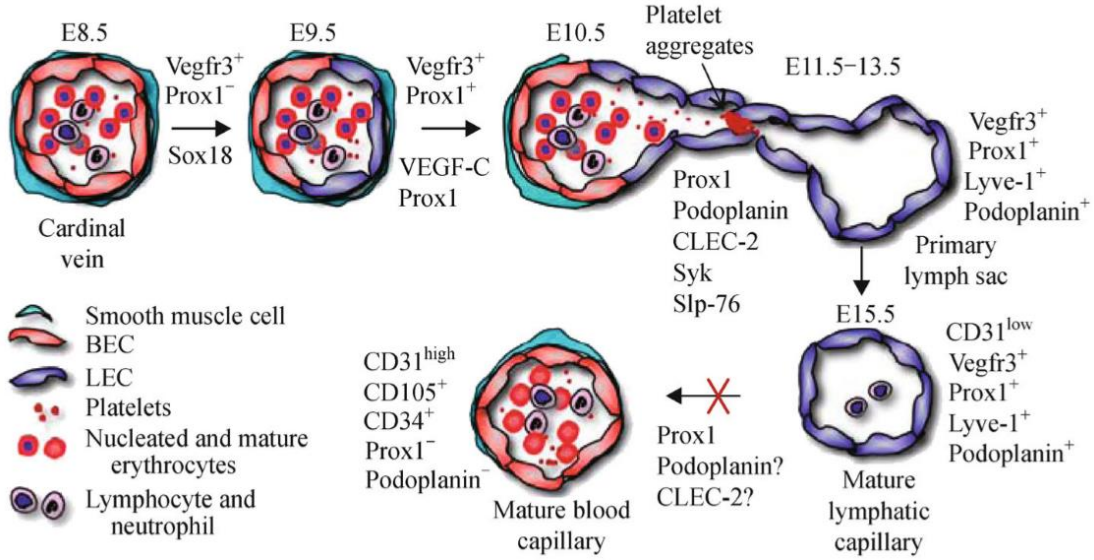

Fig 3. The embryonal lymphangiogenesis. At E8.5, cardinal vein ECs become lympsatic competent. At E9–E9.5, a subset of cardinal vein ECs begins expressing Sox18 and subsequently, Prox-1 at E9.75. Starting at E10.5, podoplanin is expressed in ECs. At E11.5, primary lymph sac is formed from sprouted LECs, with aggregate platelets to seal and separate from the vein. Mature LVs are then developed from the primary lymph sac. Prox-1 and possibly

podoplanin are critical not only for separating blood and lymphatic vascular system, but also for maintaining LECs identity.

The lymphangiogenesis: Prox-1 leads the transcription of podoplanin

Mouse Prox-1 was named as such because of its homology to the Drosophila homeobox protein prospero [29]. During mouse embryogenesis, Prox-1 is expressed in the developing central nervous system (CNS), eye lens, pancreas, liver, skeletal muscles, and heart. Mice with tamoxifen induced deficiency of Prox-1 (induciblProx1–/–) during the embryonic, postnatal, or adult stages exhibit interconnected blood vessels (BVs) and LVs and show dedifferentiation of LECs into ECs; reduced expression of LECs markers (VEGFR-3, podoplanin, LYVE-1, etc.) and the appearance of ECs markers (endoglin, CD34, etc.) may also be notably observed [28]. These findings indicate that LECs differentiation is tightly regulated and that the differentiated LECs phenotype is a plastic and dynamic condition that depends on constant Prox-1 activity, for maintenance. However, downstream target genes of Prox-1, through which it controls the switch from ECs to LECs and maintains LECs identity, remain to be identified. In vitro, Prox-1 interacts with transcription factor COUPTFII to regulate expression of several lineage genes, including VEGFR-3, fibroblast growth factor receptor 3 (FGFR-3), and neuropilin 1 [22] [30]. However, phenotypes of mice lacking VEGFR-3, FGFR-3, or neuropilin 1 do not resemble the lymphatic defects in inducible Prox-1–/– mice [30]. When Prox-1 was adenovirally transduced into human dermal microvascular endothelial cells, expression of podoplanin was upregulated. Mice with global deletion of Podoplanin (Pdpn–/–) exhibit misconnected BVs and LVs that closely resemble those observed in inducible Prox-1–/– mice [31]. Both Prox-1 and podoplanin are also constantly expressed in LECs naturally and appear to function in an LEC-autonomous manner.

Thus, podoplanin is hypothesized to function downstream of Prox-1, and podoplanin expression is regulated by Prox-1 in LECs at the transcriptional level. Four putative binding elements for Prox1 in the 5′ upstream regulatory region of the podoplanin gene were first identified. Using chromatin immunoprecipitation assay, Prox-1 was observed to directly bind to the 5′ regulatory sequence of the podoplanin gene in LECs. DNA pull down assay confirmed that Prox-1 binds to the putative binding element. In addition, luciferase reporter assay indicated that Prox-1 binds to the 5′ regulatory sequence of podoplanin to regulate podoplaningene expression [32]. These results suggest that Prox-1 regulates podoplanin expression at the transcriptional level in the lymphatic vascular system. Thus, podoplanin potentially serves as a major downstream target gene of Prox-1 in the pathway essential for differentiation and maintenance of lymphatic identity. As described, mature LECs express Lyve-1, VEGFR-3, Prox-1 andpodoplanin; all of those protein and transcription factors are very important for the formation and, scientifically, for the identification of the LVs.

The heart depends heavily on its lymphatic network for the return of the blood circulation of extravasated molecules and fluids. Accordantly, surgical obstruction of cardiac lymphatics rapidly leads to myocardial edema with well-described acute, and chronic, as well deleterious, effect on cardiac function [21].

In the cartoon below (Fig 4) is described the mechanism of BVs and LVs separation [28].

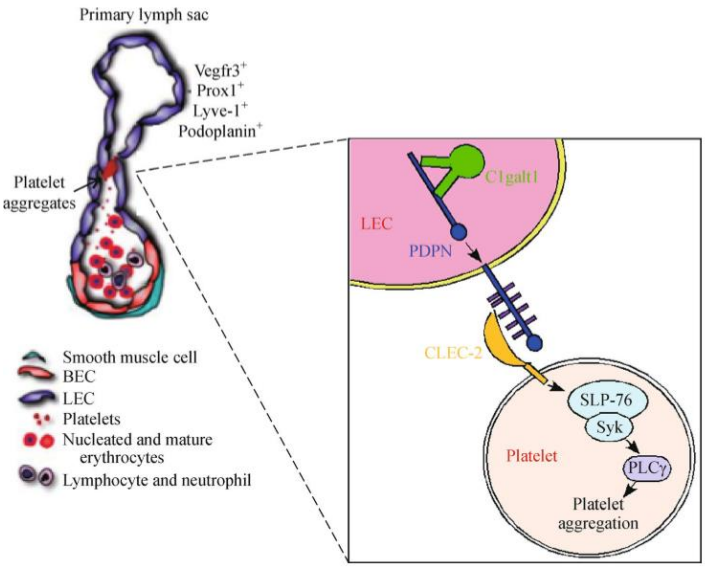

Fig 4. The separation of the lymphatic vessels from the cardinal vein. Podoplanin is O-glycosylated during biosynthesis in LECs. Cell surface exposed podoplanin binds to platelet receptor CLEC-2 and activates the Syk tyrosine kinase and SLP-76 adaptor protein. Syk/SLP-76 signaling leads to downstream activation of phospholipase C-γ2 (PLC-γ2), resulting in platelet activation. Aggregated platelets form a plug to seal off the growing primary lymph sac from the cardinal vein.

The lymphatic system in the heart

In the heart, the cardiac lymphatic system is crucial for the control of intra-myocardial pressure and prevention of swelling, lipid transport (major source of energy for myocytes), and balanced regulation of tissue inflammation (reviewed in [33] [34]). Although little is known about the distribution and activity of cardiac lymphatic vessels (CLVs), there is a documented link between lymphatic malfunction and cardiovascular diseases, including post-MI edema, fibrosis and scarring, and the evolution of congestive heart failure [35] [36].

Based on the hitherto reported data, the adult cardiac lymphatic vasculature consists of a network of sub-epicardial and sub-endocardial vessels and a plexus of myocardial capillaries of various diameters and variable concentrations in the different regions of the heart [37] [34] [38] [39]. The intramyocardial lymphatics drain centrifugally, with each contraction, toward the superficial epicardial lymphatic network composed of both blunt-ended capillaries and larger precollectors and valved collecting ducts, with empty into periaortic and paratracheal lymph nodes [21].

By employing immunohistochemical labeling LYVE-1, Prox-1, VEGFR-3, it was established that the localization and morphology of CLVs are substantially altered in pathological conditions [40] [21, 36]. Acutely after MI, the density of CLVs increases in the early phases of wound granulation and is further elevated at later stages of tissue repair, superseding the number of blood vessels (BVs) in the scar [36] [41] [21]. The post-MI lymphangiogenesis in the human heart is mostly apparent in the scar, infarct border zone (BZ) and reactive pericarditis [36]. Likewise, in murine models of MI, the development of new CLVs is primarily detected in severely damaged myocardium and the adjacent BZ [42] [43]. There is evidence that CLVs are involved in adverse ventricular remodeling [42], potentially promoting the maturation of fibrosis and formation of a stable scar [41] [43]. Yet, experimentally-induced impairment in cardiac lymph flow leads to exacerbated and prolonged inflammation after MI [33] [35], and promoting post-MI lymphangiogenesis is suggested to facilitate structural and functional recovery of the mouse and rat hearts [44] [21]. Thus, lymphangiogenic processes in the infarcted heart may have pleiotropic effects on the fibrogenic responses and scar maintenance.

Importantly, the cellular sources of the CLVs in the healing MI remain to be revealed. In order to recognize putative cell populations participating in post-MI lymphangiogenesis and fibrosis during different phases of the wound repair, we performed characterization of the distribution of

an established lymphendothelial epitopes, podoplanin, LYVE-1, Prox-1 and VEGFR-3, along with the analysis of cell phenotypic markers associated with angiogenic and fibrogenic responses, including CD34, platelet-derived growth factor receptor (PDGFR) α and PDGFRβ, vimentin, and α-smooth muscle actin (α-SMA). Our data point to an unexpected heterogeneity in the podoplanin-positive cardiac cell compartment, which might be significant for the processes of CLV growth after injury, development of fibrosis and scar maintenance.

In the three pictures (Fig 5) is shown the lymphatic vasculature in blue and the blood vasculature in white in thick sections of a mouse heart. Respectively from the left were pictured the epicardium, mid-myocardium and the endocardium; notice the distribution of the LVs along with the BVs and the major lymphatic collectors in the epicardium.

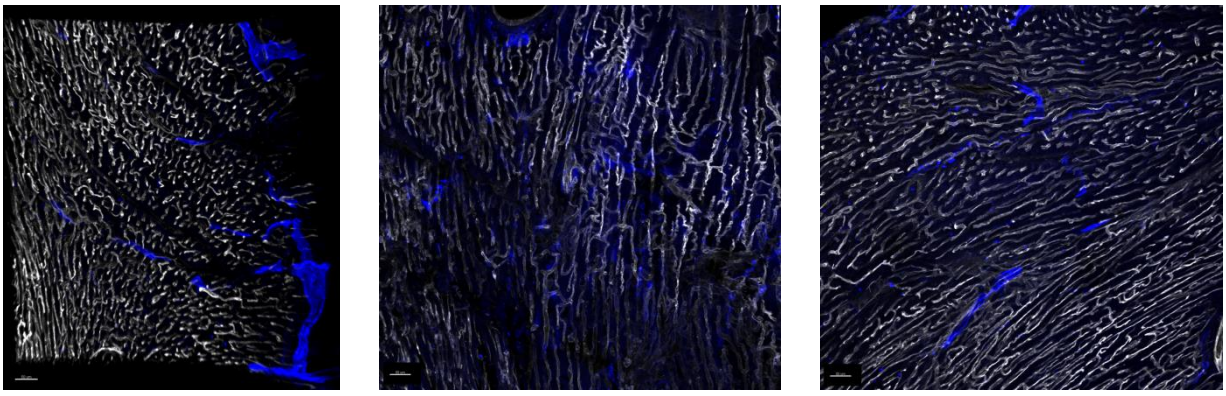

Fig 5. The distribution of the lymphatic system in the heart. In the three pictures is shown the lymphatic vasculature in blue (LVs stained together with LYVE-1 and podoplanin) and the BVs in white (stained with isolectin B4) in thick sections (250μm) of a mouse heart. Respectively from the left was pictured the epicardium, mid-myocardium and the endocardium. In the epicardium are very well visible (on the right) the sub epicardial lymphatic collectors that are located under need the pericardium. The myocardial and the sub endocadial lymphatic vasculature run parallel to the blood vasculature in a very well orchestrate organization.

As expected, the distribution of the LVs in the scar is different compared to the healthy tissue, the lymphangiogenesis supersedes the angiogenesis as it is shown in the picture below (Fig 6). Notice that the lymphatic vasculature is stained in white and the blood vasculature in blue. In order to show the scar structure, the heart has been labeled in green with α-SMA.

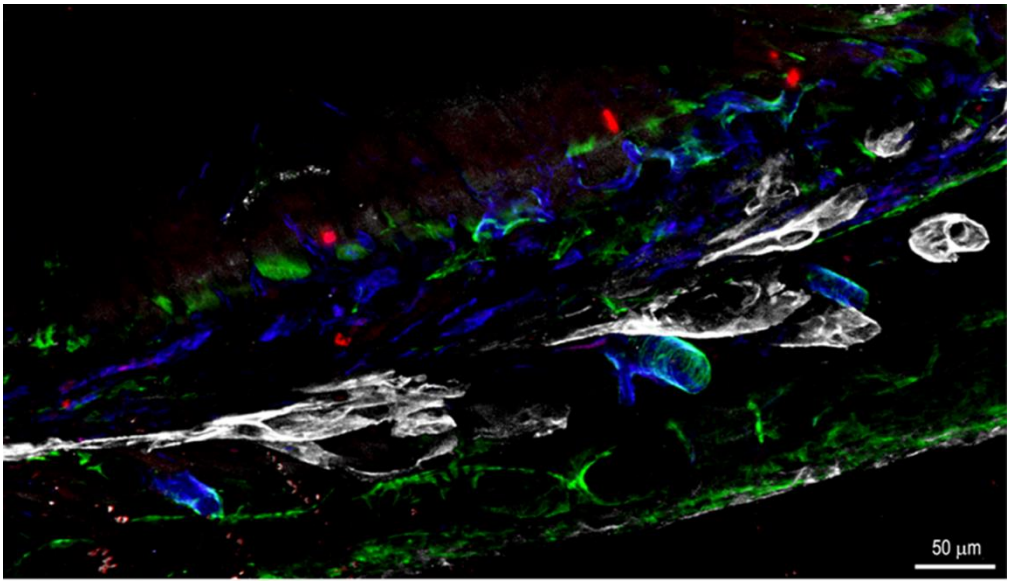

Fig 6. The distribution of the lymphatic system in the scaring heart. Below is shown a 3-D reconstruction of a thick section (250µm) of an infarcted mouse heart. Respectively the BVs are stained in blue with the isolectin B4 and the LVs are labeled in white with LYVE-1 and podoplanin. The scar tissue is stained with α-SMA, as a marker of fibrotic tissue. The section of the scar tissue, as it is shown before with the Masson trichrome staining is very thin. As said, during the scar formation the lymphangiogenesis superseding the angiogenesis.

Podoplanin, a small protein with many faces

Based our observations, podoplanin is highly expressed not only by the LECs, but by different type of cells at the time of inflammation; this heterogeneous cell cohorts that express podoplanin contribute to scar tissue biology in early and advanced phases of scar maturation.

Podoplanin is a 36- to 43-kDa mucin-type transmembrane protein. It has homologues in humans, mice, rats, dogs, and hamsters and is relatively well conserved between species. It has been reported to bind CLEC-2, which is highly expressed by platelets and immune cells; podoplanin also binds the CD44 and CD9 involved in cell motility and metastasis of immune and cancer cells [45].

podoplanin it has been identified and studied in many different contexts since it can be found on the surface of many types of cells originating from various germ layers. Thus, it has been given several names.

Podoplanin was first described on LECs as the E11 antigen [46] and on fibroblastic reticular cells (FRCs) of lymphoid organs and thymic epithelial cells as gp38 [47]. Podoplanin is also homologous to T1a/rTI$_{40}$, one of the first molecular markers of alveolar type I epithelial cells [48, 49], PA2.26, which is upregulated in skin keratinocytes upon injury [50], OTS-8, a molecule induced in osteoblasts upon phorbol ester treatment [51], and Aggrus, a platelet-aggregating factor [52]. Finally, this molecule was given the name podoplanin due to its expression on kidney podocytes and possible involvement in the flattening of podocyte foot processes [53].

While podoplanin expression patterns in many of these cells have been well characterized, there is still little known about the physiological functions of this protein.

Besides the lymphangiogenesis and LVs distribution, the setting in which podoplanin has been most extensively studied is cancer [45]. The link between the lymphangiogenesis and cancer is

correlated with poor prognosis in cancer patients with increased lymphangiogenesis [45]. PDPN is often used as a diagnostic marker [53] [54] [55]since is upregulated on tumor cells themselves in several cancer types, including squamous cell carcinoma of the lung, head, and neck [56] [57] [58] [59]malignant mesothelioma[60] [61] skin cancers, osteosarcomas, gliomas and brain tumors[62] [63]. Podoplanin is often expressed at the leading invasive edge of tumors and appears to play a role in Epithelial-Mesenchymal Transition (EMT), invasion, and metastasis [59]. Interactions between CLEC-2 and podoplanin in tumors also likely play a role in tumor progression and metastasis due to platelets interacting with tumor cells [64]. However, the exact mechanism of podoplanin action in tumor cells is still unclear; in some cases, podoplanin expression mediates the downregulation of E-cadherin and promotes EMT [57], while in others, podoplanin expression enhances tumorigenesis and metastasis in the absence of EMT [59]. *In vitro* studies have provided compelling evidence that forced expression of podoplanin in cells that normally lack this protein results in a more mesenchymal phenotype, actin-rich filopodia, and increased migration and invasion, as discussed above [57] [59].

Interestingly, podoplanin is also upregulated by cancer-associated fibroblasts (CAFs) in the stroma surrounding various tumors, including adenocarcinomas and colorectal cancers [65]. Generally, the expression of podoplanin on CAFs is associated with poor prognosis. While these studies illustrate that podoplanin expression in CAFs is linked to poor prognosis for patients, it is important to keep in mind that the effect of podoplanin^{+} CAFs likely depends on the type of tumor cells and the tissue from which the CAFs originate. In fact, one study of colorectal CAFs found that podoplanin expression was correlated with a better prognosis [66].

Recently, the expression of podoplanin has been correlated with chronic inflammatory diseases characterized by hyper proliferation and an infiltrate of immune cells like psoriasis [67] and

rheumatoid arthritis [45]; not only, podoplanin is upregulated in experimental autoimmune encephalomyelitis (EAE), where it is believed to accelerate inflammation and disease progression [68]. We are the first in describing and characterizing the expression of podoplanin in the process of scarification in the heart.

In the table below (Fig 7) are summarized the organs where podoplanin is expressed and its function [45].

Organ	Time of expression	PDPN function	Reference
Central nervous system	Beginning day E9, becomes restricted to choroid plexus in adult mouse	No specific function reported during development; high PDPN expression in brain tumors	Williams et al. (1996), Kaji et al. (2012), Peterziel et al. (2012)
Heart	Expressed in entire organ on day E9; continued expression in adult heart	Required for normal heart development, specifically for EMT in epicardium-derived cells	Martin-Villar et al. (2005), Mahtab et al. (2008, 2009), Douglas et al. (2009)
Lungs	Appears in foregut on day E9 before lung buds; subsequently restricted to alveolar type I epithelial cells	Required for lung development; specifically the effective maturation of alveolar type I epithelial cells	Ramirez et al. (2003)
Intestine	Expressed on day E9 in foregut; continued expression in lamina propia	No specific function determined	Farr et al. (1992a), Williams et al. (1996)
Lymphoid organs	Present in spleen 4 days postnatally; in adult, expression by FRCs, LECs, and FDCs in lymph node and spleen, and thymic medullary epithelial cells	Required for proper formation and organization of lymph nodes and spleen; necessary for efficient DC migration to and within lymph nodes; highly expressed by stroma and some T cells in ectopic lymphoid tissue	Farr et al. (1992a), Bekiaris et al. (2007), Raica et al. (2010), Peters et al. (2011), Acton et al. (2012), Yu et al. (2007)
Immune cell	**Expression pattern**	**Function**	**Reference**
T cell	Expressed only on T_H17 cells, not other subsets	Plays a role in T_H17-driven development of ectopic germinal centers in EAE	Peters et al. (2011)
Macrophages	Expressed by inflammatory macrophages, such as thioglycollate-elicited peritoneal macrophages	Possibly plays a role in response to fungal infections; can activate platelet aggregation	Hou et al. (2010), Kerrigan et al. (2012)

Fig 7. Podoplanin expression and function. In the table are listed the major organs where podoplanin is expressed and its function along to the belonged organ.

The importance of podoplanin in the organ development

Podoplanin is first expressed in the developing mouse embryo on day E9 in the foregut, proepicardial organ, and central nervous system [49] [69]. Throughout development, it is also expressed in the fetal rat kidney, choroid plexus, intestine, and esophagus [49]. Over time, podoplanin expression is increasingly restricted such that in an adult animal, podoplanin is predominantly expressed in alveolar type I cells, mature osteoblasts, LECs, and FRCs in the T cell zone of lymphoid organs [46] [49] [58]. PDPN is critical for normal development of some of these organs and has been well studied in podoplanin-deficient animals. *Pdpn*$^{-/-}$ mice develop normally until around day E10, which coincides with the appearance of podoplanin protein. From days E10–16, approximately 40% of podoplanin$^{-/-}$ embryos die; the ones that survive to birth die within a few days [69]. The defect in blood-lymphatic vascular separation is the phenotype most extensively studied in podoplanin-deficient mice. On day E11.5, podoplanin first appears in the developing circulatory system on Prox-1^{+} LECs [58]. It was first reported by Schacht et al. (2003) that podoplanin$^{-/-}$ mice have abnormal LVs that cannot properly regulate lymph flow and that this defect did not appear in blood vessels. These findings were further supported by Fu et al. (2008), who reported that endothelial cell expression of podoplanin was responsible for a blood-lymphatic misconnection. Furthermore, continued expression of podoplanin into adulthood was required to maintain proper vascular architecture, as an inducible deletion of T-synthase, a major glycosyltransferase required for O-glycan synthesis and normal levels of podoplanin expression, showed similar blood-lymph mixing [31].

During the embryogenesis, the interaction of platelet CLEC-2 and podoplanin on LECs induces platelet aggregation and prevents blood from flowing into new LVs budding from the cardinal vein. Furthermore, injecting a podoplanin-blocking antibody or otherwise inhibiting platelet

aggregation is sufficient to disrupt lymphatic development [70]. Overall, the model that has emerged indicates that during the budding of the lymph sac from the cardinal vein, podoplanin becomes upregulated on Prox-1^+ LYVE-1^+ LECs and binds with CLEC-2 on platelets. This interaction activates downstream signaling in platelets, which results in platelet aggregation. This aggregation then allows for a complete separation of the budding LVs from the developing BVs.

In addition to its role in LVs development, podoplanin may play a role in the development or maintenance of lymphoid organ architecture, alveolar type I cells and alveoli structure and heart formation [45]

Podoplanin is highly necessary for proper development of the heart. podoplanin is first expressed in the proepicardial organ on day E9.5 and by day E12.5, it is expressed in most of the heart. Without podoplanin expression, the hearts of developing mice exhibit hypoplasia in the pulmonary vein, left atrium dorsal wall, and the atrial septum [71]. In this setting, the lack of Podoplanin leads to a dysregulation of EMT, a process that involves the transition of sessile epithelial cells into more motile mesenchymal cells through the downregulation of epithelial markers, such as adhesion molecules like E-cadherin [72]. In podoplanin-deficient mice, the epicardium-derived cells responsible for cardiac development show increased levels of E-cadherin and decreased levels of RhoA compared with their wild-type counterparts, which is indicative of impaired EMT [69]. While podoplanin has been shown to play a role in regulating EMT [57], these studies are the first evidence that podoplanin may play a role in physiological instances of EMT in non-transformed cells.

Overall, podoplanin is crucial for the development of multiple organs interestingly, podoplanin serves diverse functions in these organs. In some instances it is required for CLEC-2-dependent platelet aggregation, but in others it seems to have an intrinsic effect on proliferation or

differentiation in a specific cell type [45]. This raises the question of whether podoplanin function could to some degree be tissue specific. The range of physiological effects downstream of podoplanin expression may be due to different protein interactions and binding partners in diverse cell types.

In the cartoon below are summarized the main transcription factor and cytokines that can enhance and promote the podoplanin transcription (Fig 8) [45].

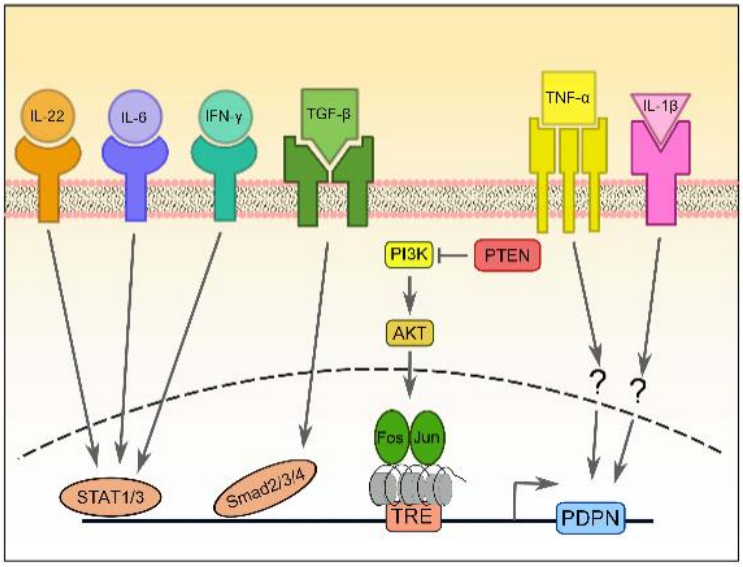

Fig 8. Transcription of podoplanin. The transcription of podoplanin can be led by different type of stimuli; the major activators of the transcription are pro-inflammatory cytokines.

Podoplanin signaling and molecular pathways

Podoplanin contains a single transmembrane domain, a short, nine amino acid cytoplasmic tail, and a heavily glycosylated extracellular domain [57]. While there are no obvious conserved protein domains in podoplanin, several studies have identified specific residues on podoplanin that mediate interactions with other proteins. The first hints at the cellular function of podoplanin came from [50], who discovered that podoplanin was upregulated in keratinocytes from induced

epidermal carcinogenesis and was localized to membrane protrusions such as fillopodia and lamellipodia. Podoplanin co-localized with ezrin, radixin, and moesin (ERM) family proteins, and was later found to directly bind ezrin and moesin. The ERM proteins function as connectors between integral membrane proteins and the actin cytoskeleton. Thus, this interaction likely underlies many of the effects that podoplanin has on cytoskeleton.

Podoplanin also interacts with two integral membrane proteins that could help to further explain how it affects cell motility and metastasis: CD44 and CD9.

CD44is widely expressed, affects many cellular functions such as migration and adhesion, and the expression of some isoforms is linked to more invasive cancers. Martín-Villar et al. (2010) noted that CD44 and podoplanin were coordinately upregulated in aggressive cancer cell lines and subsequently found that they directly bind to one another. This interaction is dependent on correct glycosylation of the extracellular domain of podoplanin, and CD44 expression is required for podoplanin-induced cell migration [57].

Additionally, Nakazawa et al. (2008) found that podoplanin directly interacts with the tetraspanin CD9 through transmembrane domains 1 and 2 of CD9. CD9 acts as a tumor suppressor in many cancers [73], and co-expression of CD9 and podoplanin resulted in a CD9-mediated decrease of Podoplanin-induced metastasis. CD9 inhibited podoplanin-mediated platelet aggregation without directly interfering with CLEC-2 binding of podoplanin [74]. This finding indicates that CD9 potentially disrupts CLEC-2 multimerization, which is required for downstream signaling. These interactions provide some insight into how podoplanin can exert striking effects on actin cytoskeleton rearrangement, cell motility, and metastasis.

The only known receptor for podoplanin is CLEC-2, a C-type lectin that is expressed by platelets, neutrophils, monocytes and dendritic cells (DCs) [75]. Glycosylation of T34 on

podoplanin is required for CLEC-2 binding of podoplanin. This amino acid resides in the platelet-aggregation stimulating (PLAG) domain, which is highly conserved between podoplanin homologues [76]. The effect of CLEC-2 engagement by podoplanin has been extensively studied in platelets; however, the effect of this interaction in podoplanin-expressing cells has not been addressed.

Podoplanin interacts with galectin-8 on LECs, and this interaction is also dependent on podoplanin glycosylation [77]. Galectin-8 can have varying effects on adhesion depending on whether it is secreted or membrane-bound [45]; it seems that podoplanin binding to galectin-8 may affect LECs adhesion, but additional studies are needed to fully elucidate the consequences of this interaction.

Podoplanin also binds CCL21 with high affinity, and this interaction is also dependent on glycosylation of podoplanin [78]. This interaction has interesting implications for lymphocyte trafficking, as both LECs and FRCs express CCL21 to direct lymphocyte and DCs trafficking to the T zone of lymph nodes [79].

It has yet to be examined whether the above binding partners of podoplanin are cell-type specific or how interaction with one protein affects the binding of podoplanin to another interacting molecule. With the exception of the ERMs and CD44, it remains unclear whether podoplanin can bind to several of these proteins at one time or whether such interactions might be mutually exclusive. A more global understanding of these various interactions is critical to our overall understanding of podoplanin's molecular functions and downstream signaling [45].

The cartoon below (Fig 9) represent the molecular interactions of podoplanin with its receptor CLEC-2 and the bindings with CD44 and CD9 [45].

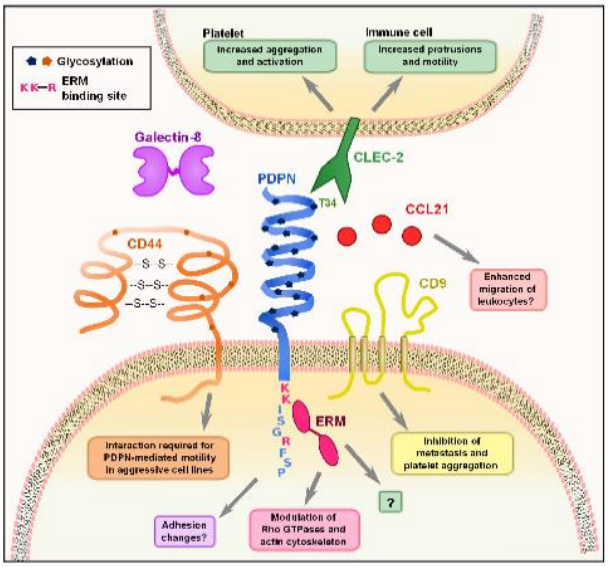

Fig 9. Podoplanin binding. Podoplanin has its own receptor called CLEC-2, but is able to interact also with CD44 and CD9 as it is shown in the figure.

Podoplanin: the joker protein

In conclusion, podoplanin is a very interesting protein; it is expressed in a variety of different type of cells and in different context; a multitude of stimuli can drive podoplanin expression, including physiological differentiation factors in embryogenesis, potentially malignant factors such as pro-tumorigenic signaling pathways in cancer and pro-inflammatory cytokines in immune diseases or scar formation. podoplanin orchestrates the lymphatic and the immune system but also the malignancy of tumors. Different pathways controlling podoplanin upregulation or downregulation could result in the activation or inhibition of distinct downstream signaling pathways and therefore different cellular outcomes.

There are still many unknown about podoplanin biology that remain to be answered and the future studies will provide critical insights into whether podoplanin can be used as a specific

marker for the diagnosis of “heathy” fibrosis and a target for the inhibition of inflammation besides that the metastasization.

Aims

The majority of data examining the function and signaling pathways of podoplanin are from studies of podoplanin expression in lymphangiogenesis and cancer, while these studies certainly provide critical insight into cellular and molecular aspects of podoplanin biology, it is important to understand whether podoplanin functions similarly in non-pathological settings and in cell types where it isn't naturally expressed.

The aim of this project is to describe in a time dependent manner the expression of podoplanin in the scar formation after MI and analyze the co-expression of podoplanin with several markers that where not associated with the podoplanin expression before.

The results of the study will provide terrific information regarding the biology of the healing heart after MI; a better understanding of the environment of the scar it will improve the feasible but modest therapy for the cardiac regeneration that are currently carried on.

Materials and Methods

Myocardial infarction

Experiments were conducted according to the NIH Guide for the Care and Use of Laboratory Animals and were approved by the Institutional Animal Care and Use Committee (IACUC). C57BL/6 and BDF1 Kit/GFP transgenic [80] mice were used interchangeably with identical results. Myocardial infarction (MI) was induced in female mice to reduce biological variability related to sex at 2-3 months of age as follows: animals were anesthetized with isoflurane 1.5% and ventilated, under sterile conditions the thorax was opened via the third costal space, the atrial appendage elevated, the left coronary artery located (S2, Fig 1), and a silk braided suture (6-0) was inserted and tightened around the vessel near the origin. Then, the chest was closed and pneumothorax reduced by negative pressure, and the animals were allowed to recover. Sham-operated (SHAM) mice were subjected to an identical surgery procedure, with the exception that the suture was not tightened around the artery. Non-operated (NO) mice served as additional controls. At the time of sacrifice (S2, Fig 2), with the animals under deep anesthesia, bilateral thoracotomy was performed, the hearts were removed and either fixed and processed for histological analysis, or enzymatically digested [81] for single-cell assessment by flow-cytometry, as described below.

Immunohistochemistry of thin cardiac sections

Hearts were perfused with 10% formalin, fixed and embedded in paraffin. Cardiac tissues were cut into 4 μm-thick sections. Following deparaffinization, rehydration, and heat-induced antigen retrieval (pH 6.0), samples were indirectly immunolabeled with commercially-available primary antibodies and corresponding fluorophore-conjugated secondary reagents; a complete list of

antibodies is provided in the S1 Table. Nuclei were counterstained with Hoechst 33342 (Life Technologies) or 4',6-diamidino-2-phenylindole dihydrochloride (DAPI; Sigma-Aldrich). Multiple sections from the hearts of at minimum 4 mice for each time point after MI and 3 mice per sham-operated group were examined, and representative micrographs are included in the figures. Images were acquired with Olympus FluoView FV100 laser scanning confocal microscope equipped with CCD camera (Bio-Rad), using 20X, 40X and 60X objectives. Optical sections (ΔZ= 0.5 to 1 μm) spanning the sample thickness were projected into a single plane for each color channel and merged using Adobe Photoshop (Adobe) or Imaris (Bitplane) software. Alternatively, the sections were blocked with hydrogen peroxide and indirectly immunolabeled with MOMA-2 or F4/80 antibodies (see S1 Table), followed by the development with diaminobenzidine (DAB) substrate kit (Vector) and counterstaining with hematoxylin and eosin (Poly Scientific R&D Corp.). Images were acquired using Olympus BX63 light microscope (Olympus Scientific Solutions Americas) with 20X and 40X objectives and assembled in Adobe Photoshop. Quantitative image analysis was performed with NIH ImageJ by scoring multiple imaging fields of 0.4 mm^2 (20X objective) and 0.045 mm^2 (60X objective) for every indicated time point after MI in the border zone (BZ) and remote area (RA) as follows: Podoplanin labeling was measured as % area above binary threshold of positive pixels out of total area populated by cells. Podoplanin co-labeling with LYVE-1, CD34 and VEGFR-3 was calculated using JACoP plugin to determine the degree of co-localization (ranging from the minimum of "0" to maximum of "1") by Manders' overlap coefficient, i.e., the fraction of intensity in a channel of interest located in the pixels displaying above the threshold signal in the podoplanin channel. The occurrence of Prox-1, PDGFRα or PDGFRβ staining in podoplanin-positive cells

was assessed by counting the % of double-labeled cells from the total podoplanin-positive population in the imaging field.

Immunolabeling of thick cardiac sections

Hearts were perfused with 4% paraformaldehyde and stored at 4ºC. Sections of 75 to 250 µm were prepared using Leica VT1200 vibrating blade microtome (Leica Biosystems), and indirectly immunolabeled employing the reagents detailed in the S1 Table, and Alexa Fluor 647-conjugated isolectin GS-IB4 (Life Technologies). Images were acquired with Olympus FluoView FV100 laser scanning confocal microscope using 10X and 20X objectives. Optical sections (ΔZ=1.5 to 2.5 µm) were projected into a single plane for each color channel, and merged using Adobe Photoshop or Imaris software. Representative micrographs are included in the figures.

Flow-cytometry analysis of isolated cardiac cells

Infarcted (MI) and sham-operated (SHAM) C57BL/6 mice were euthanized at 2 days after surgery, as described above. Non-operated (NO) age-matched animals were used as controls. The hearts were excised and extensively washed in phosphate buffered saline. The cardiac tissues were minced and subjected to repetitive rounds of enzymatic digestion with collagenase type 2 (Worthington Biochemical Corp.) until complete dissociation. Larger cells, such as mature myocytes, were precipitated, and the supernatants containing small cell populations were filtered through 40 µm cell strainers. High cell viability after isolation (~98%) was confirmed by flow-cytometry based on 7-AAD (BD Biosciences) exclusion. Samples were then either immediately stained with podoplanin and VEGFR-3, or fixed in 4% paraformaldehyde and

immunolabeled for podoplanin only, or podoplanin in conjunction with either LYVE-1, PECAM-1, CD34, Ly6C, CD11b, F4/80, PDGFRα or PDGFRβ. Prox-1 labeling was performed after the incubation of unfixed cells with podoplanin antibody, using fixation and permeabilization reagents from the transcription factor staining buffer set (affymetrix eBioscience) according to manufacturer's instructions. The antibodies used for flow-cytometry are listed in the S1 Table. Non-immune normal goat, rabbit, syrian hamster and rat IgGs and isotype controls (detailed in the S1 Table) were employed as negative controls for the respective antigen-specific labeling. Similar procedures for mouse cardiac cell isolation and antibodies for the detection of podoplanin, LYVE-1, F4/80 or PDGFRα by flow-cytometry, were recently reported by other groups [82] [83]. Samples were acquired with BD FACSCantoII (BD Biosciences) and analyzed using FlowJo software (Tree Star Inc.). Single cells were gated using FSC-A/SSC-A followed by FSC-H/FSC-W and SSC-H/SSC-W in all experiments. Compensation settings, gating of positive populations and calculations of % positive cells were performed based on non-immune and isotype IgGs and fluorescence minus one controls.

Statistical analysis

Data were presented as values for individual mice and means. Statistical analysis was performed with two-tailed *t*-test or one-way ANOVA and Tukey's *post hoc* test for multiple comparisons using GraphPad Prism (GraphPad Software).

Results

Podoplanin in the infarcted heart: a time dependent expression

In order to study the lymphangiogenesis and the appearance of the mesenchymal markers in acutely and chronically infarcted myocardium, we implemented immunohistochemical analysis of the tissue sections obtained from non-operated mouse hearts, as well as cardiac samples at 4 and 8 hours (<1day), 2 days, 2 weeks and 1 month after coronary artery ligation, and sham-operated animals.

The established markers used for the identification of LVs are LYVE-1 and podoplanin and it is well-documented that the lymphangiogenesis in the infarcted heart is peaking with the development of fibrosis and commencement of scar maturation [41] [21] [84].

We observed that at the time of ischemia and consequential necrosis [41] [85], there was a slight decrease in podoplanin-labeled cells and structures in the necrotic area when compared to a corresponding myocardial region in non-operated hearts, as illustrated by 8 hours after MI, (Fig 1A). Those findings are in agreement with previous ones in humans [41]. Surprisingly, at 2 days after MI, there was a more than a 6-fold increase in the podoplanin immunoreactivity in the infarct BZ relative to earlier time points after MI (< 1 day) or myocardial area remote to infarction (RA) (Figs 1A, 1B and 1E). As it is shown in the Fig 1A, 2 days after MI, all of the migratory cells that are recruited in the early stage of tissue granulation express podoplanin; interestingly podoplanin positive cells are located only in the BZ of the MI and they don't infiltrate yet in the necrotic tissue suggesting that the immune cells recruited in the early stages of MI barely co-stain with podoplanin (S2, Fig 5).

By flow-cytometry evaluation of isolated cardiac cells, we established that the frequency of podoplanin was relatively low in non-operated and sham-operated non-infarcted mouse hearts

(Fig 1C). In line with immunohistochemical findings on the podoplanin accumulation in the infarct BZ, by flow-cytometry analysis we determined that in the total infarcted hearts the occurrence of podoplanin-expressing cells versus non-operated and sham-operated counterparts was associated with more than three-fold increase (Fig 1C).

Importantly, our funding are in line a recent study combining immunohistochemical and flow-cytometry assessments of the mouse cardiac cellular composition, similarly reports that in homeostatic conditions, the podoplanin-positive cells are rare, constituting less than 5% of the myocardial endothelial cell population [83].

Accordingly, during early inflammatory responses to tissue damage [85], there were no observable differences in the presence of LYVE-1-positive CLVs in proximity to the injured area (Fig 1E). In the infarcted myocardium, similarly to remote areas and sham controls, the LYVE-1 labeling coincided with podoplanin almost exclusively in the vessel endothelium (Fig 1E-1H). In contrast, at the time of the appearance of podoplanin-positive cells at 2 days after MI, the co-labeling of LYVE-1 with podoplanin in the infarct BZ was substantially diminished (Fig 1E and 1F).

We observed, shortly after MI, a robust accumulation of interstitial podoplanin-positive/LYVE-1-negative cells in the infarct BZ (Fig 1E and 1F; 2 days), and a lesser extent podoplanin-positive/LYVE-1-negative counterparts in the RA (Fig 1G; 2 days).

Quantitatively, as compared to RA, in the infarct BZ there was more than a 30-fold decrease in the proportion of podoplanin-positive structures displaying the co-staining with LYVE-1 (Fig 1F, graph; 2 days). In support, flow-cytometry suggested that a much smaller fraction of podoplanin and LYVE-1 double-positive cells resided in the heart after MI compared to non-operated and sham-operated conditions (S2, Fig 3**)**.

Similarly to the co-expression of podoplanin with LYVE-1also the co-labeling with a pan-endothelial marker PECAM-1 was significantly reduced after MI in the cohorts of podoplanin-presenting cells (S2, Fig 3); further demonstrating that a large share of podoplanin-bearing cells appearing after infarction in the myocardial interstitium did not display markers of mature endothelium.

Subsequently, at 2 weeks after MI, at the maturation phase of wound healing, the density of podoplanin-labeled cells and CLVs was further elevated in the scar and BZ. We quantify an additional 1.7-fold increase in the podoplanin-labeled tissue area relative to 2 days, and a 10-fold rise relative to inflammatory stage (< 1 day) (Fig 1B and 1D-1F; 2 weeks), or the remote RA (Fig 1B and 1G) and non-operated myocardium (Fig 1 and 2A; 2 weeks).

In the healing scar, podoplanin immunoreactivity was apparent in LYVE-1-negative cell cords (Fig 1E and 1F; 2 weeks) and the proportion of podoplanin-positive cells co-labeled with LYVE-1 at 2 weeks after MI was almost 15 times lower than in the RA (Fig 1F, graph; 2 weeks) suggesting that LYVE-1 is expressed in podoplanin positive cells only il CLVs and not in the interstitial podoplanin positive cells. T

hese podoplanin-presenting LYVE-1-negative cells were aligned with the extracellular matrix (Fig 3A; 2 weeks) and formed capillary-like structures, which occasionally expressed CD34 (Fig 3B). The co-labeling of podoplanin with CD34 was more readily detectable at the time of scar maturation at 2 weeks compared to an earlier stage of acute injury at 2 days (Fig 3B), with a 3-fold increase in the co-localization coefficient relative to 2 days (Fig 3C; graph). Indeed, as evaluated by flow cytometry, shortly after MI there were no significant changes in the proportion of CD34-positive cells within podoplanin-presenting populations versus sham-operated controls (S2, Fig 3, Panel B; CD34). Intriguingly, the podoplanin-expressing cells also frequently

encircled the BVs in the fibrotic region and neighboring myocardium (Fig 1F, Fig 3D and 4D; 2 weeks), which might point to their origin from perivascular cells or the cells recruited from circulation.

At one month after MI, when the scar is well mature and the lost tissue is replaced by nonfunctional cells, the podoplanin labeling in the infarcted area and BZ remained high with no significant changes versus 2 weeks after MI (Fig 1B, 1D and 1F). As expected [41] [43], the presence of LYVE-1- and podoplanin-positive CLVs was prominent (Fig 1D-1F, 1H and Fig 2B; 1 month), supporting the notion that lymphatics, once formed, persist in the scarred tissue [41] [42] [21] [86]. Simialr to that, the co-staining of podoplanin with CD34 was also increased in the maturing scar like it was at 2 weeks after MI (Fig 3B; 2 weeks and Fig 3C; 1 month, and Fig 3C; graph), with an almsot 5-fold rise in podoplanin co-localization coefficient with CD34 relative to 2 days (Fig 3C; graph). Correspondingly to the early stage of scar maturation, the podoplanin-expressing population in the mature scar was dominated by the LYVE-1-negative multicellular assemblies (Fig 1E and 1F; 1 month), which were observed aligned with fibronectin deposits in the scar (Fig 3A; 1 month) and at the outline of small and large blood vessels (Fig 4; 1 month). In contrast, there was no such accumulation of the podoplanin-labeled cellular aggregates in the RA not affected by the infarction (Fig 1F, graph, RA and Fig 1G; 1 month). Quantitatively, there was more than a 10-fold decrease in the podoplanin and LYVE-1 co-localization in the chronic scar and BZ compared to RA (Fig 1F; 1 month). Collectively, these findings point to a correlation between the presence of podoplanin-expressing LYVE-1-negative cells at different stages of cardiac healing and the development of CLVs and fibrosis after MI.

Of interest, the growth of CLVs and appearance of podoplanin-positive interstitial cells were not detected in the sham-operated animals (Fig 1H; 1 month SHAM). Likewise, there were no

significant differences in the frequency of podoplanin between the sham- and non-operated hearts at 2 days after surgery (Fig 1C). These data underscore a specific effect of the MI-induced injury on the podoplanin expression and lymphangiogenesis.

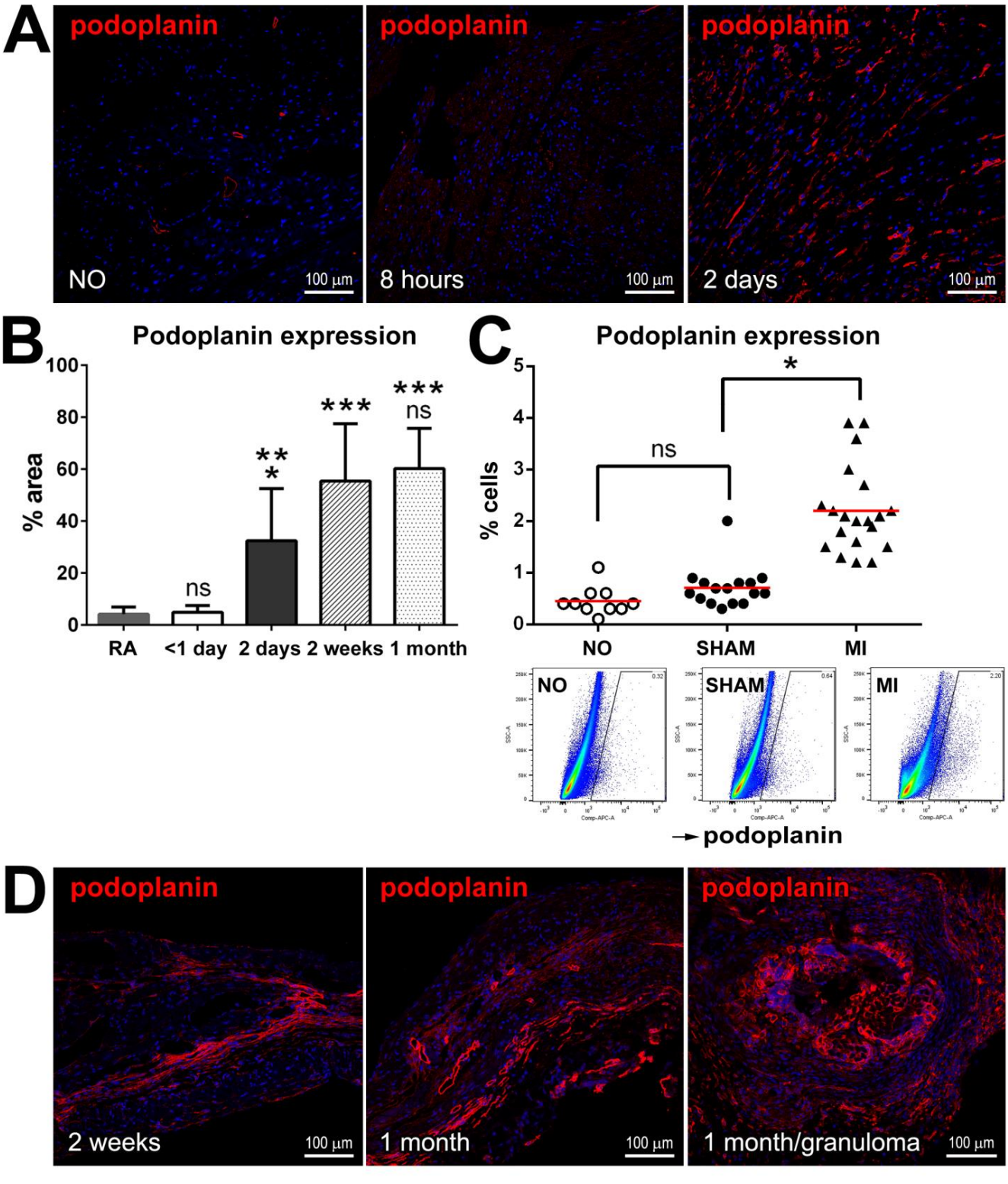
A
podoplanin
NO
100 µm
podoplanin
8 hours
100 µm
podoplanin
2 days
100 µm
B
Podoplanin expression
% area
100
80
60
40
20
0
ns
**
*
***
***
ns
RA
<1 day
2 days
2 weeks
1 month
C
Podoplanin expression
% cells
5
4
3
2
1
0
*
ns
NO
SHAM
MI
NO
SHAM
MI
podoplanin
D
podoplanin
2 weeks
100 µm
podoplanin
1 month
100 µm
podoplanin
1 month/granuloma
100 µm

Figure 1

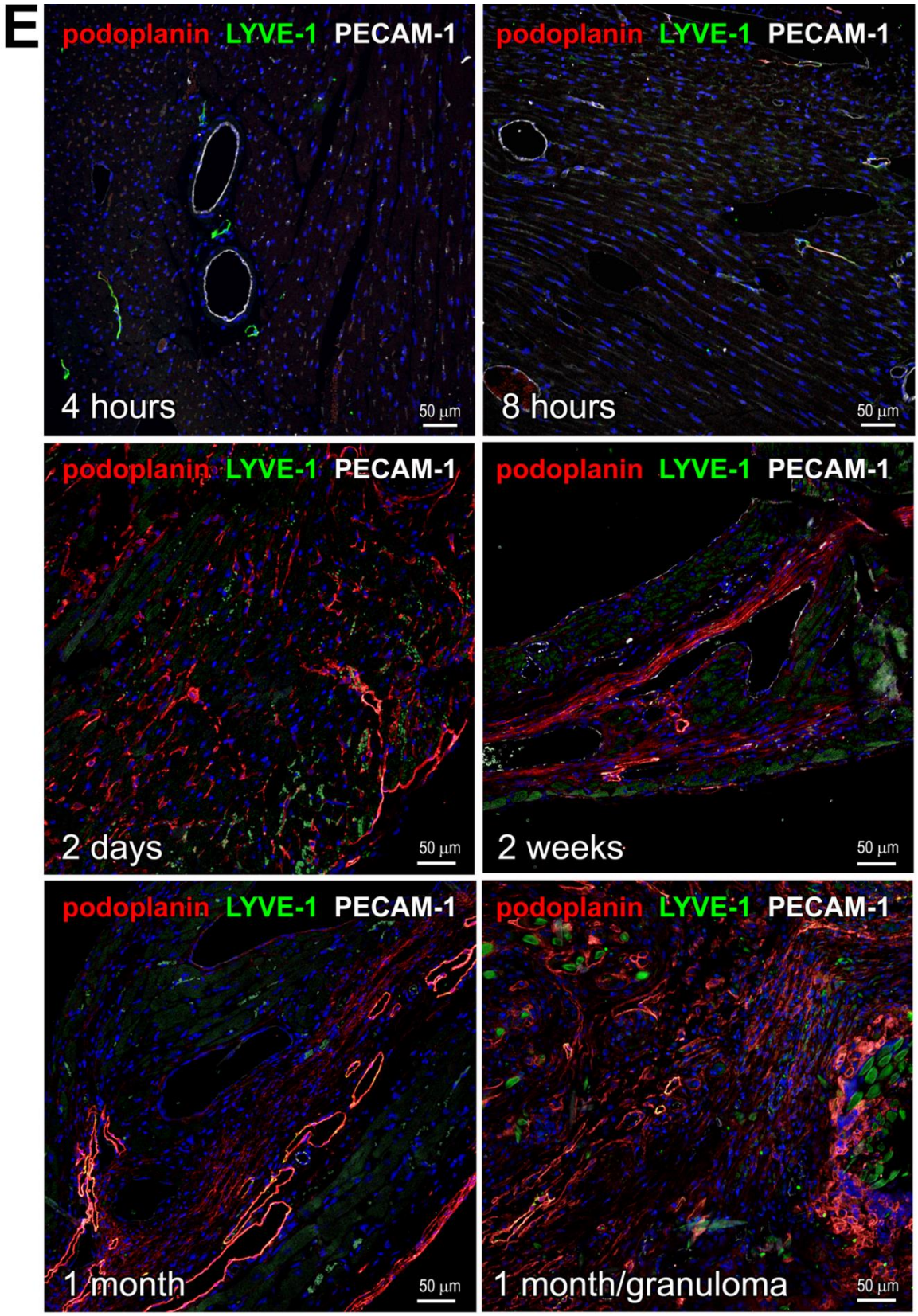
E
podoplanin LYVE-1 PECAM-1
4 hours
50 µm
podoplanin LYVE-1 PECAM-1
8 hours
50 µm
podoplanin LYVE-1 PECAM-1
2 days
50 µm
podoplanin LYVE-1 PECAM-1
2 weeks
50 µm
podoplanin LYVE-1 PECAM-1
1 month
50 µm
podoplanin LYVE-1 PECAM-1
1 month/granuloma
50 µm

Fig 1 (cont.)

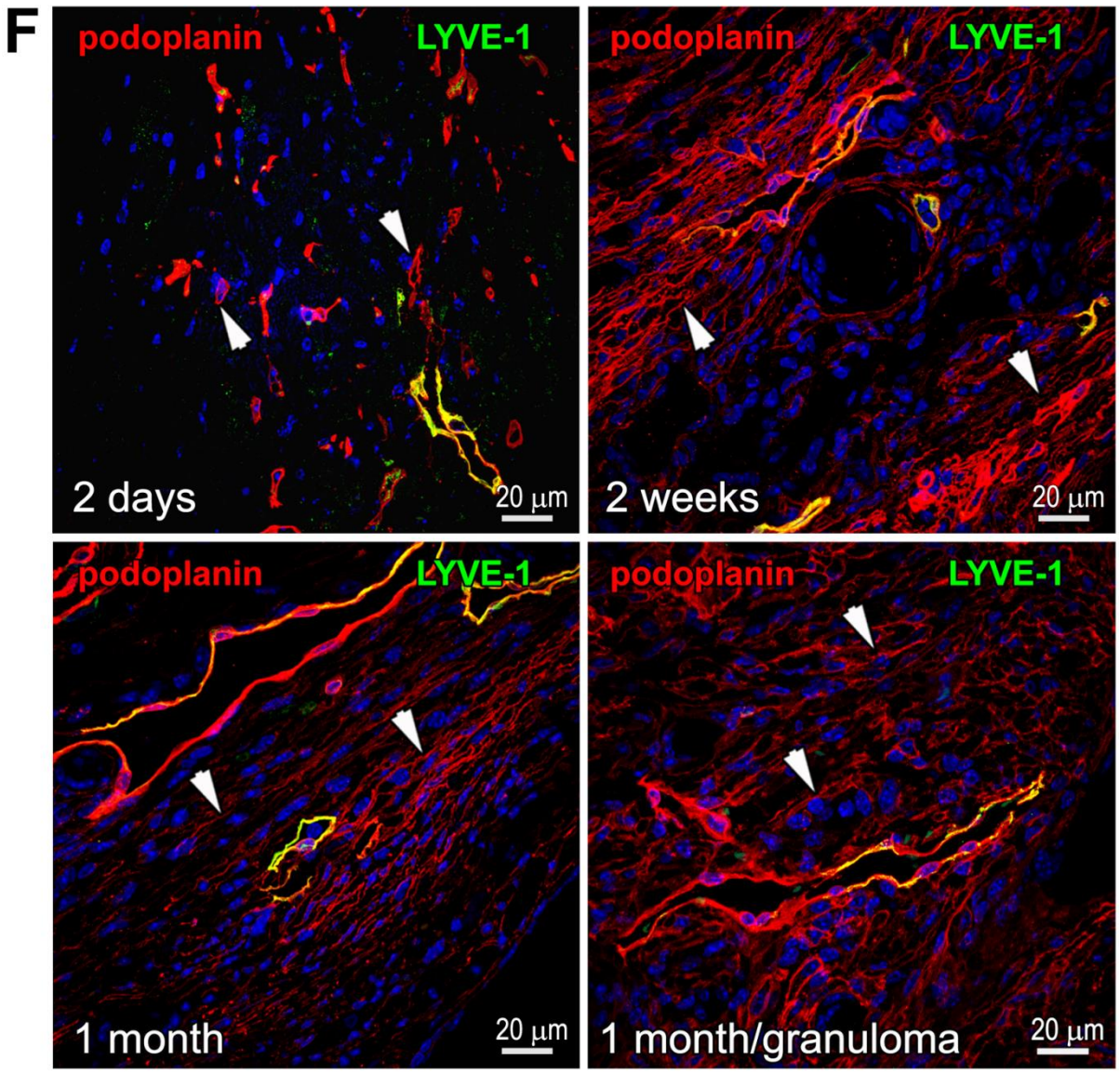
F
podoplanin
LYVE-1
2 days
20 μm
podoplanin
LYVE-1
2 weeks
20 μm
podoplanin
LYVE-1
1 month
20 μm
podoplanin
LYVE-1
1 month/granuloma
20 μm

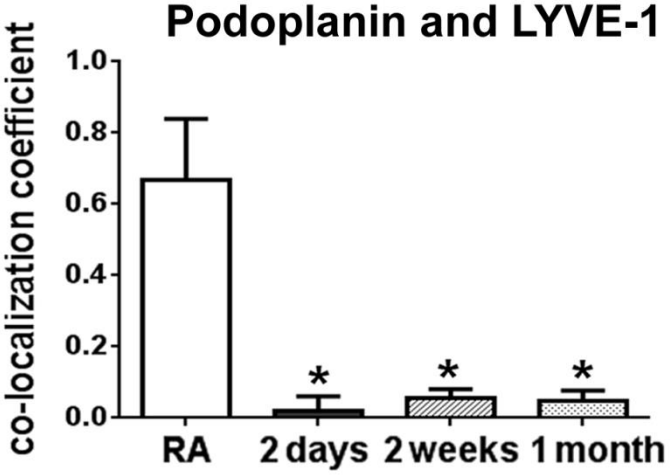
Podoplanin and LYVE-1
co-localization coefficient
1.0
0.8
0.6
0.4
0.2
0.0
*
*
*
RA
2 days
2 weeks
1 month

Fig 1 (cont.)

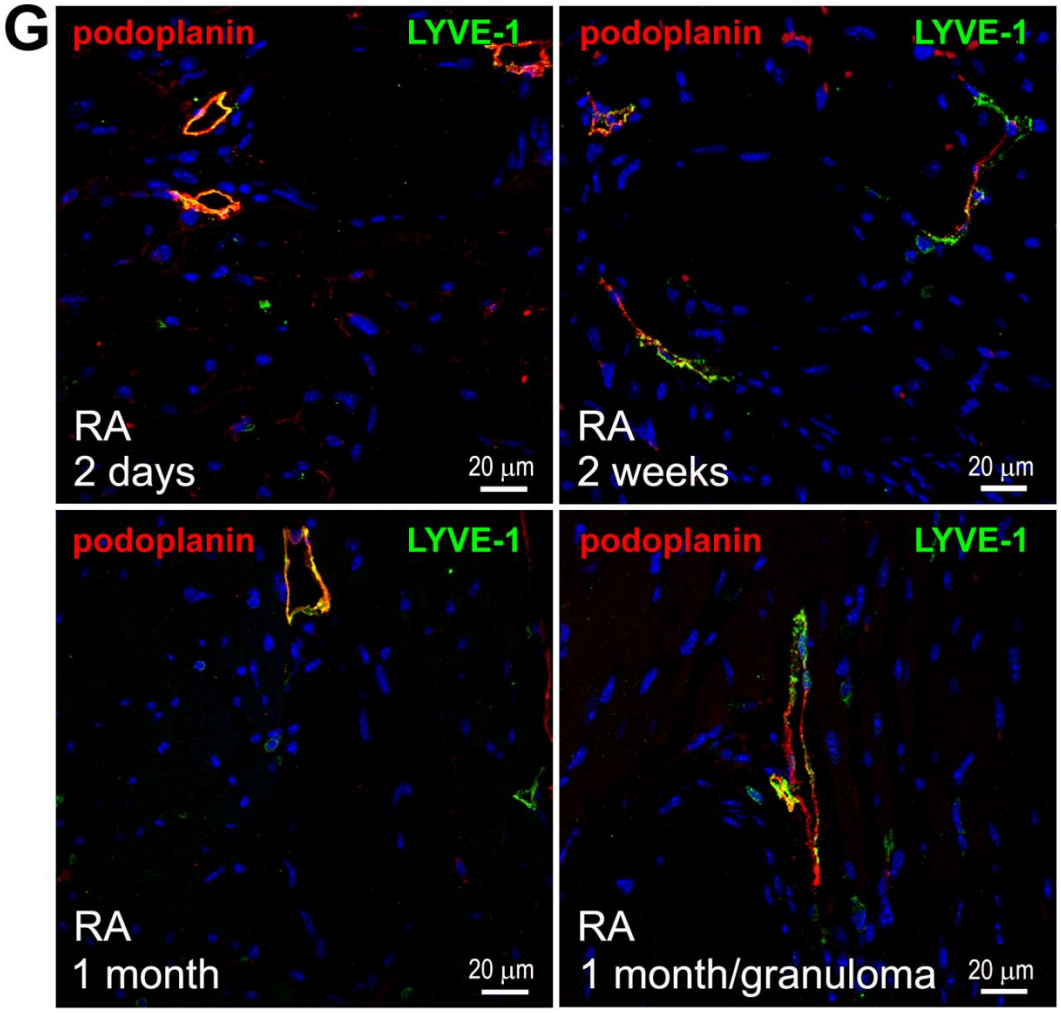
G
podoplanin
LYVE-1
RA
2 days
20 μm
podoplanin
LYVE-1
RA
2 weeks
20 μm
podoplanin
LYVE-1
RA
1 month
20 μm
podoplanin
LYVE-1
RA
1 month/granuloma
20 μm

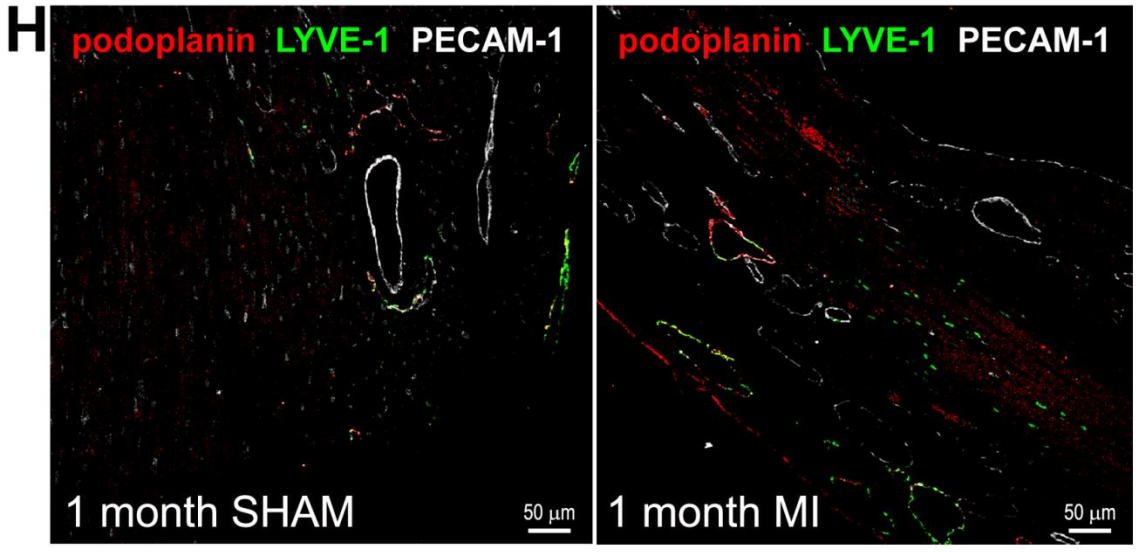
H
podoplanin
LYVE-1
PECAM-1
1 month SHAM
50 μm
podoplanin
LYVE-1
PECAM-1
1 month MI
50 μm

Fig 1 (cont.)

Fig 1. Podoplanin expression in the infarcted and non-infarcted hearts. (**A**) Thin cardiac sections from non-operated (NO) mice and animals at the indicated times after MI were indirectly immunolabeled with podoplanin (red). Nuclei, blue. Areas neighboring the necrotic myocardium are shown for the infarcted hearts. Note the increase in podoplanin immunoreactivity at 2 days after MI. (**B**) Quantitative image analysis of the changes in podoplanin immunolabeling in thin cardiac sections in the infarcted myocardium at the indicated times after MI. RA, remote area. Data represent mean and SD of % area stained with podoplanin; n=6-10 image fields per group. By one-way ANOVA, *P < 0.02 for 2 days vs. RA, 2 weeks, or 1 month; **P = 0.0017 for 2 days vs. <1 day; ***P < 0.0001 for RA vs. 2 weeks or 1 month and for <1 day vs. 2 weeks or 1 month; ns, non-significant for < 1 day vs RA, and for 1 month vs. 2 weeks. (**C**) Flow-cytometry analysis of the frequency of podoplanin-positive cells in the hearts of non-operated (NO), and the sham-operated (SHAM) and infarcted (MI) mice at 2 days after surgery. Graph depicting data from individual animals (upper row) and representative flow-cytometry scatterplots (lower row) are shown. n=10-20 animals per treatment; mean values are represented by the red line on the graph. By one-way ANOVA, *P < 0.0001 for MI vs. SHAM or NO; ns, not significant for SHAM vs NO. (**D**-**H**) Thin cardiac sections obtained at the indicated times after MI were indirectly immunolabeled with antibodies that recognize podoplanin (**D**-**H**; red), LYVE-1 (**E**-**H**; green), and PECAM-1 (**E** and **H**; grey). Nuclei, blue. Corresponding single channel images (**E**-**H**) are included in S2 Fig 1. Areas affected by ischemia are depicted in **D**-**F**; Remote area (RA) is shown in **G**. SHAM, sham-operated in **H**. In **F**, the arrowheads in representative images (upper panels) point to the examples of podoplanin-positive LYVE-1 negative cells. Note the accumulation of LYVE-1 positive CLVs (red and green) as well as podoplanin-expressing cells lacking the LYVE-1 labeling (red only) in the infarcted myocardium

as opposed to RA and SHAM. Quantitative image analysis (lower panel) of the podoplanin co-labeling with LYVE-1 is included in the graph. Data represent mean and SD of the co-localization coefficient measured at indicated times after MI and the remote area (RA); n=5-10 image fields per group. By one-way ANOVA, *P < 0.0001 for RA vs. 2 days, 2 weeks or 1 month; no significant changes between 2 days and 2 weeks and 1 month.

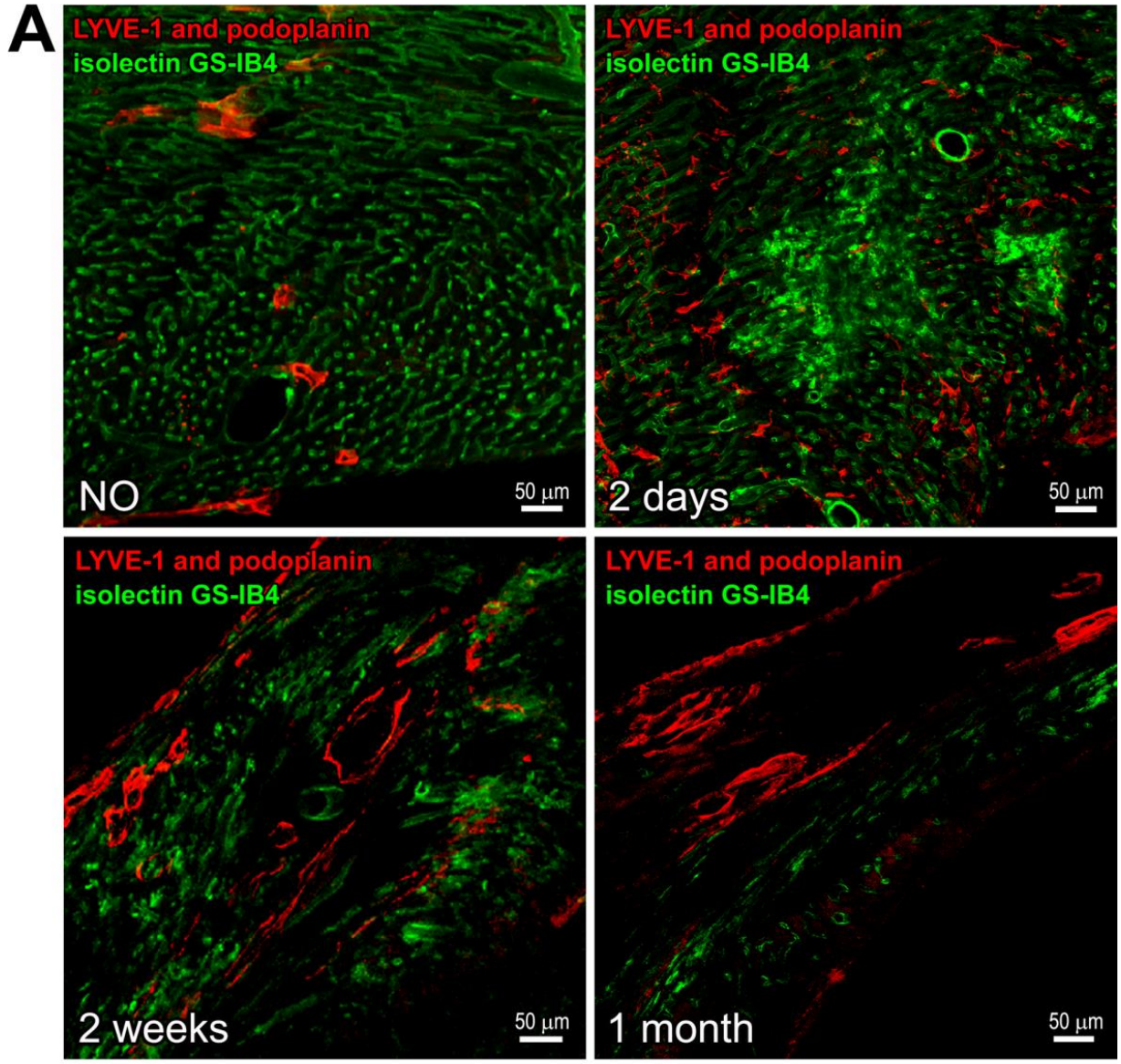

Fig 2

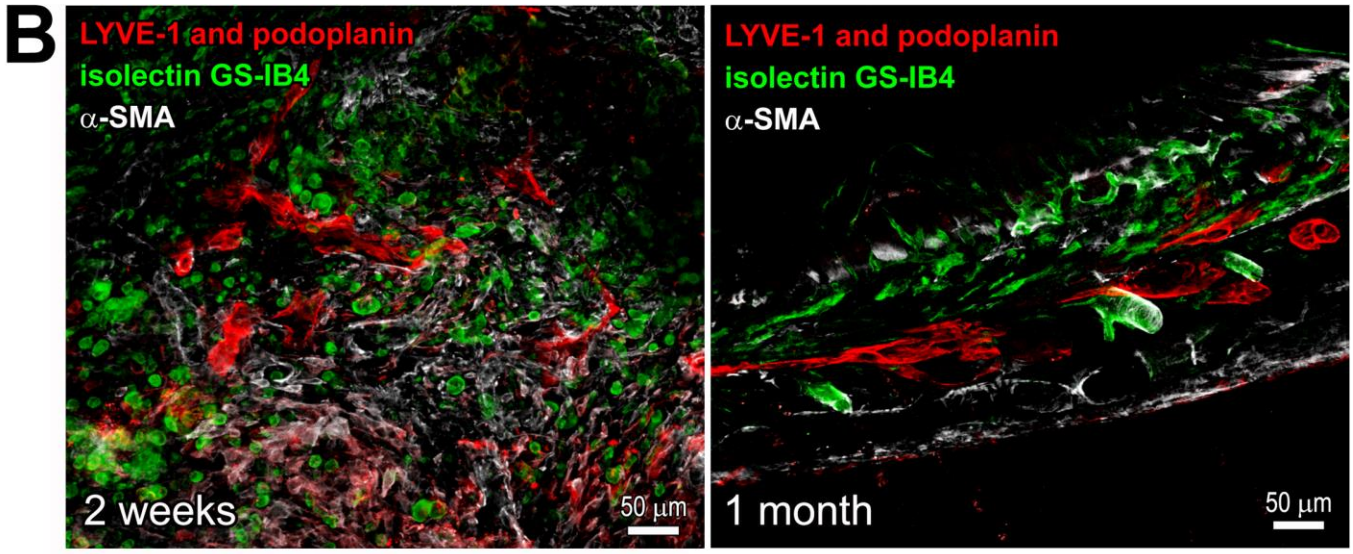

Fig 2 (cont.)

Fig 2. CLVs in the forming and mature scar. Thick cardiac sections were indirectly immunolabeled with the mix of LYVE-1 and podoplanin antibodies (**A**,**B**; red) and α-SMA antibody (**B**; grey), and co-stained with isolectin GS-IB4 (**A**,**B**; green). NO, non-operated. Time after MI is indicated. Corresponding single channel images are included in S2 Fig 2. CLVs are recognized by the staining with podoplanin and LYVE-1. In **A**, note the changes in the abundance and distribution of the vessels and LYVE-1 and podoplanin immunolabeled cells at different stages of infarct healing. In **B**, α-SMA-positive cells are apparent in the fibrotic tissue and the coating of large vessels.

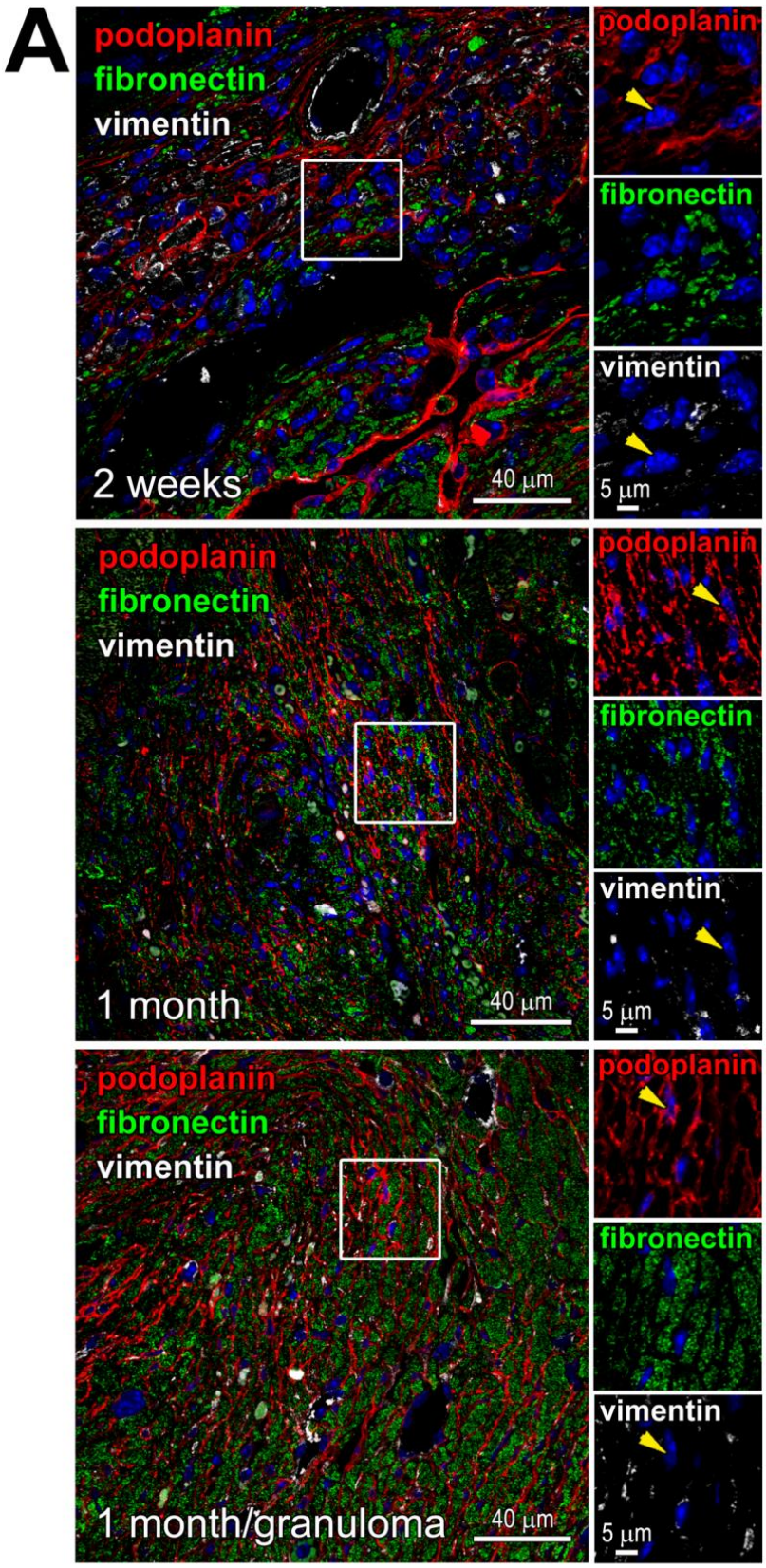
A
podoplanin
fibronectin
vimentin
2 weeks
40 μm
podoplanin
fibronectin
vimentin
5 μm
podoplanin
fibronectin
vimentin
1 month
40 μm
podoplanin
fibronectin
vimentin
5 μm
podoplanin
fibronectin
vimentin
1 month/granuloma
40 μm
podoplanin
fibronectin
vimentin
5 μm

Fig 3

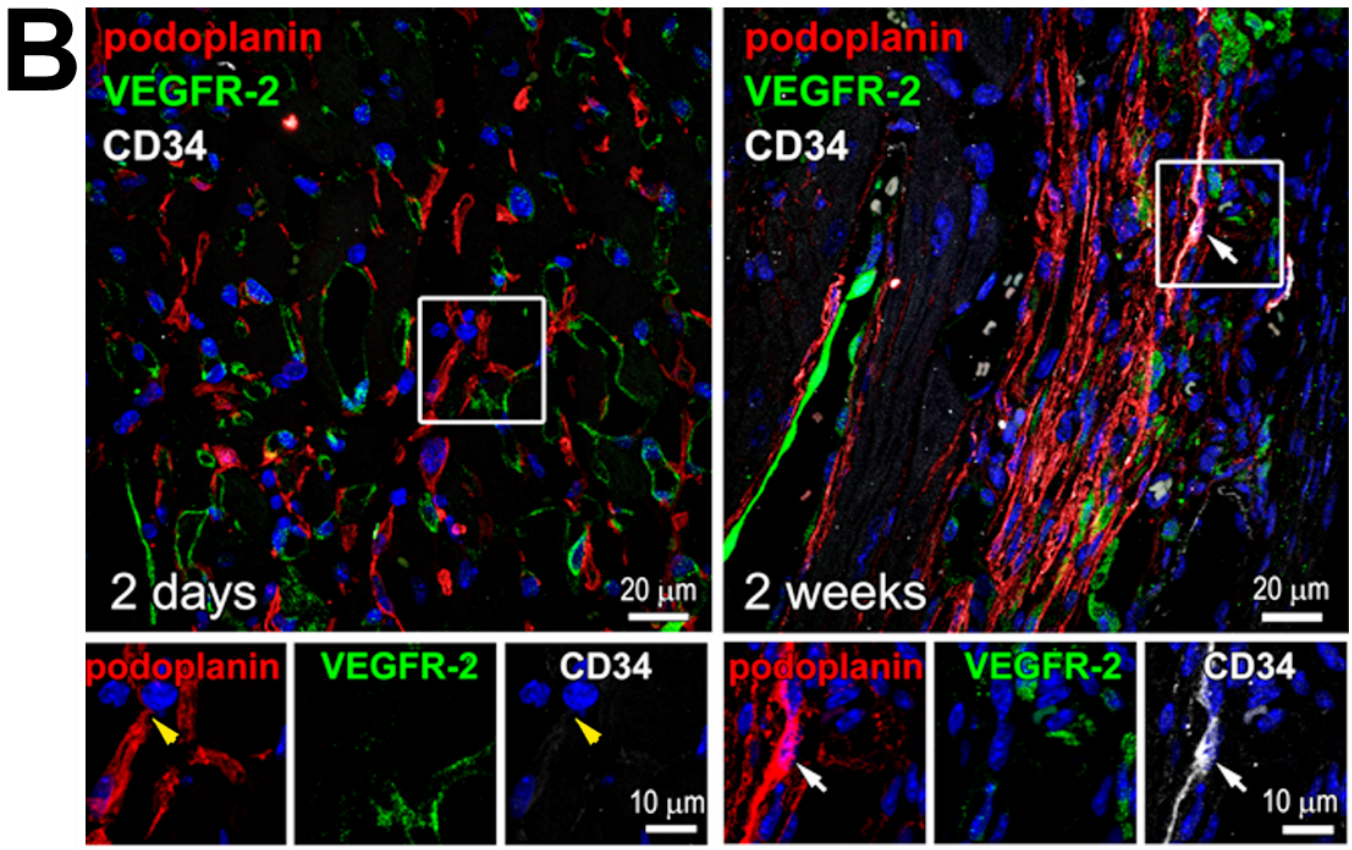
B
podoplanin
VEGFR-2
CD34
2 days
20 µm
podoplanin
VEGFR-2
CD34
2 weeks
20 µm
podoplanin
VEGFR-2
CD34
10 µm
podoplanin
VEGFR-2
CD34
10 µm

Fig 3 (cont.)

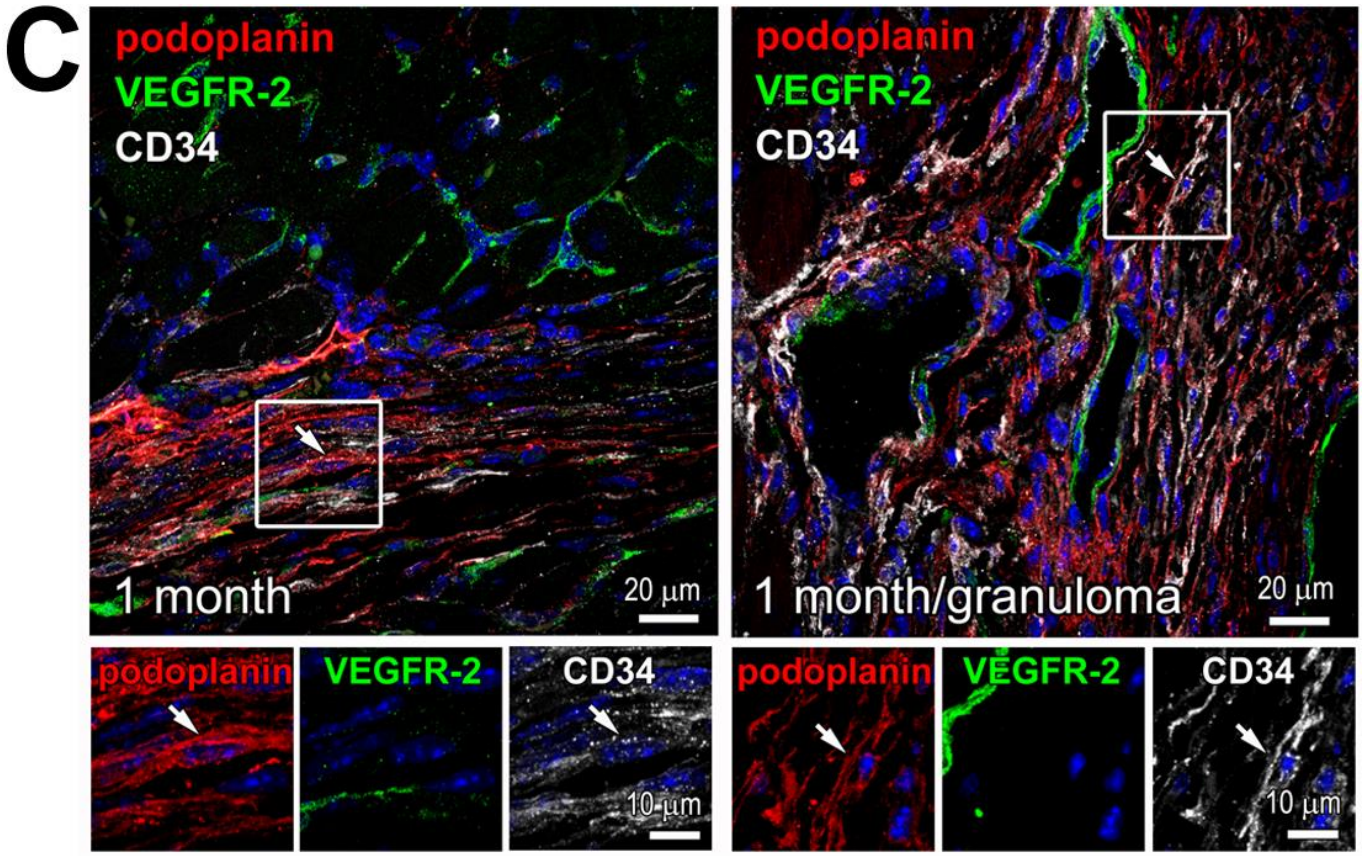
C
podoplanin
VEGFR-2
CD34
1 month
20 μm
podoplanin
VEGFR-2
CD34
1 month/granuloma
20 μm
podoplanin
VEGFR-2
CD34
10 μm
podoplanin
VEGFR-2
CD34
10 μm

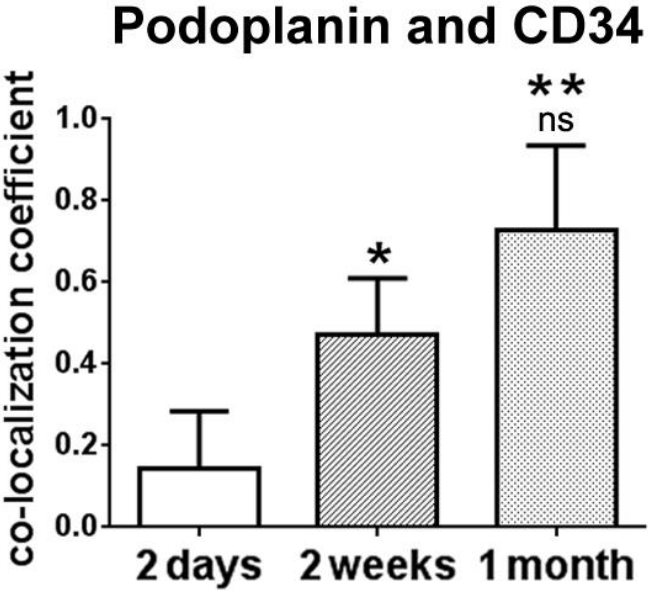
Podoplanin and CD34
co-localization coefficient
1.0
0.8
0.6
0.4
0.2
0.0
*
**
ns
2 days
2 weeks
1 month

Fig 3 (cont.)

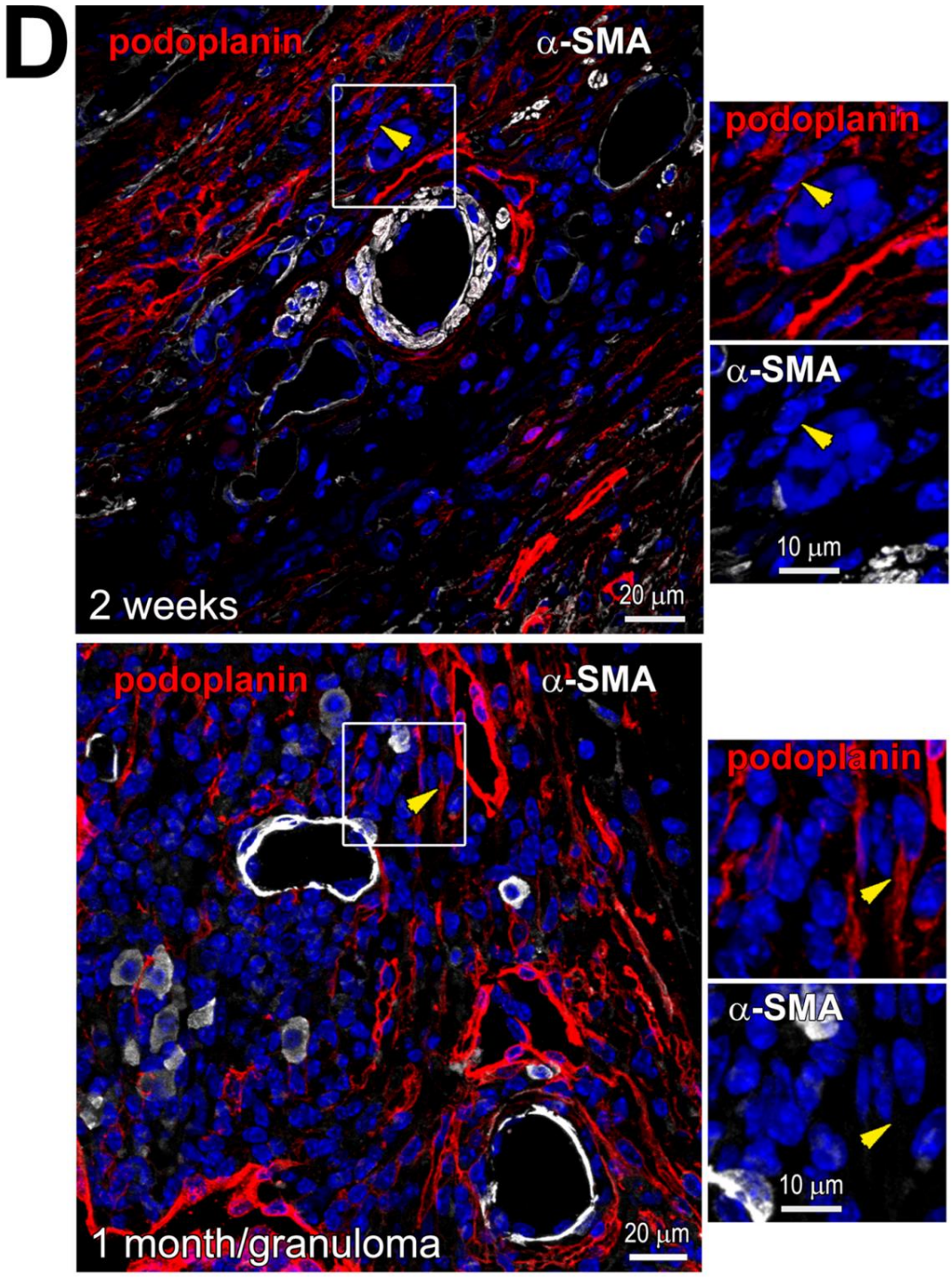
D
podoplanin
α-SMA
2 weeks
20 μm
podoplanin
α-SMA
10 μm
podoplanin
α-SMA
1 month/granuloma
20 μm
podoplanin
α-SMA
10 μm

Fig 3 (cont.)

Fig 3. Phenotype of podoplanin-positive cells in the fibrotic tissue. Thin cardiac sections were indirectly immunolabeled with antibodies that recognize podoplanin (red) and either fibronectin and vimentin (**A**; green and grey, respectively), VEGFR-2 and CD34 (**B** and **C**; green and grey, respectively), or α-SMA (**D**; grey). Nuclei, blue. Time after MI is indicated. Areas in rectangles are shown at higher magnifications in the adjacent images for each color channel. Note that vimentin (**A**) or α-SMA (**D**) labeling is rarely detectable in podoplanin-expressing cells (examples are pointed by yellow arrowheads). In **B** and **C**, the podoplanin-presenting cells show minimal VEGFR-2 labeling. At 2 days after MI, the podoplanin-bearing cells mostly do not co-stain with CD34 (exemplified by yellow arrowheads). Starting 2 weeks after MI, the CD34 staining is present in irregular capillary-like structures (examples are indicated by white arrows). In **C**, quantitative image analysis demonstrating changes in the podoplanin co-labeling with CD34 at indicated times after MI is included in the graph (lower panel). Data represent mean and SD of the co-localization coefficient; n=5-6 image fields per group. By one-way ANOVA, *$P < 0.02$ for 2 weeks vs. 2 days; **$P < 0.0001$ for 1 month vs. 2 days; ns, not-significant 1 month vs. 2 weeks.

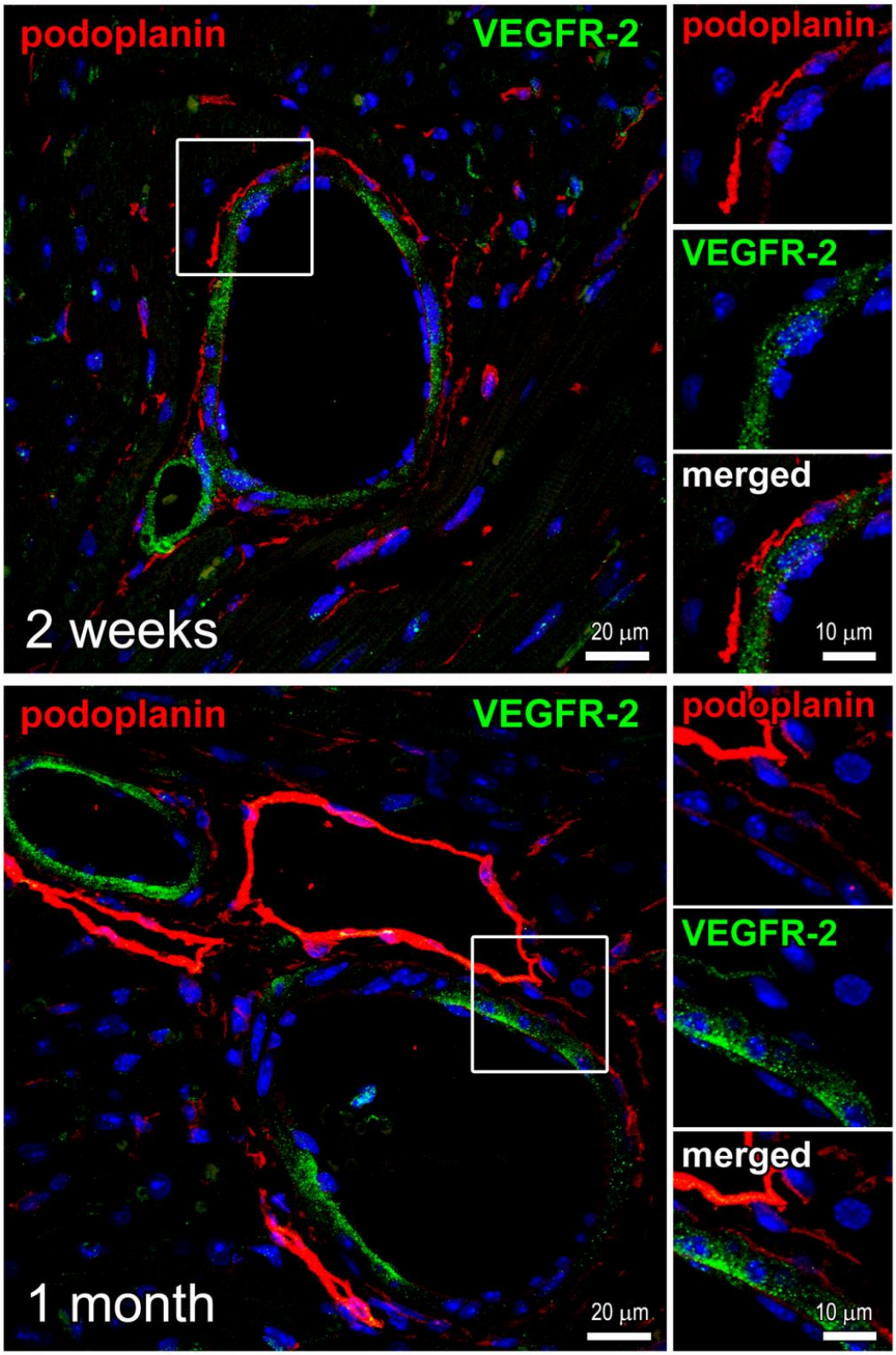
podoplanin
VEGFR-2
2 weeks
20 μm
podoplanin
VEGFR-2
merged
10 μm
podoplanin
VEGFR-2
1 month
20 μm
podoplanin
VEGFR-2
merged
10 μm

Fig 4

Fig 4. Perivascular localization of the podoplanin-expressing cells. Thin cardiac sections were indirectly immunolabeled with podoplanin (red) and VEGFR-2 (green) antibodies. Nuclei, blue. Time after MI is indicated. Areas in rectangles are shown at a higher magnification in the adjacent images for each color channel and merged. Note the podoplanin-positive cells encircling the VEGFR-2-labeled BVs.

Podoplanin-positive cell population manifest a variable expression of the lymphatic endothelial cell markers Prox-1 and VEGFR-3 in the heart

In order to assess the lymphangiogenic potential of the podoplanin-bearing cells in the infarcted myocardium, we evaluated the presence of a lymphatic endothelial cell-specific transcription factor Prox-1 [87] [88] in this population. We noted that along with the expected localization in the nuclei of the endothelium of CLVs (Fig 5A-5C; arrows), Prox-1 staining was detectable also in the podoplanin-positive cells not organized into vessel-like structures (Fig 5A-5C; white arrowheads) at different times after MI. Quantitatively, as detected by flow-cytometry the frequency of Prox-1 expression in podoplanin-positive cells was diminished at 2 days after MI as compared to sham-operated hearts (S2, Fig 3 Panel B; Prox-1). These data are consistent with the findings on a lower presence of LYVE-1 and PECAM-1 in the podoplanin-expressing cell cohorts, thus validating the theory that a large proportion of podoplanin-bearing cells appearing acutely after injury do not possess differentiated lymphatic endothelial phenotype.

The occurrence of Prox-1 in the infarcted myocardium was generally high at the later stages of wound repair (Fig 5B, 5C; 2 weeks and 1 month) confirming that the neo lymphangiogenesis is required for the scar maturation and the resolution of inflammation. However, there was no direct correlation between the incidences of podoplanin and Prox-1 in these cell cohorts (Fig 5B

and 5C; yellow arrowheads). Despite a major rise in the abundance of podoplanin-presenting cells in the scarred tissue (Fig 1B and 1D-1F; 2 days versus 2 weeks and 1 month), we observed that the percentage of podoplanin-labeled Prox-1-positive cells in the injured area remained similar at all the time points after MI (Fig 5C; graph), supporting the notion that many of the newly-appearing podoplanin-expressing cells in the fibrotic area are Prox-1 negative and that Prox-1 is closely correlated only with the lymphatic lineage.

VEGFR-3 is another characteristic marker of the lymphatic endothelial cell activation and differentiation [88, 89]. The expression of the VEGFR3 was discontinuous compared with constant presence of LYVE-1 in the CLVs (Fig 5E-5G; white arrows) of the infarcted myocardium, and only occasionally found in the podoplanin-positive cells populating the infarct BZ shortly after MI (Fig 5E and 5G; 2 days). By flow-cytometry, the frequency of VEGFR-3 co-staining with podoplanin was not affected by acute myocardial injury as compared to non-operated and sham-operated animals (S2, Fig 3 Panel B). The level of VEGFR-3 immunolabeling was augmented at the later phases of infarct healing at 2 weeks and 1 month, and the co-staining of VEGFR-3 with podoplanin was intensified at these stages (Fig 5F and 5G; white arrowheads). These data suggest that VEGFR3 is highly expressed in the CLVs cells only when the lymphatic vessel is mature and well formed, this theory is confirmed quantitatively: more than a 5-fold elevation in the co-localization of podoplanin with VEGFR-3 was found at the time of scar formation and maturation relative to 2 days after MI (Fig 5G; graph). Yet, VEGFR-3-expression was frequently lacking in podoplanin-presenting cells (Fig 5F and 5G; yellow arrowheads).

Our analysis, along with the quantitative data, show that the appearance of Prox-1 or VEGFR-3 in a subset of podoplanin-expressing cells suggests their commitment to the LECs fate.

At the same time, the absence of lymphendothelial epitopes in a large group of podoplanin-positive cells might signify an alternative differentiation pathway, or, most importantly that different type of cells that are recruited for the granulation and the scar formation after MI express podoplanin in response to the inflammation similarly to cancer cells; it is very important to keep in mind that podoplanin is involved in cell migration and the receptor C-LEC2 is highly expressed in immune cells.

In contrast to VEGFR-3, the presence of VEGFR-2, a very well-known marker of endothelial cells, was rarely detected in podoplanin-bearing interstitial cells and CLVs in the infarcted heart (Fig 3B, 3C and Fig 4). This is in agreement with previous reports demonstrating that in the mouse, VEGFR-2 is restricted to the activated blood endothelium and not to the lymphatic ones [90].

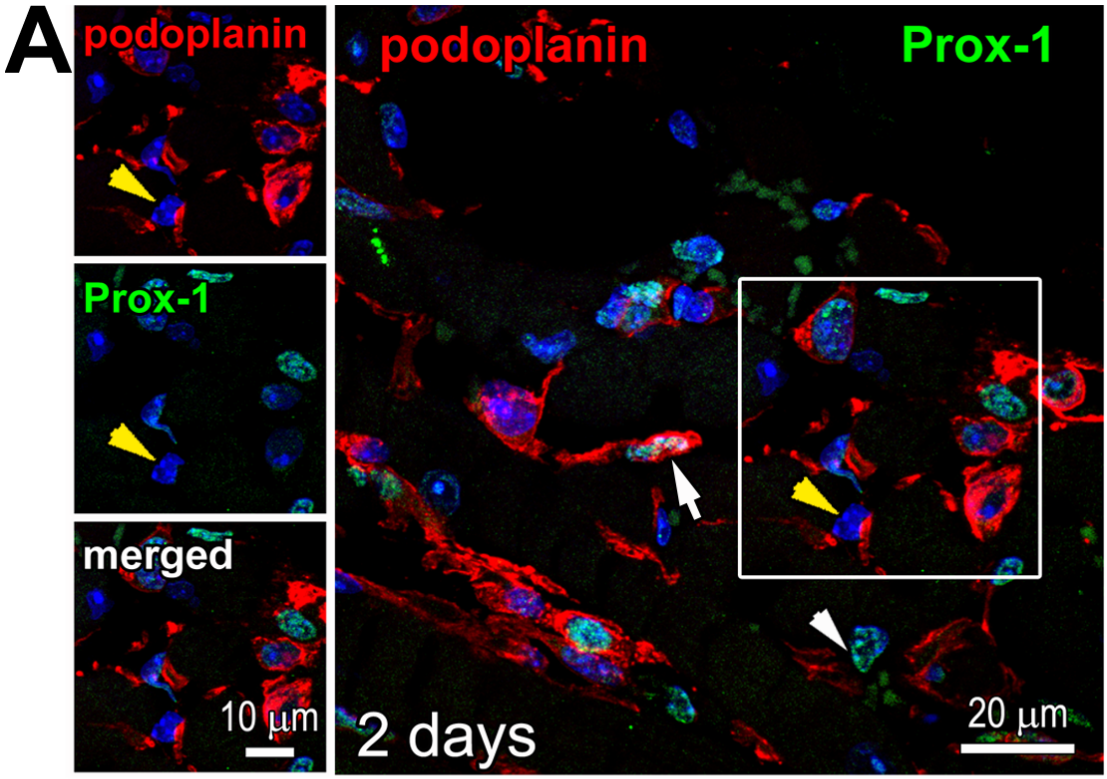

Fig 5

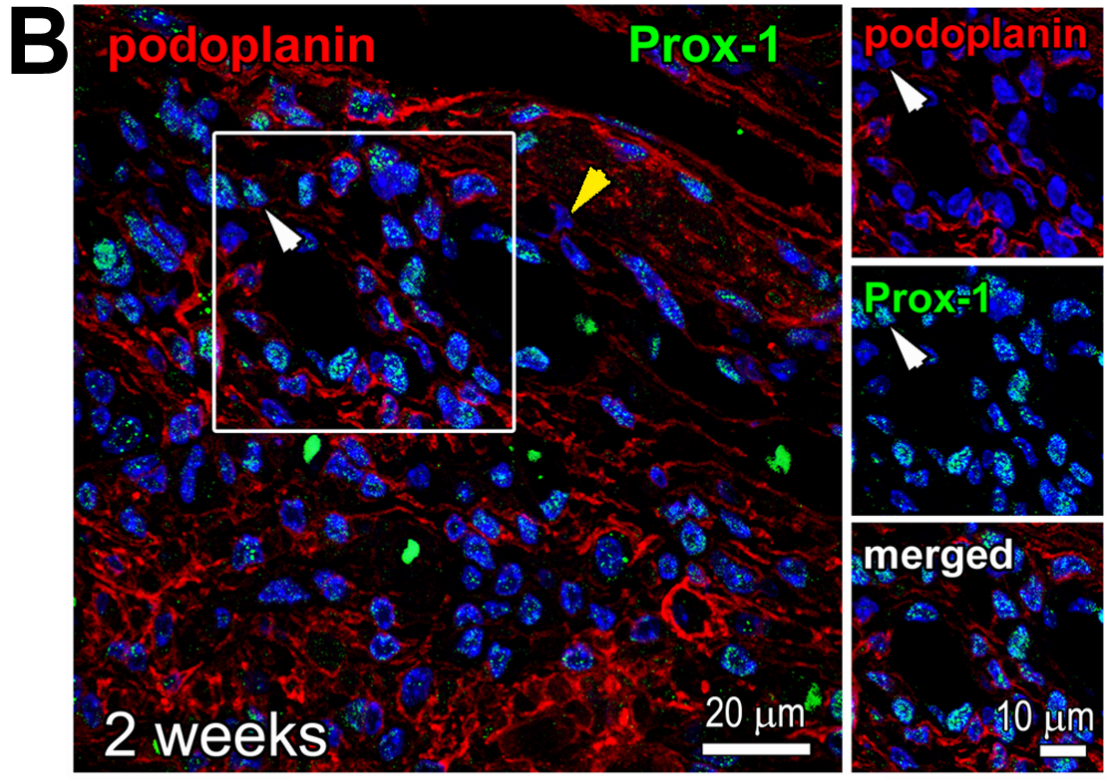

Fig 5 (cont.)

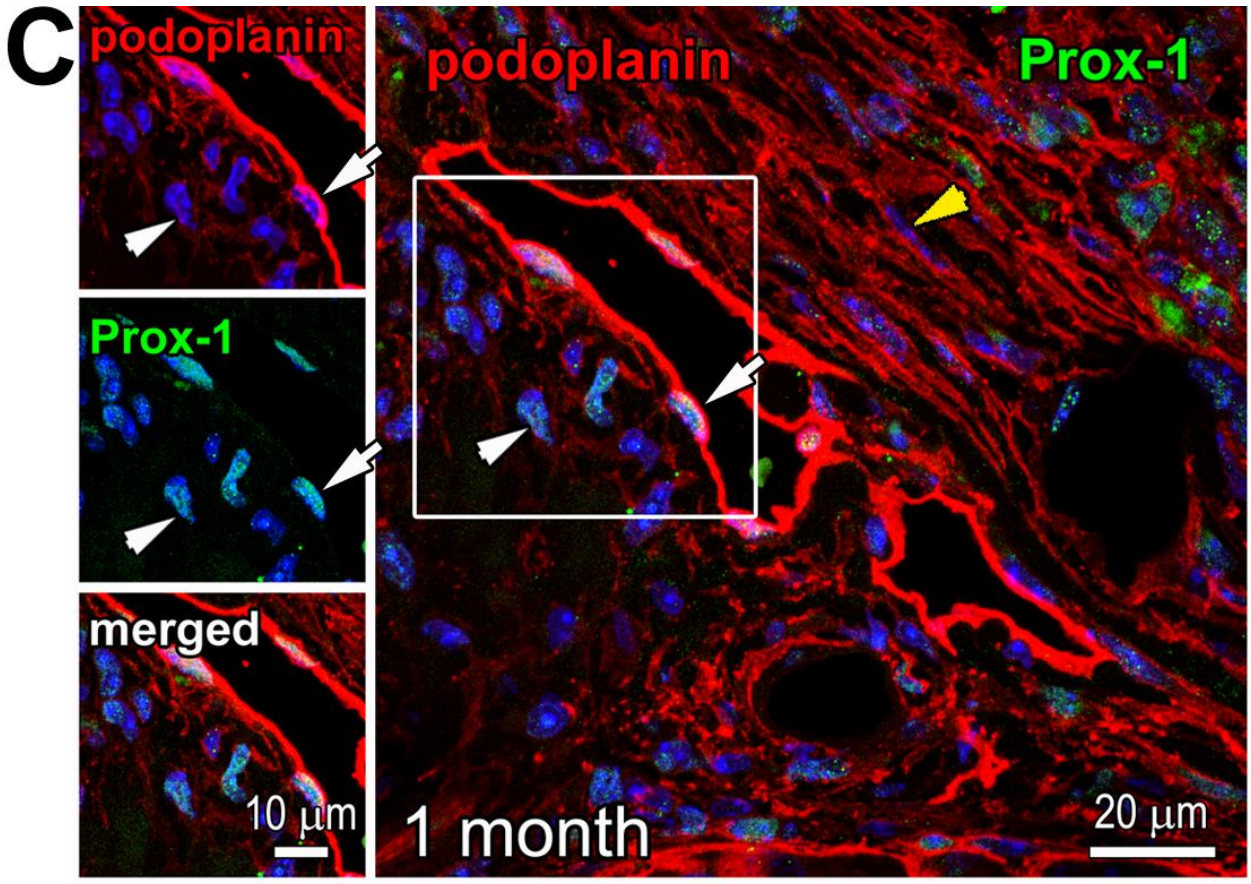
C
podoplanin
Prox-1
merged
10 μm
podoplanin
Prox-1
1 month
20 μm

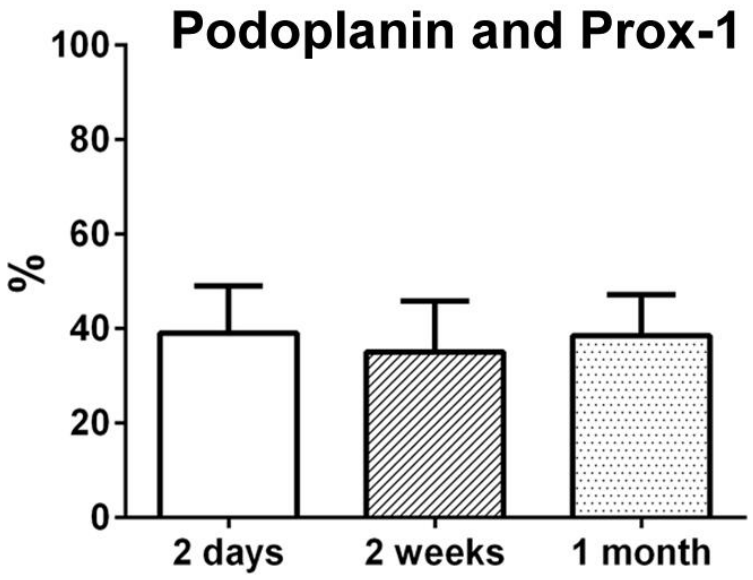
Podoplanin and Prox-1
100
80
60
40
20
0
%
2 days
2 weeks
1 month

Fig 5 (cont.)

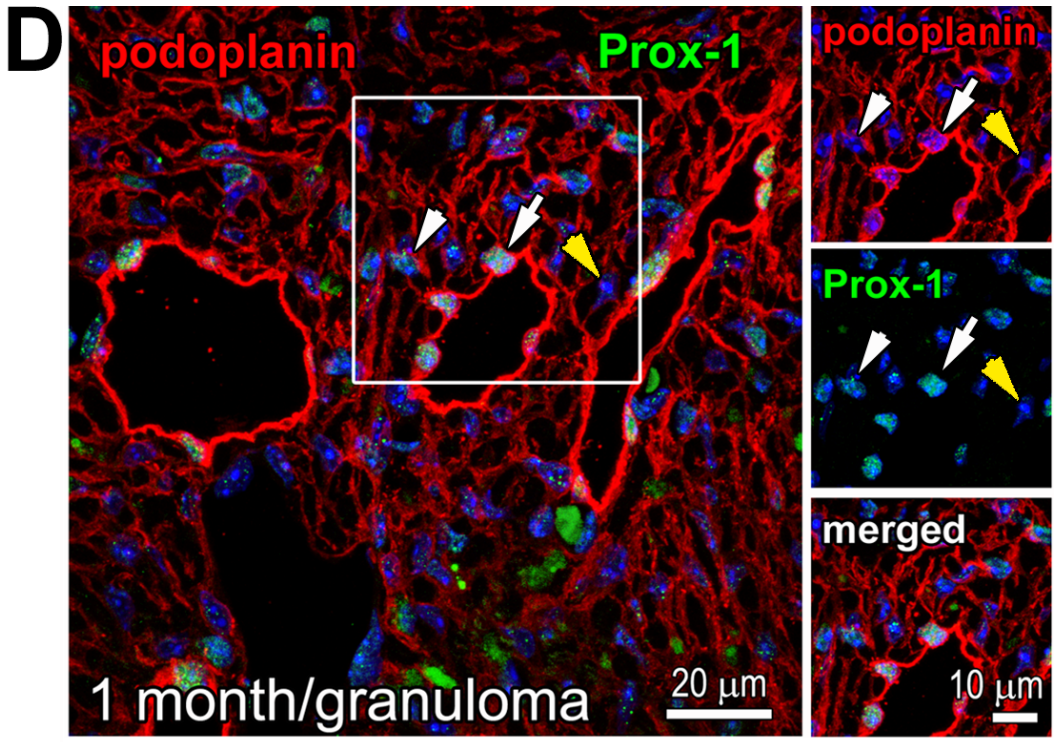

Fig 5 (cont.)

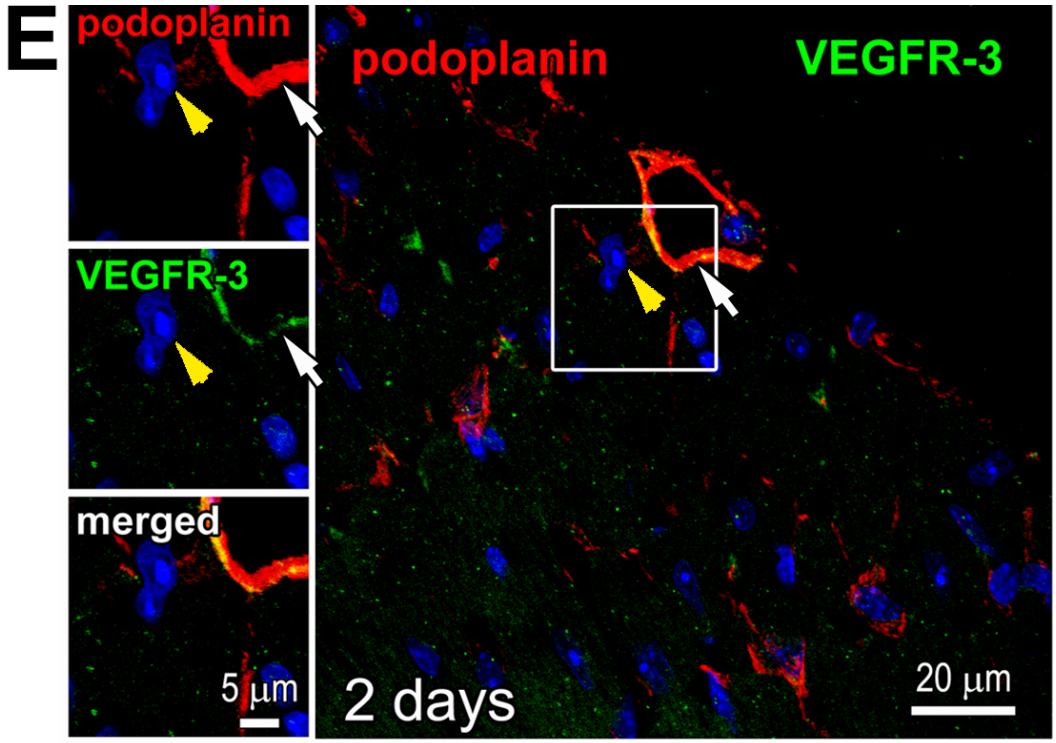

Fig 5 (cont.)

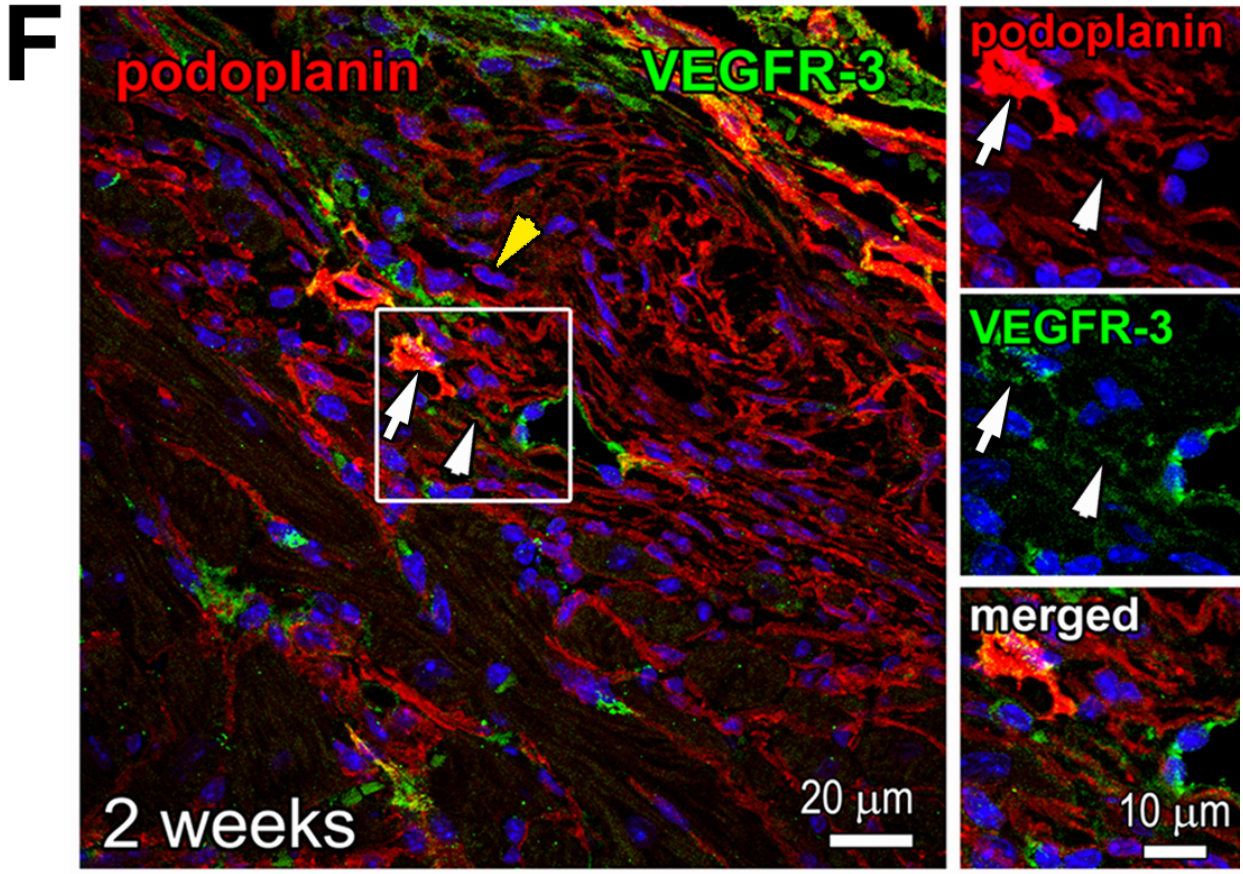
F
podoplanin
VEGFR-3
2 weeks
20 μm
podoplanin
VEGFR-3
merged
10 μm

Fig 5 (cont.)

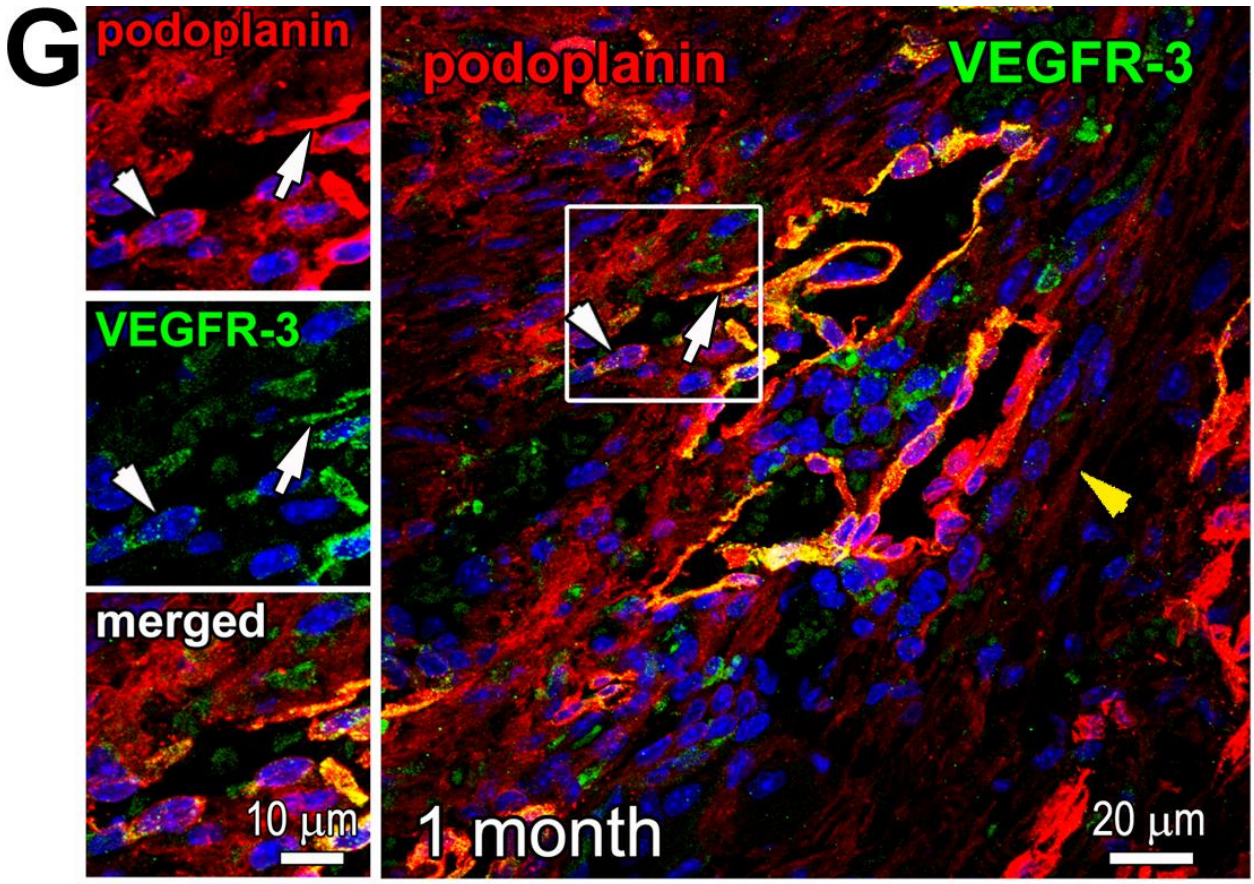
G
podoplanin
VEGFR-3
merged
10 μm
podoplanin
VEGFR-3
1 month
20 μm

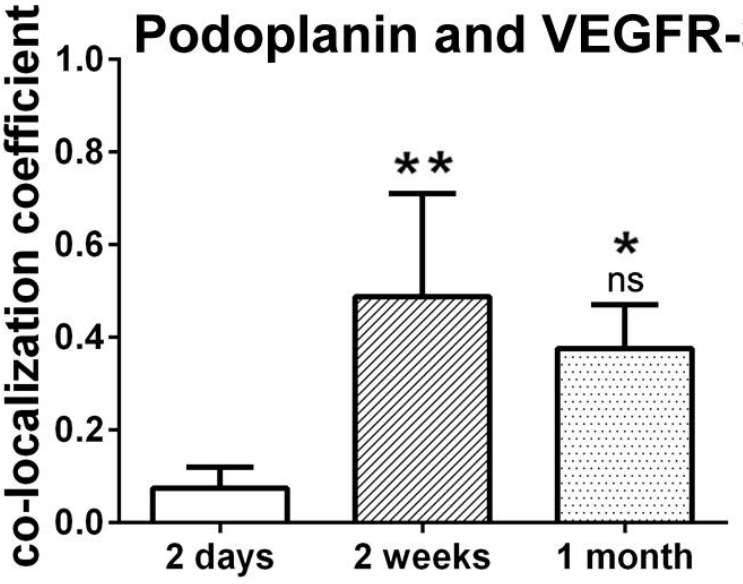
Podoplanin and VEGFR-3
co-localization coefficient
1.0
0.8
0.6
0.4
0.2
0.0
**
*
ns
2 days
2 weeks
1 month

Fig 5 (cont.)

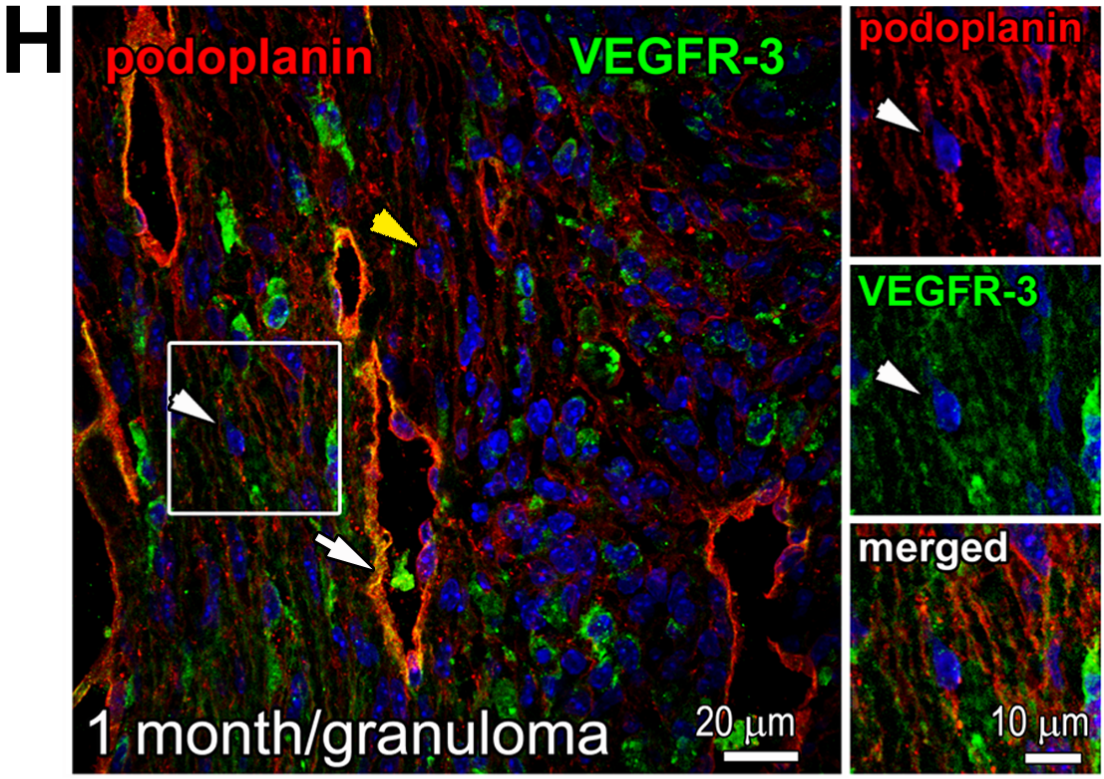

Fig 5 (cont.)

Fig 5. Variable expression of Prox-1 and VEGFR-3 in podoplanin-positive cells in the infarcted heart. Thin cardiac sections were indirectly immunolabeled with antibodies that recognize podoplanin (red) and either Prox-1 (**A-D**; green) or VEGFR-3 (**E-H**; green). Nuclei, blue. Time after MI is indicated. Areas in rectangles are shown in the adjacent images for each color channel and merged. White arrows indicate examples of Prox-1 or VEGFR-3 labeling in the lymphatic endothelial cells of CLVs, and white arrowheads point to the examples of Prox-1 or VEGFR-3 staining in podoplanin-expressing interstitial cells. Yellow arrowheads exemplify instances of podoplanin-positive cells in which Prox-1 or VEGFR-3 expression was undetectable. Note the consistent detection of Prox-1 and VEGFR-3 in CLVs, and the heterogeneity in Prox-1 and VEGFR-3 labeling intensity in podoplanin-stained cells not

organized into vessels. In **C**, quantitative image analysis (graph, lower panel) of the fraction of podoplanin-expressing cells co-labeled with Prox-1 is shown at indicated times after MI. Data represent mean and SD of the % double-positive cells out of all podoplanin-positive cells in the imaging field; n=6-9 image fields per group. By one-way ANOVA, no significant changes between were groups. In **G**, quantitative image analysis (graph, lower panel) of the podoplanin co-labeling with VEGFR-3 is shown. Data represent mean and SD of the co-localization coefficient measured at indicated times after MI; n=4-7 image fields per group. By one-way ANOVA, **P = 0.002 for 2 weeks vs. 2 days; *P = 0.009 for 1 month vs. 2 days; ns, not-significant 1 month vs. 2 weeks.

Podoplanin-positive cell population show a time dependent positivity to mesenchymal markers PDGFRα and PDGFRβ

In the infarcted myocardium, the heightened expression of PDGFRα, PDGFRβ and their PDGF ligands coincides with angiogenesis and inflammatory and fibrogenic responses, indicating a role in wound repair processes [91] [92]. We found, by flow-cytometry analysis of all of the small cardiac cells isolated from acutely infarcted hearts, that the podoplanin-presenting cells in the infarcted heart were distinctly PDGFRα-positive (S2, Fig 4). Those data were confirmed by the immunohistochemistry assessment of myocardium at the different times after MI (Fig 6A-6C; white arrowheads, and Fig 6C; graph). Since PDGFRα expression is associated with the properties of immature mesenchymal cells [93, 94], the concordance of PDGFRα and podoplanin staining suggests that cardiac podoplanin-positive cells contain a population with progenitor cell capabilities.

Similarly to the PDGFRα, the PDGFRβ is a marker of pericytes and perivascular progenitor cells cells with endothelial and fibrogenic potential [95], but, unlike PDGFRα, the presence of PDGFRβ was infrequent in the podoplanin-presenting cells early after MI (Fig 6E; 2 days, yellow arrowheads, Fig 6G; graph,). However, we noticed that the level of PDGFRβ expression and co-staining with podoplanin were strongly elevated at the later stages of infarct healing and in the mature scar (Fig 6F and 6G; 2 weeks and 1 month, white arrowheads), reaching approximately 100% co-labeling of podoplanin-positive cells with PDGFRβ (Fig 6E, graph; 2 weeks and 1 month).

Interestingly, in the infarcted myocardium, PDGFRβ labeling was abundant not only in the CLVs but also in the BVs (Fig 6I). A recent lineage-tracing analysis shows that PDGFRβ-positive endothelium contributes to the CLV formation during embryonal development [96], implying that upon severe tissue injury, blood endothelial cells acquire the lymphatic endothelial cell phenotype. Such endothelial cell plasticity has been previously described in cultured cells and for the tumor vasculature [97, 98]. We report, confirming the literature, that Prox-1 is expressed in the nuclei of podoplanin-negative cells of the BVs (Fig 6I; arrows).

Although the expression of PDGFR α or β is often related to the fibrogenic behavior and associated with the myofibroblast phenotype of cells [93] [99] [100], we found that the podoplanin-positive populations in the scar occasionally exhibited fibroblast markers vimentin (Fig 3A; yellow arrowheads) or a myofibroblast protein α-SMA (Fig 3D; yellow arrowheads). This data suggests that the podoplanin is not a marker of maturing fibrogenic cells.

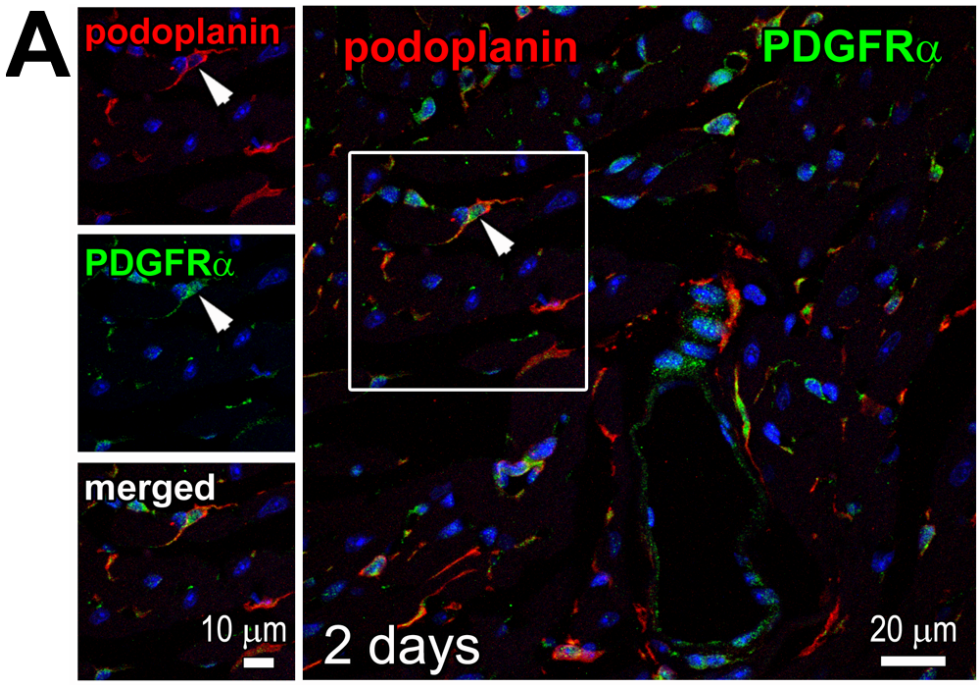

Fig 6

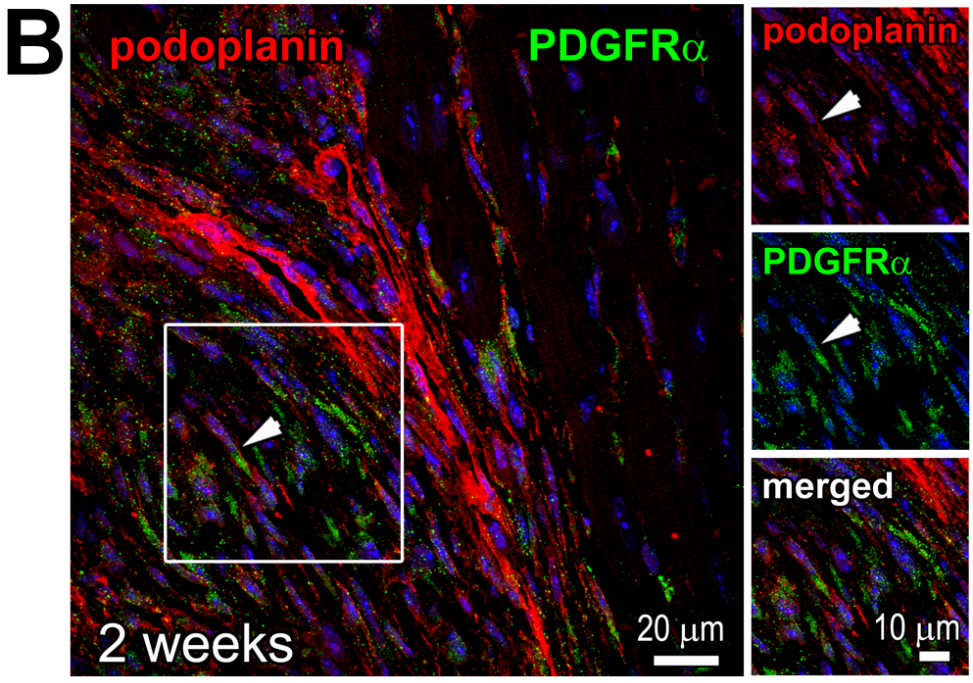

Fig 6 (cont.)

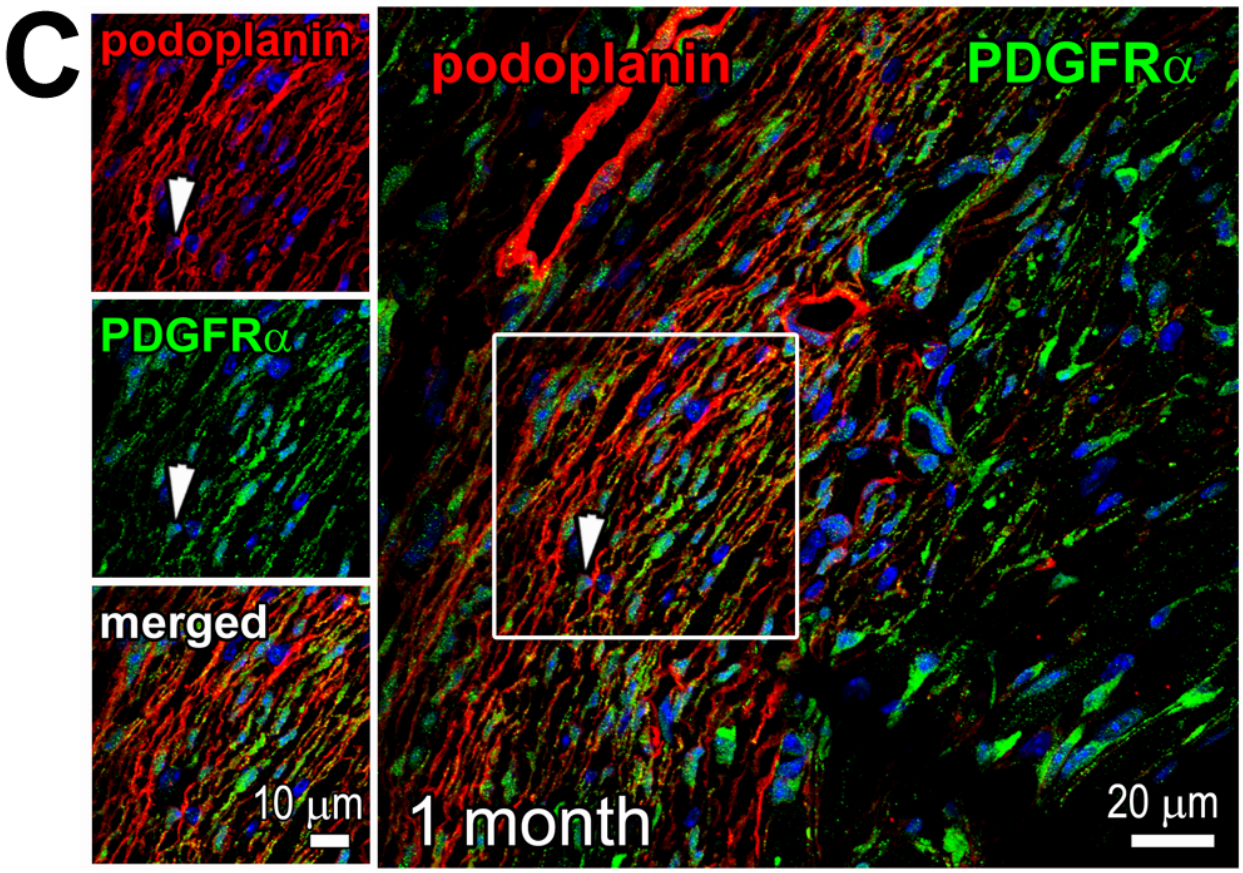
C
podoplanin
PDGFRα
merged
10 μm
podoplanin
PDGFRα
1 month
20 μm

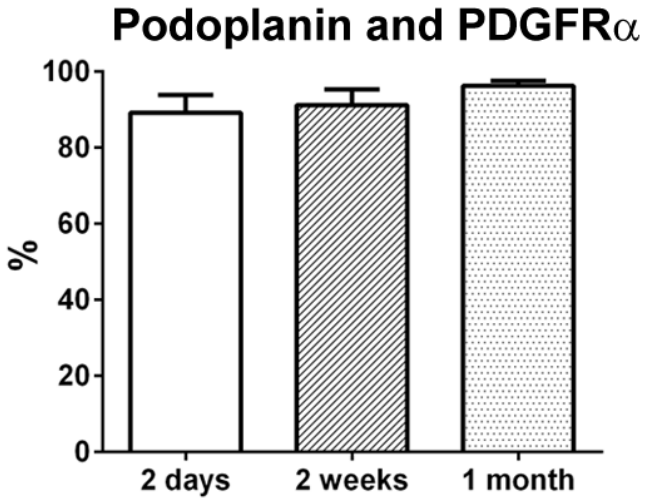
Podoplanin and PDGFRα
100
80
60
40
20
0
%
2 days
2 weeks
1 month

Fig 6 (cont.)

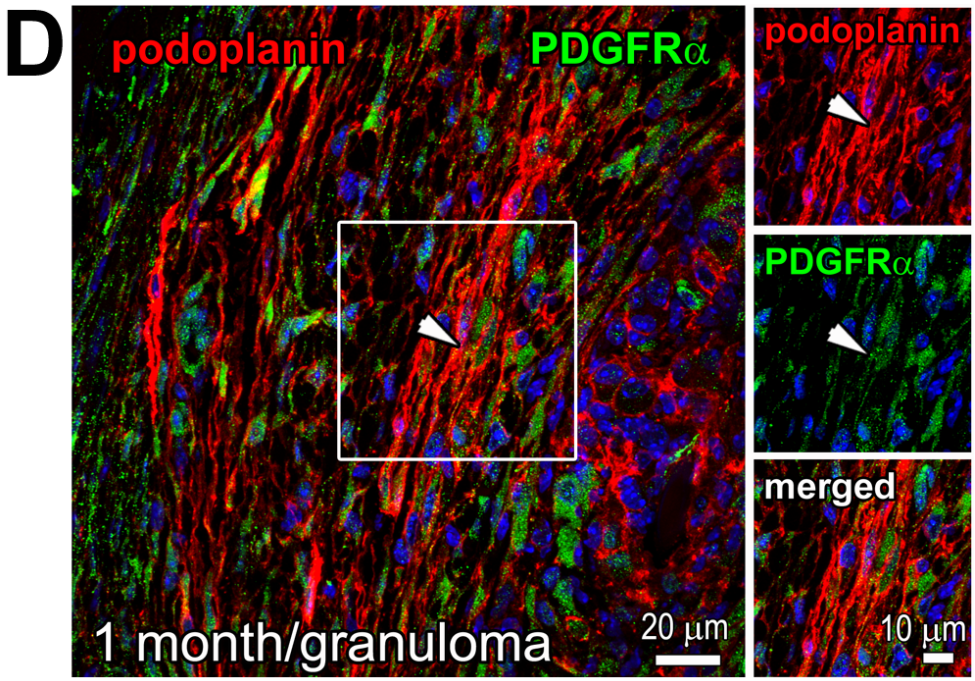

Fig 6 (cont.)

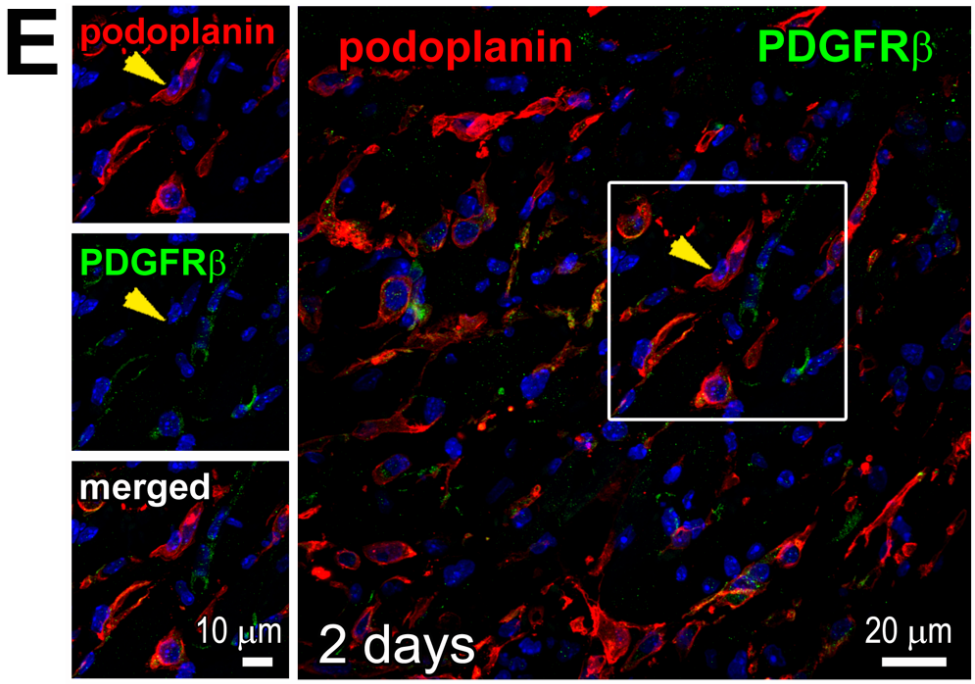

Fig 6 (cont.)

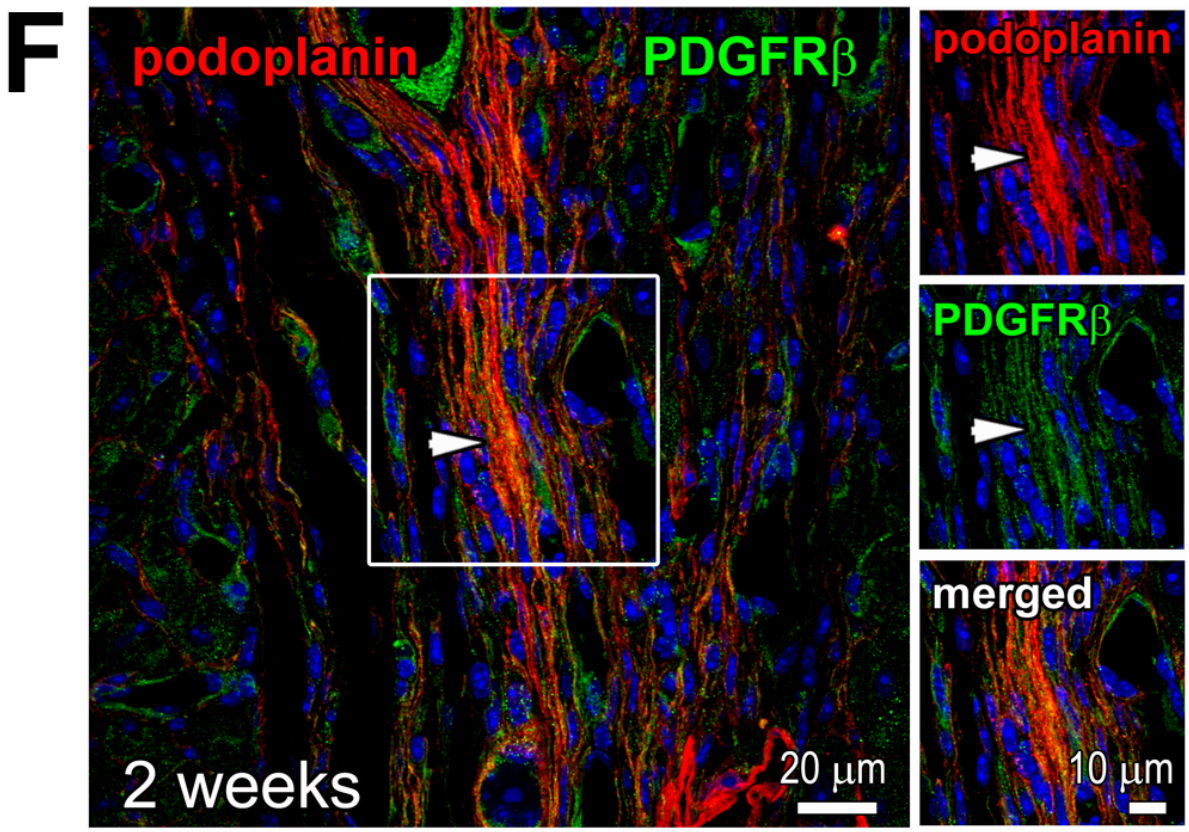
F
podoplanin
PDGFRβ
2 weeks
20 μm
podoplanin
PDGFRβ
merged
10 μm

Fig 6 (cont.)

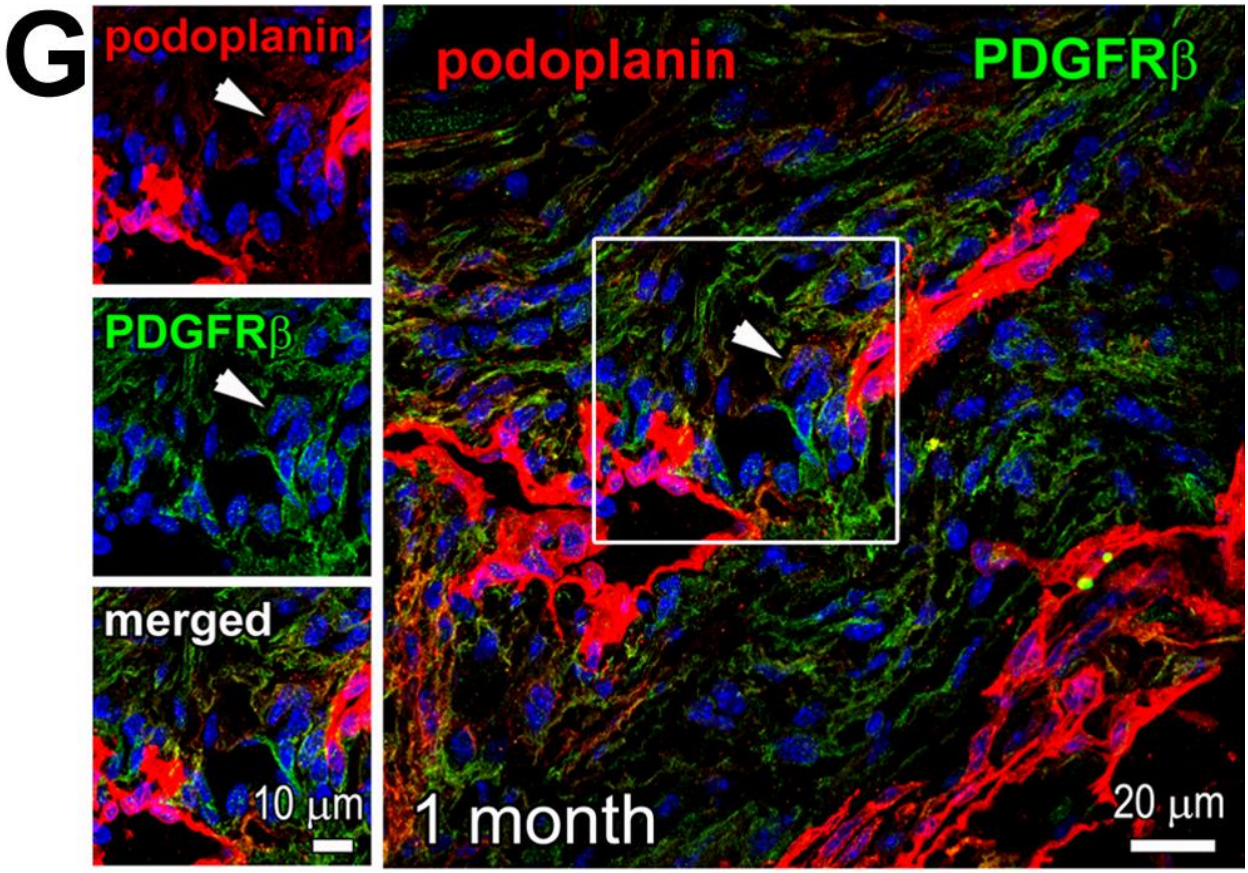
G
podoplanin
PDGFRβ
merged
10 μm
podoplanin
PDGFRβ
1 month
20 μm

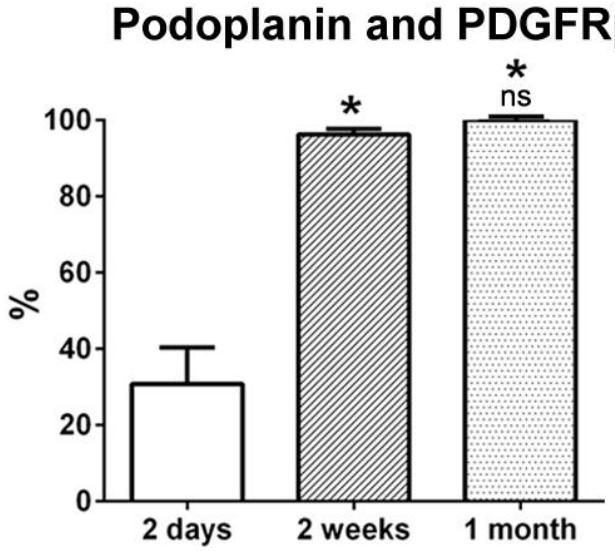
Podoplanin and PDGFRβ
%
100
80
60
40
20
0
*
*
ns
2 days
2 weeks
1 month

Fig 6 (cont.)

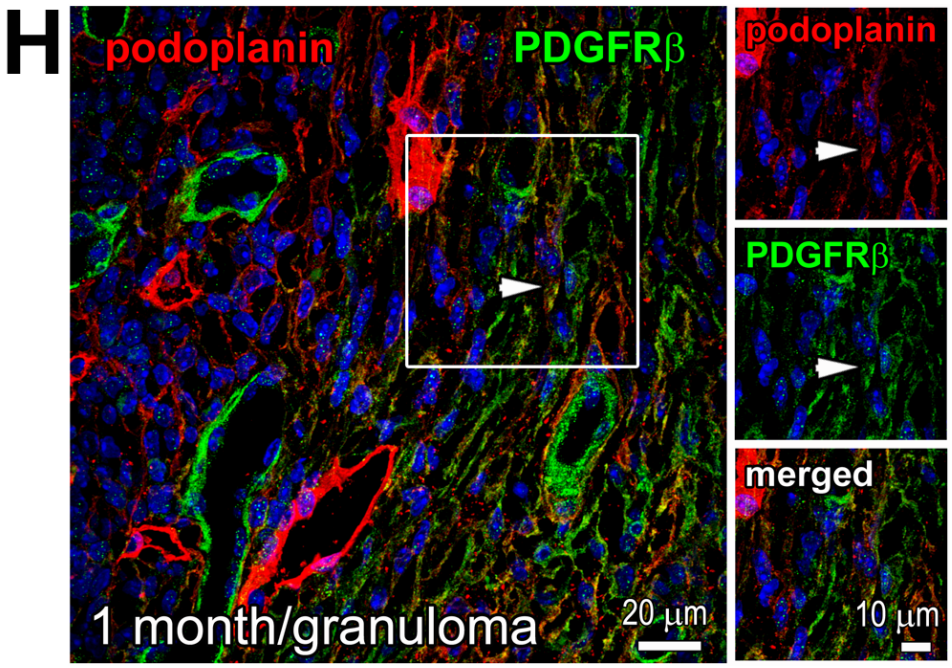

Fig 6 (cont.)

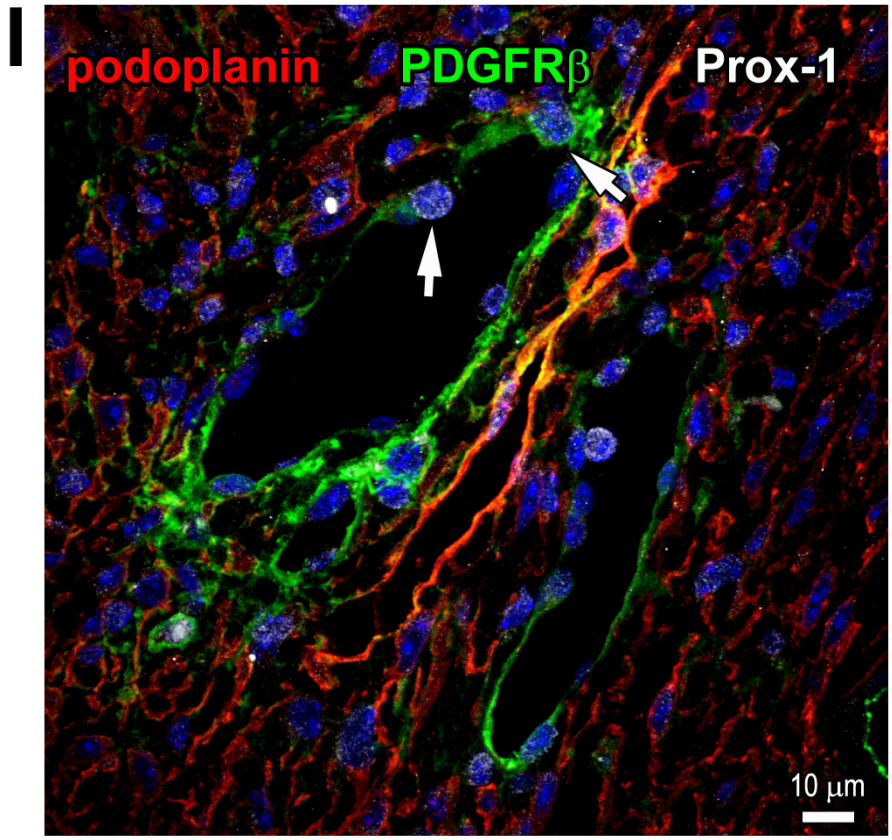

Fig 6 (cont.)

Fig 6. Expression of PDGFRα and PDGFRβ in podoplanin-positive populations. Thin cardiac sections were indirectly immunolabeled with podoplanin (red) and either PDGFRα (**A**-**D**; green), PDGFRβ (**E**-**H**; green), or PDGFRβ and Prox-1 (**I**; green and grey, respectively) antibodies. Nuclei, blue. In **A**-**H**, time after MI is indicated. Areas in rectangles are shown in the adjacent images for each color channel and merged. In **A**-**D**, podoplanin is frequently co-stained with PDGFRα at every time point; examples are indicated by white arrowheads. In **E**, podoplanin-positive cells are mostly PDGFRβ-negative, as exemplified by yellow arrowheads. In **F**-**H**, PDGFRβ distinctly co-stained with podoplanin. In **C** and **G**, quantitative image analysis (graphs, lower panels) of the fraction of podoplanin-expressing cells co-labeled with PDGFRα (**C**) and PDGFRβ (**G**) are shown at indicated times after MI. Data represent mean and SD of the % double-positive cells out of total podoplanin-positive cells; n=5 image fields per group. By one-way ANOVA for PDGFRβ, *P < 0.0001 for 2 days vs. 2 weeks or 1 month; ns, not-significant for 1 month vs. 2 weeks. In **I**, arrows point to the examples of Prox-1 staining in the nuclei of PDGFRβ-positive podoplanin-negative BVs.

The role of inflammation in the recruitment of podoplanin-expressing cells

Inflammation-induced lymphangiogenesis is a well-established phenomenon implicated in wound healing responses sine the lymphangiogenesis is needed for the resolution of the inflammation and the return of the immune cells back to the circulation [86] [101] [102].

In the present study we also examined few cases of MI with higher inflammation, like granulomas. Granuloma is a form of inflammatory reaction described for several diseases. It is noted that nodules of granulomas in different tissues are characterized by the presence of podoplanin-positive cells and LVs of heterogeneous and atypical morphology, which frequently

express PDGFRβ [90, 95] [103] [104], resembling the podoplanin-labeled cells in the chronically infarcted heart (Fig 6G; 1 month).

Few experimental mice developed granulomas near to the insertion of a suture thread within the myocardium.

We found a high density of podoplanin labeling in the granuloma nodules in the heart (Fig 1D-1F, and Fig 3A and 3C; 1 month/granuloma), but not in the RA of the same samples (Fig 1G; 1 month/granuloma). Importantly, the frequency of podoplanin-positive cells that express Prox-1 or VEGFR-3 was increased in the scar and BZ in the cardiac samples with MI and granulomas as compared to MI only (Fig 5C and 5G; 1 month and Fig 5D and 5H; 1month/granuloma), as expected in a highly inflammatory environment.

Although the lymphangiogenic responses in the infarcted myocardium with granulomas were apparently amplified relative to MI only (Fig 1D), the phenotypic features of podoplanin-labeled cells in the hearts with granulomas, including vascular markers (Fig 3C; 1 month/granuloma) and PDGFRα and PDGFRβ (Fig 6D and 6H, 1month/granuloma), were similar to the ones observed in the absence of granuloma (Fig 3C and Fig 6C and 6G; 1 month). This suggests that the surge in podoplanin expression following acute MI is at least partly driven by inflammation.

The inflammatory reaction to myocardial injury is evident by a time-dependent accumulation of immune cells, including macrophages. In murine embryos and pathological conditions, cells that exhibit traits of macrophages display characteristics of lymphatic endothelial cells and localize in the regions of lymphatic vessel growth, serving as a source of lymphangiogenic factors, and potentially integrating into newly-formed vessels [105] [106]. We did not detect the presence of monocyte-macrophage markers MOMA-2 (Fig 7A), F4/80 (Fig 7B), or CD11b and Ly6C (S2,

Fig 5) in the infarcted myocardial areas that were characterized by the accumulation of podoplanin-positive cells (Fig 1).

In order to confirm that podoplanin is partially expressed by the immune cells, we performed a flow-cytometry analysis. As previously said, the immune cells show the ligands for podoplanin and barely the podoplanin itself.

By flow-cytometry we documented that at 2 days after MI on average only 20% of podoplanin-positive cells in the infarcted heart were labeled with either F4/80, CD11b (Fig 7C) or Ly6C (S2, Fig1; Panel 5) antibodies. These data indicate that the podoplanin-expressing pools in the heart in majority do not correspond to maturing macrophages, although, as discussed below, their hematopoietic origin cannot be excluded [107].

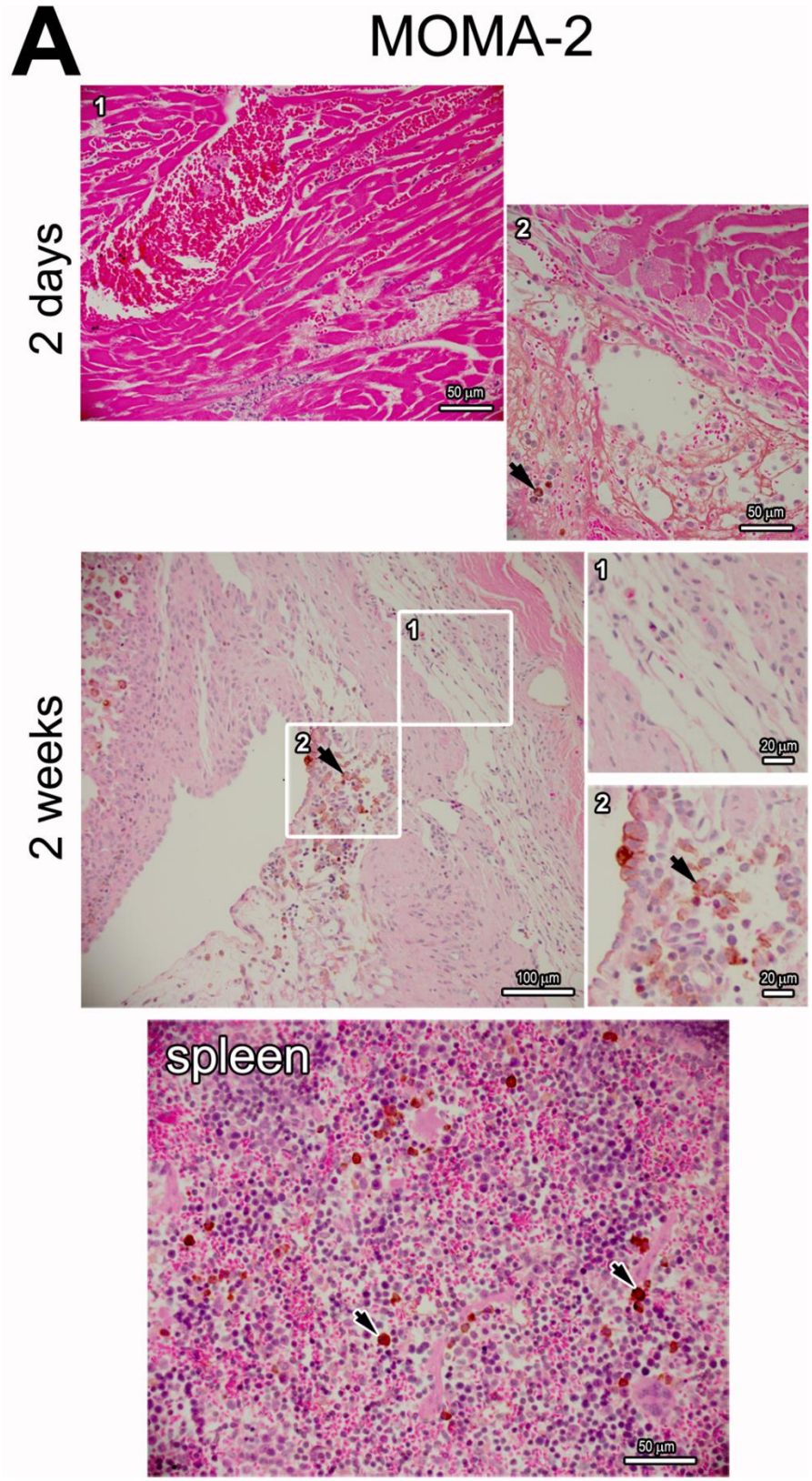
A
MOMA-2
2 days
1
50 µm
2
50 µm
2 weeks
1
2
100 µm
1
20 µm
2
20 µm
spleen
50 µm

Fig 7

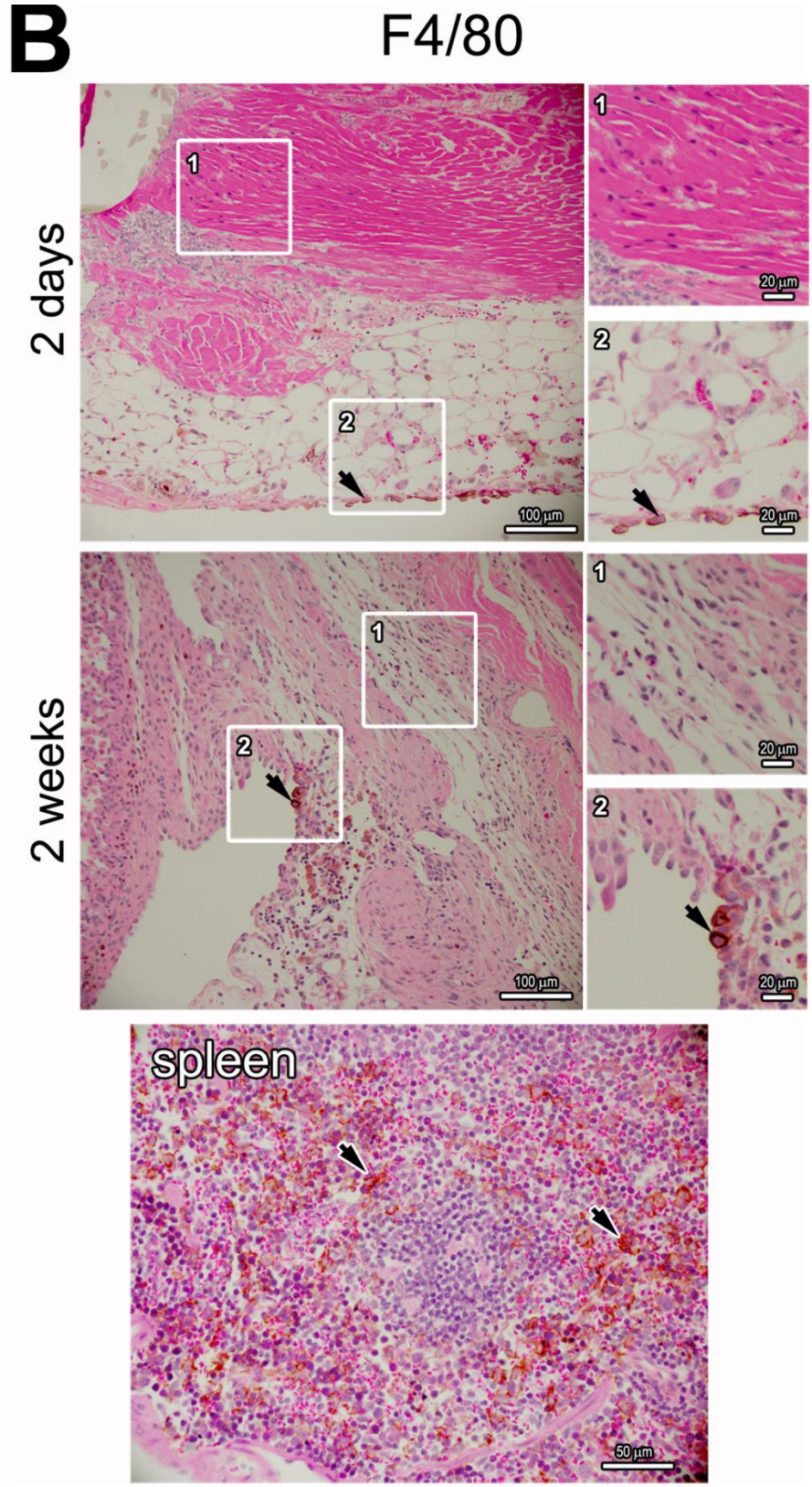

Fig 7 (cont.)

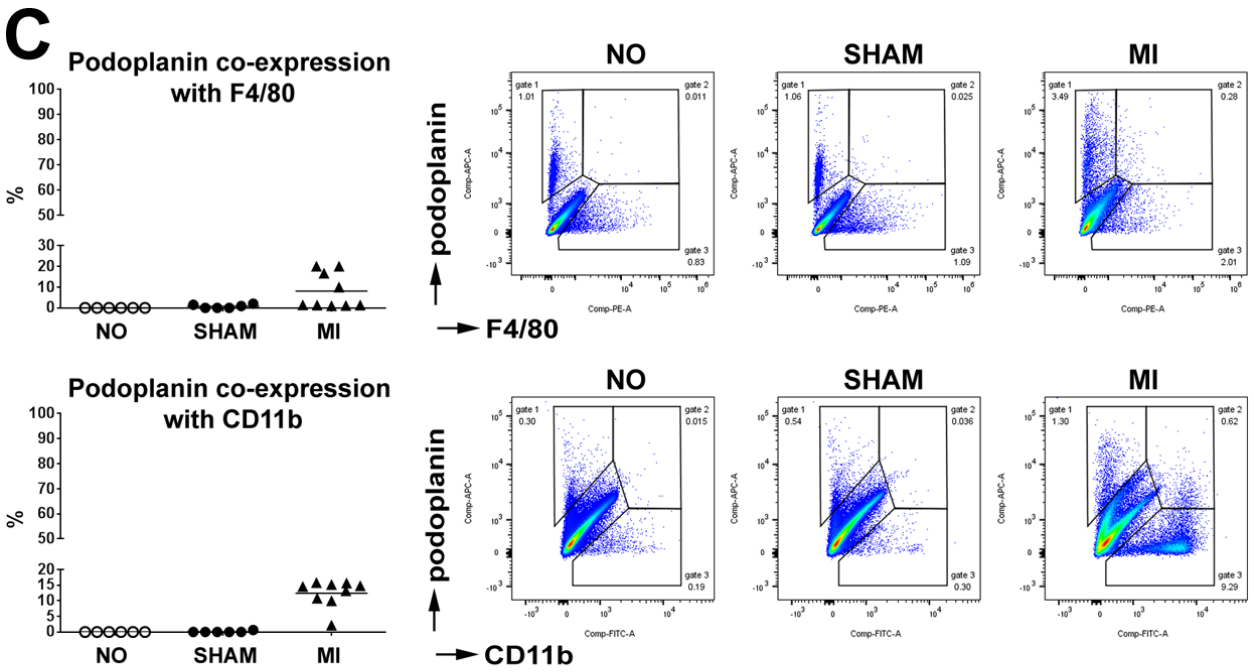

Fig 7 (cont.)

Fig 7. Low expression of monocyte-macrophage markers in the populations of podoplanin-positive cells in the infarcted myocardium. (**A**,**B**) Thin cardiac sections were indirectly immunolabeled with MOMA-2 (**A**) or F4/80 (**B**) antibodies and counterstained with hematoxylin and eosin. Time after MI is indicated. Spleen sections were included as positive controls. Areas in rectangles with the corresponding numbers are shown at a higher magnification in the adjacent insets. Note the presence of cells immunoreactive for MOMA-2 or F4/80 (arrows) in the inflamed epicardium (2 days, insets 2), myocardial interstitium (2 weeks, insets 2) and spleen, but not in the BZ of necrotic myocardium (2 days, insets 1) or the maturing scar (2 weeks, insets 1). (**C**) Flow-cytometry analysis of the F4/80 or CD11b expression in the podoplanin-positive cohorts populating the hearts of non-infarcted (NO), sham-operated (SHAM) and infarcted (MI) mice at 2 days after surgery. Graphs displaying individual values and the respective means (left),

as well as representative scatterplots (right) are shown. Data represent frequency of double-positive cells within podoplanin-labeled populations (calculated as % cells in gate 2 out of the sum of cells in gate 1 and gate 2).

Discussion

In the present work we studied the healing process and scar formation in the heart using MI as a model of the lymphangiogenic and fibrogenic responses. We identified a hitherto unconsidered glycol protein named podoplanin as a master regulator of different stages of myocardial wound repair after infarction.

We established that shortly after MI, at the time corresponding to the later phases of granulation of the necrotic tissue in the infarcted myocardium, the well-defined lymphatic marker podoplanin was expressed more than six-fold in the areas neighboring the infarction as compared to remote area, and we fund a three-fold increase in the frequency of podoplanin-positive cells in the whole heart relative to non-operated and sham operated controls.

These newly-appearing podoplanin-presenting cells not organized into vessels-like structures were predominantly LYVE-1-negative and exhibited a heterogeneous phenotype in terms of various markers of mesenchymal and endothelial fates.

We characterized the podoplanin cohort of cells by co-immunolabeling with several markers in a time dependent manner.

The immunolabeling profile of podoplanin-expressing cells at the different stages of infarct repair is summarized in Table1.

The presence of podoplanin-bearing cells was mainly prominent in the areas of future lymphangiogenesis at the infarct BZ; furthermore the abundance of podoplanin was elevated

almost two-fold in the healing and maturing scars but not the RA, concomitantly with the previously reported increase in LYVE-1 and VEGFR-3-positive CLVs [41] [43] and the buildup of fibronectin deposits [86] [87].

The fate of podoplanin positive cells it would have been predictable based on the knowledge already present in literature, but a very detail observation showed that cells positive to podoplanin were not lineaged only into the lymphatic fate.

Of note, the expansion of podoplanin-positive compartment and CLVs was not noticeable in the myocardium of sham-operated animals. We also establish a detailed characterization of the accumulation of podoplanin-labeled multicellular assemblies intensified in vicinity of myocardial granuloma nodules, exhibiting similarities to encapsulating peritoneal sclerosis [103] and pulmonary sarcoid granulomas [104].

Based on our observation the inflammatory processes might play a significant role in the recruitment of podoplanin-bearing LYVE-1-negative cells to the site of myocardial repair or the activation of podoplanin expression in responsive cell cohorts, not only for the lymphangiogenesis but also for the renovation of the necrotic tissue.

Podoplanin is expressed in a variety of different type of cells and in different context; a multitude of stimuli can drive podoplanin expression, including physiological differentiation factors in embryogenesis, potentially malignant factors such as pro-tumorigenic signaling pathways in cancer and pro-inflammatory cytokines in immune diseases, so, we cannot exclude that the scar formation environment it stimuli the over expression of podoplanin.

Indeed, inflammation and neoplastic growth alter the podoplanin level in various cell types, impacting their differentiation status and migratory behavior [108] [109]. In addition, homing of circulating cells is proposed to contribute to the LVs formation under inflammatory conditions

[107] [110], with evidence that rare bone marrow-derived podoplanin-positive cells express Prox-1 and function as lymphatic endothelial progenitors [110].

Although the podoplanin-mediated signaling pathway is not sufficiently understood, the expression of podoplanin is cognate toLECs; and inflammatory lymphangiogenesis is attenuated if podoplanin activity is lacking [28] [111]. Podoplanin deficiency impairs cardiac development [28], while continuous expression of podoplanin into adulthood is required to maintain functional lymphatic vasculature [108] [112].

We detected the presence of canonical lymphendothelial markers Prox-1 and VEGFR-3 within the cohort of podoplanin-positive LYVE-1-negative cells (Table 1), which might be indicative of their differentiation into LECs of CLVs. We confirmed that Prox-1 is required for the transcription and that VEGFR3 is essential for the lymphatic vessel formation.

Additionally, a hematoendothelial epitope CD34 was observed in podoplanin-presenting cells, and its expression was augmented with time after MI (Table 1). CD34 labeling may signify a hematopoietic origin of these cells, or, an endothelial progenitor one. Moreover, CD34 upregulation distinguishes lymphatic endothelium in tumors [113]. Hence the presence of CD34 in podoplanin-expressing cells and vessels of the chronically infarcted heart might point to their activated diseased state.

Nevertheless, a considerable fraction of the podoplanin-presenting cells, which was seemingly indistinguishable from the above cell group in terms of morphology [108] and tissue location, did not exhibit any of the markers associated with endothelial commitment, respectively: Prox-1, VEGFR-3, CD34 and PECAM-1.

These findings imply that podoplanin-positive compartment in the infarcted myocardium constitutes an inhomogeneous population, consisting of cells with a variable potency to adopt the

lymphatic endothelial or other cell fates. For instance, it has been documented that interstitial stroma cells acquire podoplanin expression after organ injury and in pathological conditions accompanied by fibrosis in the skin, skeletal muscle and peritoneum [114] [105] [115].

Importantly, we documented for the first time that a mesenchymal marker PDGFRα was highly represented in podoplanin-positive cells in the heart (Table 1). Cells positive to PDGFRα are proposed to function as mesenchymal progenitors, which in response to injury and inflammation reveal plasticity regarding their ability to differentiate into endothelium or act as profibrotic cells [93] [116] [99] [100]. The predisposition towards the fibrogenic phenotype is influenced by the presence of pathologies and with aging, and can be antagonized to reduce scarring and improve angiogenesis [117]. Thus, the high expression of PDGFRα, along with irregular occurrences of Prox-1 and VEGFR-3 (Table 1), might signify an alternative ability of podoplanin-bearing cells to generate LECs or fibroblasts, impacting the outcome of the myocardial repair process. Likewise, in the human liver, podoplanin discriminates disparate categories of progenitor and stromal cell subsets, which display cell fate plasticity, population growth, and alterations in the relative distribution under conditions of chronic inflammation and fibrosis [118].

PDGFRβ have been also associated with podoplanin, in fact inflamed and fibrotic tissues are characterized by the abundance of podoplanin-presenting cells of mesenchymal morphology, which often co-express PDGFRβ [95] [103] [104]; PDGFRβ is also linked to the fibrogenic activity of mural cells [100] [119]. Of interest, granuloma nodules in the heart showed similar accumulation of podoplanin and PDGFRβ co-presenting cells. In the infarcted myocardium with no granulomas, the high occurrence of podoplanin in PDGFRβ -bearing cells was apparent as well, albeit at the later stages of wound repair, concomitantly with the scar development (Table 1). Disruption of the PDGFRβ signaling impairs post-MI angiogenesis and BV maturation, and

decreases collagen content in the wound, destabilizing the scar [120]. Therefore, the acquisition of podoplanin by PDGFRβ-positive cells in the chronically infarcted myocardium might reflect their active role in lymphangiogenesis, fibrotic responses and scar maintenance.

Yet, the markers of fibroblast, such as vimentin and α-SMA, were rarely detected in podoplanin-positive cells residing in the fibrotic areas (Table 1); based on the observation on the podoplanin expression in PDGFRα and PDGFRβ cells, we can extrapolate that podoplanin is expressed mostly in progenitor cells that later can be positive to vimentin or α-SMA with a full transformation into myofibroblasts. Indeed, analogous type of PDGFRα-positive progenitors, which acquire fibrogenic behavior due to a partial endothelial-mesenchymal transition but do not become myofibroblasts, has been reported in the injured muscle [93] [99].

The growth of lymphatic network in adult organs is believed to occur as a result of the proliferative expansion and/or sprouting of new LVs from pre-existing lymphatics [86] [101] [113]. These processes are seemingly conditioned by the type of stimulus: whereas VEGFR-2 activation mainly induces vessel enlargement, VEGFR-3 signaling promotes sprouting [121] [89]. Notably, VEGFRs, as well as VEGF-C and -D ligands, are up-regulated in the peri-infarcted region [41] [96] [21] [122]. Administration of a selective VEGFR-3 agonist to the infarcted heart induces strong and sustained lymphangiogenesis [96] [21]. VEGFR-3 signaling is enhanced by mechanical stretch [115], which may explain the development of the lymphatic vasculature when interstitial pressure is elevated. Intriguingly, activation of podoplanin on the lymph node reticular cells diminishes their contractility, altering organ shape and stiffness under inflammatory conditions [123]. Thus, podoplanin-positive cells in the infarcted myocardium might affect local tissue tension, indirectly impacting VEGFR-3-stimulated CLV growth, extracellular matrix deposition and scar remodeling.

Table 1. Summary of the observed immunolabeling profile of podoplanin-expressing cells at different stages of infarct repair [(a), (b), (c), (d)].

[(a)] – designates that < 20% cells are co-labeled
[(b)] -/+ designates that 20-50% cells are co-labeled
[(c)] + designates that > 50% cells are co-labeled
[(d)] ++ designates that all the cells are co-labeled
[§]no scar was formed at 2 days
[(*)] interstitial and perivascular cells were seldom detected in the RA
[(1)]interst. and perivas. designates interstitial and perivascular cells; comparison pertanting to interstitial and perivascular podoplanin-positive cells are shaded
[(2)]lymph. vessels designates cells organized in LVs

Table 1. Summary of the observed immunolabeling profile of podoplanin-expressing cells at different stages of infarct repair [(a),(b),(c),(d)].

Time after MI	2 days			2 weeks			1 month		
Myocardial region	*BZ*[(§)]	*BZ*	*RA*[(*)]	*scar and BZ*	*scar and BZ*	*RA*[(*)]	*scar and BZ*	*scar and BZ*	*RA*[(*)]
Relative location of podoplanin-positive cells	[(1)]interst. and perivas.	[(2)]lymph. vessels	[(2)]lymph. vessels	[(1)]interst. and perivas.	[(2)]lymph. vessels	[(2)]lymph. vessels	[(1)]interst. and perivas	[(2)]lymph. vessels	[(2)]lymph. vessels
Podoplanin co-labeling with:									
LYVE-1	-	+	++	-	+	++	-	+	++
Prox-1	-/+	++	+	-/+	++	+	-/+	++	+
VEGFR-3	-	+	+	-/+	+	+	-/+	+	+
CD34	-	-	-	-/+	-/+	-/+	+	-/+	-/+
PDGFRα	++	++	-/+	++	++	-/+	++	++	-/+
PDGFRβ	-	-/+	-	++	++	-	++	++	-
α-SMA	-	-	-	-	-	-	-	-	-

Conclusion

In conclusion, our detailed spatiotemporal analysis of the acutely and chronically infarcted myocardium shows that podoplanin expression in the heart identifies structurally and phenotypically diverse cell categories, displaying epitopes of fibrogenic and endothelial commitment. The majority of data examining the function and signaling pathways of podoplanin are from studies of podoplanin expression in lymphangiogenesis and cancer, while these studies certainly provide critical insight into cellular and molecular aspects of podoplanin biology, it is important to understand whether podoplanin functions similarly in non-pathological settings and in cell types where it isn't naturally expressed.

Below, the cartoon represents a "summarized" scar tissue. Has it is shown in the histological staining, a mature scar is composed by disperse or perivascular LVs (in blue) of different size, capillaries (light purple), small and big arterioles (endothelial cell lining in purple and smooth muscle cells in deep blue) and a cohorts of cells that are scatter along the ECM. We characterized these cells, and although they have different origin or belong to different lineage they have in common the expression of podoplanin (red lining). In the cartoon all the cells that are positive to podoplanin have a red lining and in order to distinguish the populations they are exemplified with different colors: the lymphatic endothelial cells are represented in light blue, the mesenchymal progenitors in green or yellow and the endothelial progenitors in orange or yellow as well. In grey are labeled the immune cells. The colors and the characteristics are summarized in the legend.

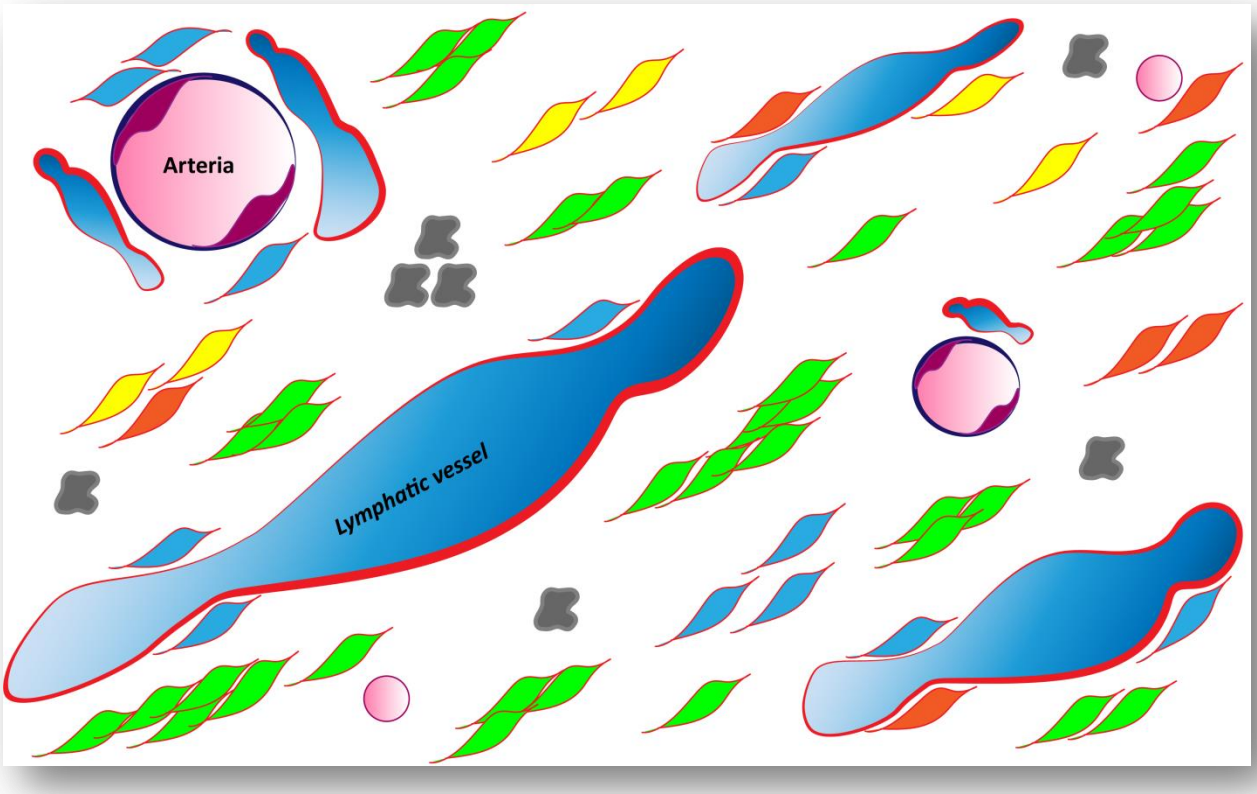
Arteria
Lymphatic vessel

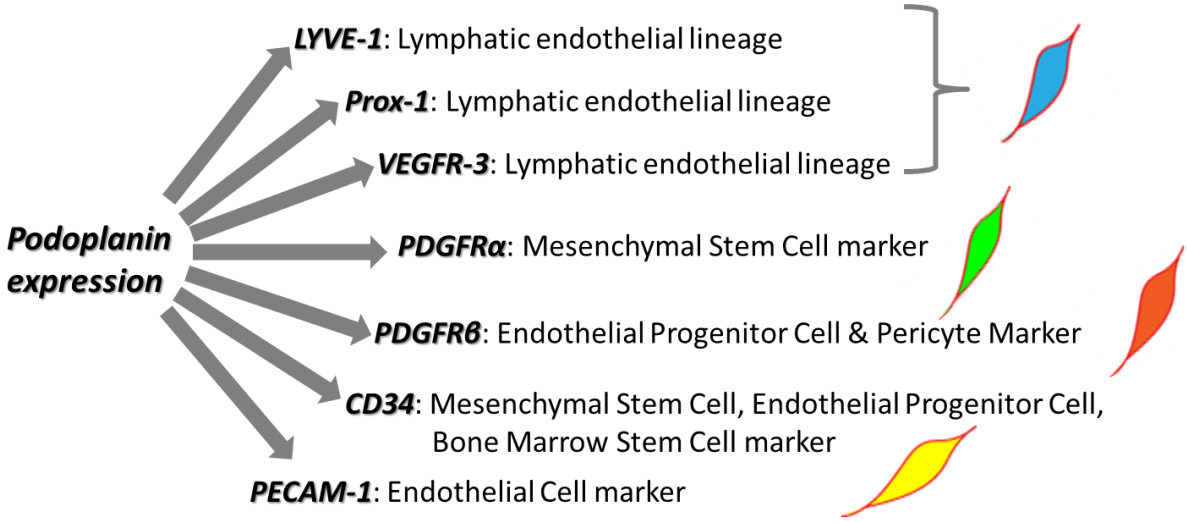
Podoplanin expression
LYVE-1: Lymphatic endothelial lineage
Prox-1: Lymphatic endothelial lineage
VEGFR-3: Lymphatic endothelial lineage
PDGFRα: Mesenchymal Stem Cell marker
PDGFRβ: Endothelial Progenitor Cell & Pericyte Marker
CD34: Mesenchymal Stem Cell, Endothelial Progenitor Cell, Bone Marrow Stem Cell marker
PECAM-1: Endothelial Cell marker

Further studies are warranted to determine whether cells with lymphangiogenic or profibrotic potentials can be recognized within the heterogeneous podoplanin-presenting populations and utilized to promote the CLV growth and attenuate the development of fibrosis after MI.

There are still many unknown about podoplanin biology that remain to be answered and the future studies will provide critical insights into whether podoplanin can be used as a specific marker for the diagnosis of “heathy” fibrosis and a target for the inhibition of inflammation besides that the metastasization.

The results of our study provided terrific information regarding the biology of the healing heart after MI; a better understanding of the environment of the scar it will improve the feasible but modest therapy for the cardiac regeneration that are currently carried on.

Disclosures

This study was developed in collaboration with Harvard University and the laboratory of Dr. Polina Goichberg at the Department of Anesthesiology, Perioperative and Pain Medicine, Brigham and Women's Hospital, Harvard Medical School, Boston, Massachusetts, United States of America.

This study also resulted in a peer-reviewed publication in PLoS-One Journal: PLoS One.

Maria Cimini, Antonio Cannatá, Gianandrea Pasquinelli, Marcello Rota and Polina Goichberg: Phenotypically heterogeneous podoplanin-expressing cell populations are associated with the lymphatic vessel growth and fibrogenic responses in the acutely and chronically infarcted myocardium. PLos One Journl. 2017; 12(3): e0173927 [124].

Supporting Information

S1 Table. Primary and secondary reagents employed for immunolabeling, light microscopy, and flow-cytometry

Primary Antibodies				
Antigen	***Manufacturer***	***Catalogue number***	***Host species***	***Applications***
podoplanin	RnD Systems	AF3244	goat	IHC(*), FC(*)
podoplanin	Thermo Fisher Scientific	MA5-1613	syrian hamster	IHC(*)
APC(§)-podoplanin	BioLegend	127409	syrian hamster	FC(*)
LYVE-1	RnD Systems	AF2125	goat	IHC(*)
LYVE-1	Abcam	ab14917	rabbit	IHC(*), FC(*)
PECAM-1	RnD Systems	AF3628	goat	IHC(*)
PECAM-1	BD Pharmingen	553370	rat	FC(*)
Prox-1	Abcam	ab37128	rabbit	IHC(*),FC(*)
Prox-1	Millipore	AB5475	rabbit	FC(*)
PDGFRα	Cell Signaling Technology	3174	rabbit	IHC(*)
PE(§)-PDGFRα	BioLegend	135905	rat	FC(*)
PDGFRα	RnD Systems	AF1062	goat	FC(*)
PDGFRβ	Cell Signaling Technology	3169	rabbit	IHC(*)
PDGFRβ	Abcam	ab51876	rat	IHC(*)
PE(§)-PDGFRβ	BioLegend	136005	rat	FC(*)
PDGFRβ	RnD Systems	AF1042	goat	FC(*)
VEGFR-3	BD Biosciences	552857	rat	IHC(*)
PE(§)-VEGFR-3	Miltenyi Biotech	130-102-216	rat	FC(*)
VEGFR-2	Cell Signaling Technology	9698	rabbit	IHC(*)
CD34	BioLegend	119301	rat	IHC(*)
PE(§)-CD34	BD Pharmingen	551387	rat	FC(*)

vimentin	Sigma-Aldrich	V2258	mouse	IHC(*)
fibronectin	Abcam	ab2413	rabbit	IHC(*)
α-SMA	Sigma-Aldrich	A2547	mouse	IHC(*)
MOMA-2	AbD Serotec	MCA519G	rat	IHC(*)
F4/80	AbD Serotec	MCA497GA	rat	IHC(*)
PE(§)-F4/80	BioLegend	123109	rat	FC(*)
CD11b	AbD Serotec	MCA74GA	rat	IHC(*), FC(*)
Ly6C	AbD Serotec	MCA2389T	rat	IHC(*)
Alexa Fluor 647-Ly6C	BioLegend	128009	rat	FC(*)
Non-immune IgGs				
Description	***Manufacturer***	***Catalogue number***	***Host species***	***Applications***
Normal IgG control	RnD Systems	AB-108-C	goat	FC(*)
Normal IgG control	RnD Systems	AB-105-C	rabbit	FC(*)
APC(§)-IgG control	BioLegend	402012	syrian hamster	FC(*)
PE(§)-IgG2a control	BioLegend	400507	rat	FC(*)
PE(§)-IgG2a control	BD Pharmingen	553930	rat	FC(*)
IgG2a control	BioLegend	400501	rat	FC(*)
APC(§)-IgG2a control	eBioscience	17-432181	rat	FC(*)
Secondary Antibodies				
Reactivity	***Manufacturer***	***Catalogue number***	***Conjugate***	***Applications***
Goat	Jackson ImmunoResearch	705-095-147	FITC(§)	IHC(*), FC(*)
Goat	Jackson ImmunoResearch	705-025-147	TRITC(§)	IHC(*)
Goat	Jackson ImmunoResearch	705-175-147	Cy(§)5	IHC(*), FC(*)
Goat	Jackson ImmunoResearch	705-605-147	Alexa Fluor 647	IHC(*), FC(*)
Goat	Jackson ImmunoResearch	705-475-003	DyLight 405	IHC(*)
Hamster	Jackson ImmunoResearch	107-166-142	Cy(§)3	IHC(*)

Hamster	Jackson ImmunoResearch	107-606-142	Cy(§)5	IHC(*)
Hamster	Jackson ImmunoResearch	107-475-142	DyLight 405	IHC(*)
Rabbit	Life Technologies	A21206	Alexa Fluor 488	IHC(*), FC(*)
Rabbit	Life Technologies	A10042	Alexa Fluor 568	IHC(*)
Rabbit	Jackson ImmunoResearch	711-605-152	Alexa Fluor 647	IHC(*), FC(*)
Rabbit	eBioscience	12-4739-81	PE(§)	FC(*)
Rabbit	Jackson ImmunoResearch	711-475-152	DyLight 405	IHC(*)
Mouse	Jackson ImmunoResearch	715-025-140	TRITC(§)	IHC(*)
Mouse	Jackson ImmunoResearch	715-605-140	Cy(§)5	IHC(*)
Mouse	Jackson ImmunoResearch	715-095-150	FITC(§)	IHC(*)
Mouse	Jackson ImmunoResearch	715-025-150	TRITC(§)	IHC(*)
Mouse	Jackson ImmunoResearch	715-175-150	Cy(§)5	IHC(*)
Mouse	Jackson ImmunoResearch	715-475-150	DyLight 405	IHC(*)
Rat	Jackson ImmunoResearch	712-095-150	FITC(§)	IHC(*), FC(*)
Rat	Jackson ImmunoResearch	712-025-150	TRITC(§)	IHC(*)
Rat	Vector	SK-4100	HRP(§)	IHC(*)

(*) IHC= immunohistochemistry; FC= flow cytometry

(§) APC=allophycocyanin; PE= phycoerythrin; FITC= fluorescein isothiocyanate; TRITC= tetramethylrhodamine; Cy= Cyanine; HRP= Horseradish peroxidase

Supporting Information Figures and Figure Captions

S2 Fig 1. Left ventricular coronary artery ligation. Myocardial infarction (MI) was induced in female mice to reduce biological variability related to sex at 2-3 months of age as follows: animals were anesthetized with isoflurane 1.5% and ventilated, under sterile conditions the thorax was opened via the third costal space, the atrial appendage elevated, the left coronary artery, and a silk braided suture (6-0) was inserted and tightened around the vessel near the origin. Then, the chest was closed and pneumothorax reduced by negative pressure, and the animals were allowed to recover. Sham-operated (SHAM) mice were subjected to an identical surgery procedure, with the exception that the suture was not tightened around the artery. Non-operated (NO) mice served as additional controls.

S2 Fig 2. Experimental model and time dependent observation. At the time of sacrifice, with the animals (MI animals, sham and controls) under deep anesthesia, bilateral thoracotomy was performed, the hearts were removed and either fixed and processed for histological analysis, or enzymatically digested for single-cell assessment by flow-cytometry, as described in the materials and methods. We chose as time points: 4h and 8h, 2 days, 14 days and 30 days after MI in order to analyze chronic and acute processes of wound healing.

S2 Fig 3. Flow-cytometry analysis of the podoplanin co-expression with LYVE-1 in cardiac cells from non-operated (NO), sham-operated (SHAM) and infarcted (MI) mice at 2 days after surgery. (**A**,**B**) Isolated cardiac cells were co-stained with podoplanin and the indicated antibodies. (**A**) LYVE-1. Representative scatterplots are shown. Numbers indicate proportions of LYVE-1-positive cells within total podoplanin-positive populations (calculated as % cells in Q2 out of the sum of Q1 and Q2). Samples labeled with non-immune IgGs (IgGs) and podoplanin

only or LYVE-1 only were used to determine the gates and calculate background. (**B**) Frequency (%) of podoplanin-positive cells co-labeled with PECAM-1, CD34, Prox-1, or VEGFR-3, respectively, was calculated as in (A). Graphs displaying values for the individual hearts and the respective means for each group (red lines) are shown. **PECAM-1**: ns, not significant; *P = 0.0001 by one-way ANOVA. **CD34**: ns, not significant for SHAM vs. MI by two-tailed *t*-test. **Prox-1**: *P = 0.0036 for SHAM vs. MI by two-tailed *t*-test. **VEGFR-3**: ns, not significant by one-way ANOVA.

S2 Fig 4. Flow-cytometry analysis of the podoplanin co-expression with PDGFRα and PDGFRβ in cells from the infarcted (MI) hearts at 2 days after surgery. Representative scatterplots (left) and the summary graph (right) displaying individual values for each heart with the respective means of the frequency of podoplanin-positive cells co-labeled with PDGFRα or PDGFRβ are shown. Calculated as % cells in gate Q6 out of the sum of the gates Q5 and Q6. Samples labeled with non-immune IgGs (IgGs) and podoplanin only, or PDGFRα or PDGFRβ only (PDGFR only), were used to determine the gates and calculate background.

S2 Fig 5. Low expression of myelo-monocytic markers in the podoplanin-positive interstitial cells. (**A**) Thin cardiac sections 1 month after MI were indirectly immunolabeled with podoplanin (red) and a combination of CD11b and Ly6C (green) antibodies. Nuclei, blue. Area in rectangle is shown at a higher magnification in the adjacent images for each color channel and merged. (**B**) Flow-cytometry analysis of the podoplanin co-expression with Ly6C in cardiac cells from the infarcted (MI) mice at 2 days after surgery. Isolated cells were co-stained with podoplanin and Ly6C antibodies. Representative scatterplots (left) and the graphs displaying individual values with the respective mean (right) are shown. Samples labeled with non-immune IgGs (IgGs) and podoplanin only or Ly6C only were used to determine the gates

and calculate the background. Data showing frequencies of double-positive cells within podoplanin-labeled populations in each heart (n=4) was calculated as % cells in gate 2 out of the sum of % cells in gate 1 and gate 2.

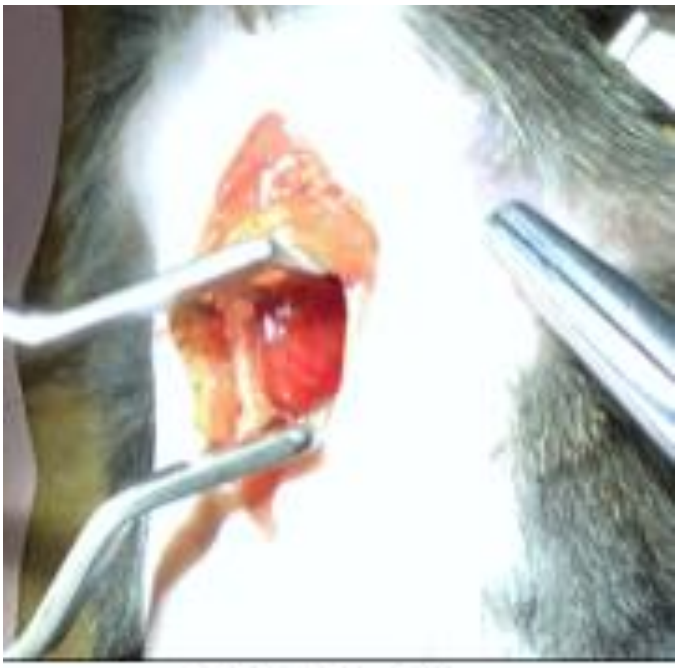

S2 Fig 1

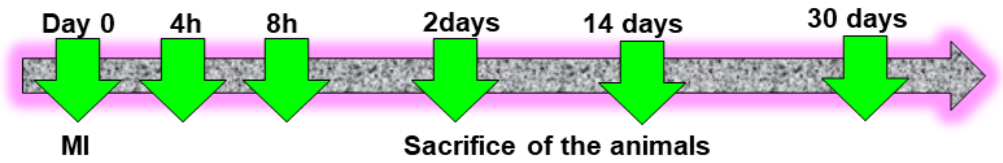

S2 Fig 2

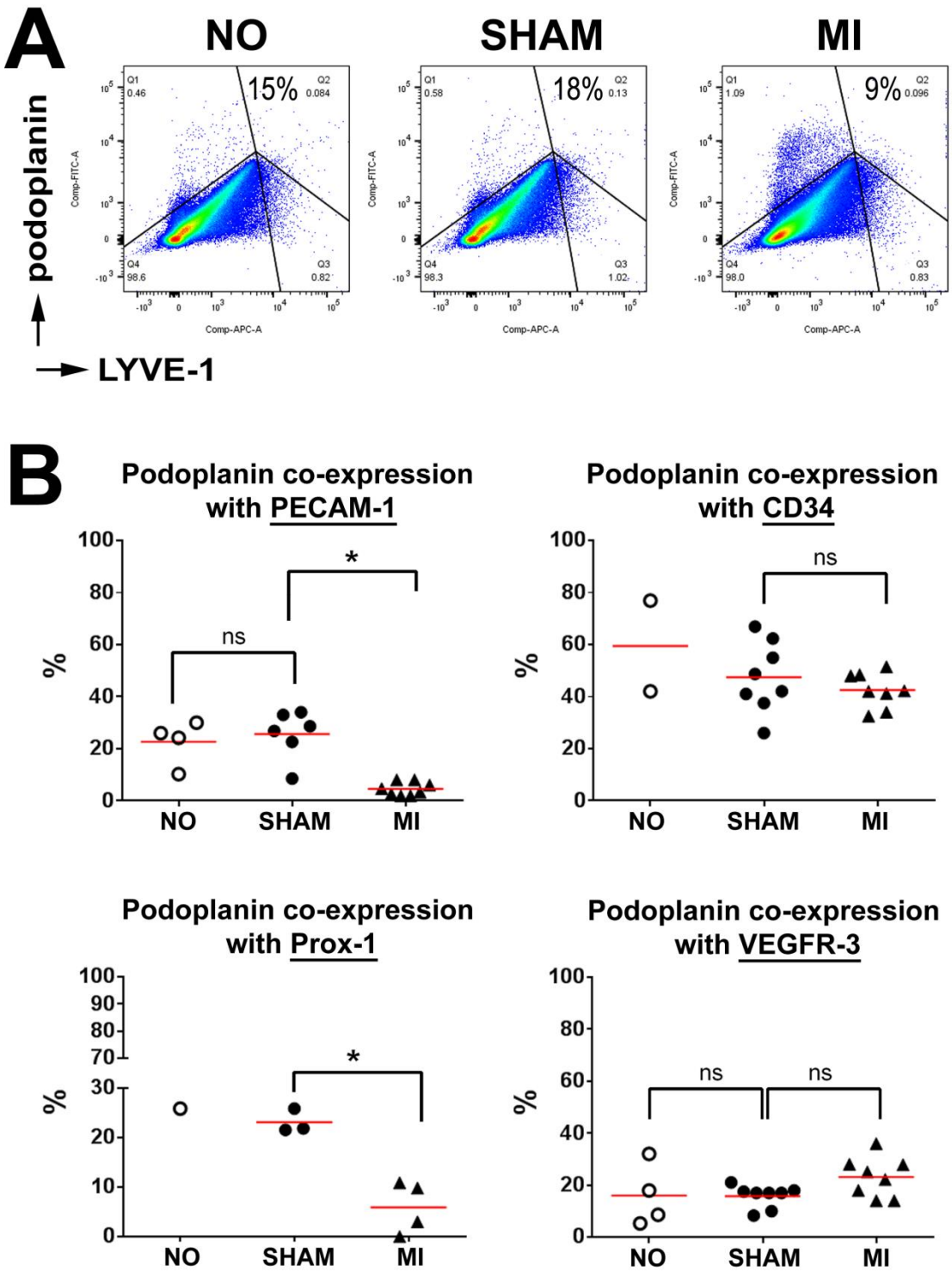
A
NO
SHAM
MI
podoplanin
LYVE-1
15%
18%
9%
B
Podoplanin co-expression with PECAM-1
Podoplanin co-expression with CD34
Podoplanin co-expression with Prox-1
Podoplanin co-expression with VEGFR-3
%
ns
*
NO
SHAM
MI

S2 Fig 3

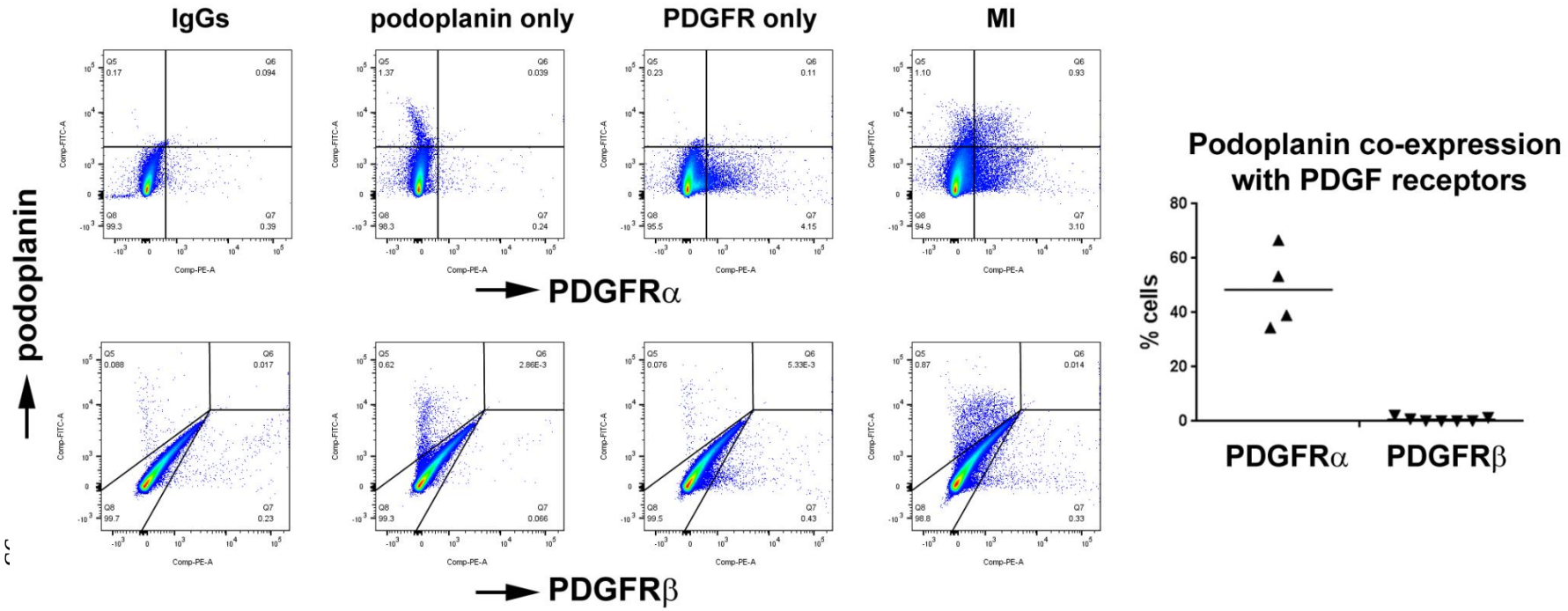
IgGs
podoplanin only
PDGFR only
MI
podoplanin
PDGFRα
PDGFRβ
Comp-FITC-A
Comp-PE-A
Q5 0.17
Q6 0.094
Q8 99.3
Q7 0.39
Q5 1.37
Q6 0.039
Q8 98.3
Q7 0.24
Q5 0.23
Q6 0.11
Q8 95.5
Q7 4.15
Q5 1.10
Q6 0.93
Q8 94.9
Q7 3.10
Q5 0.088
Q6 0.017
Q8 99.7
Q7 0.23
Q5 0.62
Q6 2.86E-3
Q8 99.3
Q7 0.066
Q5 0.076
Q6 5.33E-3
Q8 99.5
Q7 0.43
Q5 0.87
Q6 0.014
Q8 98.8
Q7 0.33

Podoplanin co-expression with PDGF receptors
% cells
80
60
40
20
0
PDGFRα
PDGFRβ

S2 Fig 4

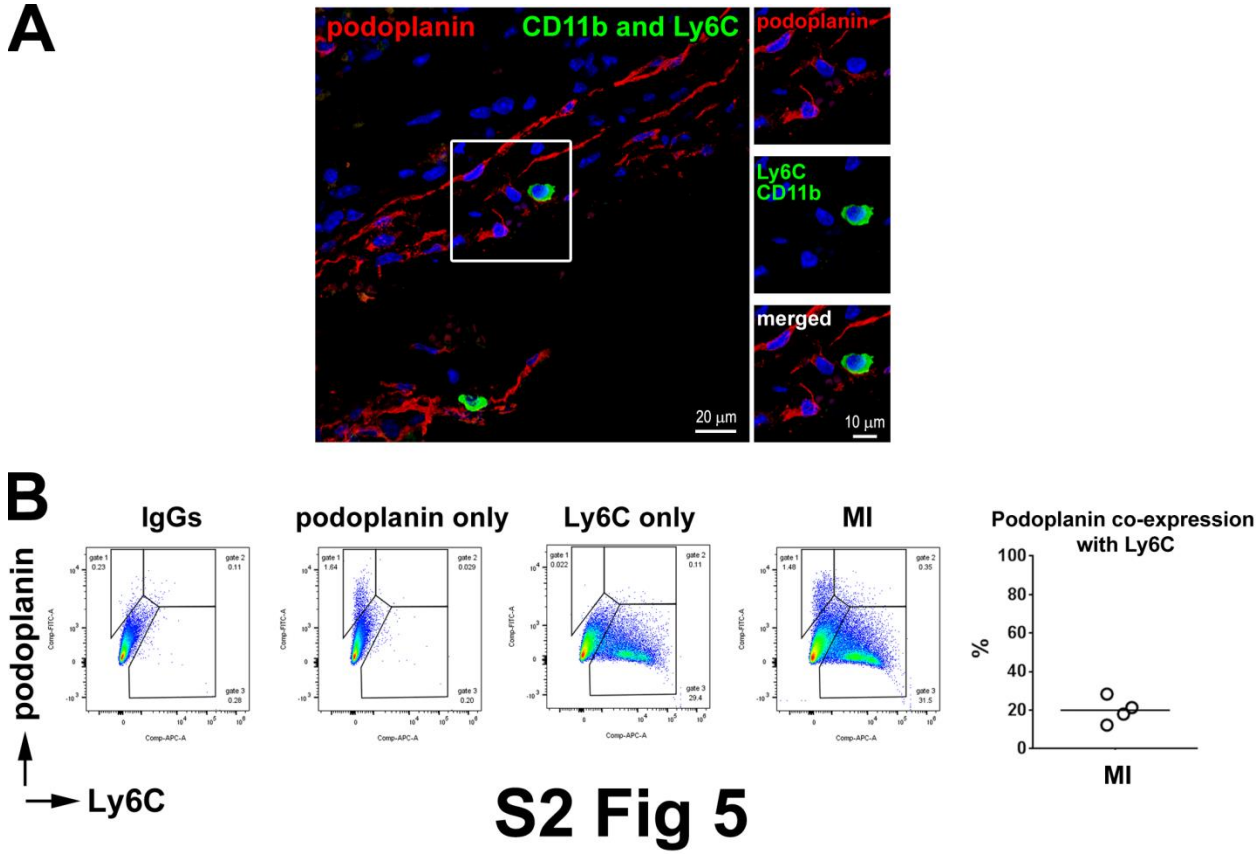
A
podoplanin
CD11b and Ly6C
podoplanin
Ly6C
CD11b
merged
20 μm
10 μm
B
IgGs
podoplanin only
Ly6C only
MI
Podoplanin co-expression with Ly6C
podoplanin
Ly6C
%
MI

S2 Fig 5

Reference

1. Moore-Morris, T., M. Puceat, and S.M. Evans, *Targeting cardiac fibroblasts: the pressure is on.* Cell Cycle, 2014. **13**(17): p. 2647-8.
2. Sangaralingham, S.J., et al., *The aging heart, myocardial fibrosis, and its relationship to circulating C-type natriuretic Peptide.* Hypertension, 2011. **57**(2): p. 201-7.
3. Platonov, P.G., et al., *Structural abnormalities in atrial walls are associated with presence and persistency of atrial fibrillation but not with age.* J Am Coll Cardiol, 2011. **58**(21): p. 2225-32.
4. Zeppenfeld, K., et al., *Catheter ablation of ventricular tachycardia after repair of congenital heart disease: electroanatomic identification of the critical right ventricular isthmus.* Circulation, 2007. **116**(20): p. 2241-52.
5. Goldsmith, E.C., et al., *Organization of fibroblasts in the heart.* Dev Dyn, 2004. **230**(4): p. 787-94.
6. Ertl, G. and S. Frantz, *Healing after myocardial infarction.* Cardiovasc Res, 2005. **66**(1): p. 22-32.
7. Czubryt, M.P., *Common threads in cardiac fibrosis, infarct scar formation, and wound healing.* Fibrogenesis Tissue Repair, 2012. **5**(1): p. 19.
8. Camelliti, P., et al., *Spatially and temporally distinct expression of fibroblast connexins after sheep ventricular infarction.* Cardiovasc Res, 2004. **62**(2): p. 415-25.
9. Virag, J.I. and C.E. Murry, *Myofibroblast and endothelial cell proliferation during murine myocardial infarct repair.* Am J Pathol, 2003. **163**(6): p. 2433-40.
10. Vanhoutte, D., et al., *Relevance of matrix metalloproteinases and their inhibitors after myocardial infarction: a temporal and spatial window.* Cardiovasc Res, 2006. **69**(3): p. 604-13.
11. Sun, Y., et al., *Infarct scar as living tissue.* Basic Res Cardiol, 2002. **97**(5): p. 343-7.
12. Fomovsky, G.M. and J.W. Holmes, *Evolution of scar structure, mechanics, and ventricular function after myocardial infarction in the rat.* Am J Physiol Heart Circ Physiol, 2010. **298**(1): p. H221-8.
13. Gabbiani, G., et al., *Granulation tissue as a contractile organ. A study of structure and function.* J Exp Med, 1972. **135**(4): p. 719-34.
14. Braitsch, C.M., et al., *Differential expression of embryonic epicardial progenitor markers and localization of cardiac fibrosis in adult ischemic injury and hypertensive heart disease.* J Mol Cell Cardiol, 2013. **65**: p. 108-19.
15. Turner, N.A. and K.E. Porter, *Function and fate of myofibroblasts after myocardial infarction.* Fibrogenesis Tissue Repair, 2013. **6**(1): p. 5.
16. Kohl, P. and R.G. Gourdie, *Fibroblast-myocyte electrotonic coupling: does it occur in native cardiac tissue?* J Mol Cell Cardiol, 2014. **70**: p. 37-46.
17. Janse, M.J. and A.L. Wit, *Electrophysiological mechanisms of ventricular arrhythmias resulting from myocardial ischemia and infarction.* Physiol Rev, 1989. **69**(4): p. 1049-169.
18. Nguyen, T.P., Z. Qu, and J.N. Weiss, *Cardiac fibrosis and arrhythmogenesis: the road to repair is paved with perils.* J Mol Cell Cardiol, 2014. **70**: p. 83-91.
19. Moccetti, T., A. Leri, and P. Anversa, *Controversy in myocardial regeneration.* Regen Med, 2015. **10**(8): p. 921-4.

20. Rog-Zielinska, E.A., et al., *The Living Scar--Cardiac Fibroblasts and the Injured Heart.* Trends Mol Med, 2016. **22**(2): p. 99-114.
21. Henri, O., et al., *Selective Stimulation of Cardiac Lymphangiogenesis Reduces Myocardial Edema and Fibrosis Leading to Improved Cardiac Function Following Myocardial Infarction.* Circulation, 2016. **133**(15): p. 1484-97; discussion 1497.
22. Lee, S., et al., *Prox1 physically and functionally interacts with COUP-TFII to specify lymphatic endothelial cell fate.* Blood, 2009. **113**(8): p. 1856-9.
23. Abraham, S., et al., *Salmonella enterica isolated from infections in Australian livestock remain susceptible to critical antimicrobials.* Int J Antimicrob Agents, 2014. **43**(2): p. 126-30.
24. Srinivasan, R.S., et al., *Lineage tracing demonstrates the venous origin of the mammalian lymphatic vasculature.* Genes Dev, 2007. **21**(19): p. 2422-32.
25. Wigle, J.T., et al., *An essential role for Prox1 in the induction of the lymphatic endothelial cell phenotype.* EMBO J, 2002. **21**(7): p. 1505-13.
26. Bertozzi, C.C., et al., *Platelets regulate lymphatic vascular development through CLEC-2-SLP-76 signaling.* Blood, 2010. **116**(4): p. 661-70.
27. Tammela, T. and K. Alitalo, *Lymphangiogenesis: Molecular mechanisms and future promise.* Cell, 2010. **140**(4): p. 460-76.
28. Pan, Y. and L. Xia, *Emerging roles of podoplanin in vascular development and homeostasis.* Front Med, 2015. **9**(4): p. 421-30.
29. Oliver, G., et al., *Prox 1, a prospero-related homeobox gene expressed during mouse development.* Mech Dev, 1993. **44**(1): p. 3-16.
30. Dumont, D.J., et al., *Cardiovascular failure in mouse embryos deficient in VEGF receptor-3.* Science, 1998. **282**(5390): p. 946-9.
31. Fu, J., et al., *Endothelial cell O-glycan deficiency causes blood/lymphatic misconnections and consequent fatty liver disease in mice.* J Clin Invest, 2008. **118**(11): p. 3725-37.
32. Pan, Y., W.D. Wang, and T. Yago, *Transcriptional regulation of podoplanin expression by Prox1 in lymphatic endothelial cells.* Microvasc Res, 2014. **94**: p. 96-102.
33. Cui, Y., *Impact of lymphatic vessels on the heart.* Thorac Cardiovasc Surg, 2010. **58**(1): p. 1-7.
34. Aspelund, A., et al., *Lymphatic System in Cardiovascular Medicine.* Circ Res, 2016. **118**(3): p. 515-30.
35. Kline, I.K., et al., *The Effects of Chronic Impairment of Cardiac Lymph Flow on Myocardial Reactions after Coronary Artery Ligation in Dogs.* Am Heart J, 1964. **68**: p. 515-23.
36. Kholova, I., et al., *Lymphatic vasculature is increased in heart valves, ischaemic and inflamed hearts and in cholesterol-rich and calcified atherosclerotic lesions.* Eur J Clin Invest, 2011. **41**(5): p. 487-97.
37. Loukas, M., et al., *The cardiac lymphatic system.* Clin Anat, 2011. **24**(6): p. 684-91.
38. Geissler, H.J., et al., *Morphology and density of initial lymphatics in human myocardium determined by immunohistochemistry.* Thorac Cardiovasc Surg, 2003. **51**(5): p. 244-8.
39. Ratajska, A., et al., *Comparative and developmental anatomy of cardiac lymphatics.* ScientificWorldJournal, 2014. **2014**: p. 183170.
40. Dashkevich, A., et al., *Morphological and quantitative changes of the initial myocardial lymphatics in terminal heart failure.* Lymphat Res Biol, 2009. **7**(1): p. 21-7.

41. Ishikawa, Y., et al., *Lymphangiogenesis in myocardial remodelling after infarction.* Histopathology, 2007. **51**(3): p. 345-53.
42. Sun, Q.N., Y.F. Wang, and Z.K. Guo, *Reconstitution of myocardial lymphatic vessels after acute infarction of rat heart.* Lymphology, 2012. **45**(2): p. 80-6.
43. Park, J.H., et al., *Endothelial progenitor cell transplantation decreases lymphangiogenesis and adverse myocardial remodeling in a mouse model of acute myocardial infarction.* Exp Mol Med, 2011. **43**(8): p. 479-85.
44. Goichberg, P., *Therapeutic lymphangiogenesis after myocardial infarction: vascular endothelial growth factor-C paves the way.* J Thorac Dis, 2016. **8**(8): p. 1904-7.
45. Astarita, J.L., S.E. Acton, and S.J. Turley, *Podoplanin: emerging functions in development, the immune system, and cancer.* Front Immunol, 2012. **3**: p. 283.
46. Wetterwald, A., et al., *Characterization and cloning of the E11 antigen, a marker expressed by rat osteoblasts and osteocytes.* Bone, 1996. **18**(2): p. 125-32.
47. Farr, A., A. Nelson, and S. Hosier, *Characterization of an antigenic determinant preferentially expressed by type I epithelial cells in the murine thymus.* J Histochem Cytochem, 1992. **40**(5): p. 651-64.
48. Rishi, A.K., et al., *Cloning, characterization, and development expression of a rat lung alveolar type I cell gene in embryonic endodermal and neural derivatives.* Dev Biol, 1995. **167**(1): p. 294-306.
49. Williams, M.C., et al., *T1 alpha protein is developmentally regulated and expressed by alveolar type I cells, choroid plexus, and ciliary epithelia of adult rats.* Am J Respir Cell Mol Biol, 1996. **14**(6): p. 577-85.
50. Scholl, F.G., et al., *Identification of PA2.26 antigen as a novel cell-surface mucin-type glycoprotein that induces plasma membrane extensions and increased motility in keratinocytes.* J Cell Sci, 1999. **112 (Pt 24)**: p. 4601-13.
51. Nose, K., H. Saito, and T. Kuroki, *Isolation of a gene sequence induced later by tumor-promoting 12-O-tetradecanoylphorbol-13-acetate in mouse osteoblastic cells (MC3T3-E1) and expressed constitutively in ras-transformed cells.* Cell Growth Differ, 1990. **1**(11): p. 511-8.
52. Kato, Y., et al., *Molecular identification of Aggrus/T1alpha as a platelet aggregation-inducing factor expressed in colorectal tumors.* J Biol Chem, 2003. **278**(51): p. 51599-605.
53. Breiteneder-Geleff, S., et al., *Podoplanin, novel 43-kd membrane protein of glomerular epithelial cells, is down-regulated in puromycin nephrosis.* Am J Pathol, 1997. **151**(4): p. 1141-52.
54. Ji, R.C., *Lymphatic endothelial cells, tumor lymphangiogenesis and metastasis: New insights into intratumoral and peritumoral lymphatics.* Cancer Metastasis Rev, 2006. **25**(4): p. 677-94.
55. Swartz, M.A. and A.W. Lund, *Lymphatic and interstitial flow in the tumour microenvironment: linking mechanobiology with immunity.* Nat Rev Cancer, 2012. **12**(3): p. 210-9.
56. Kato, Y., et al., *Enhanced expression of Aggrus (T1alpha/podoplanin), a platelet-aggregation-inducing factor in lung squamous cell carcinoma.* Tumour Biol, 2005. **26**(4): p. 195-200.

57. Martin-Villar, E., et al., *Characterization of human PA2.26 antigen (T1alpha-2, podoplanin), a small membrane mucin induced in oral squamous cell carcinomas.* Int J Cancer, 2005. **113**(6): p. 899-910.
58. Schacht, V., et al., *Up-regulation of the lymphatic marker podoplanin, a mucin-type transmembrane glycoprotein, in human squamous cell carcinomas and germ cell tumors.* Am J Pathol, 2005. **166**(3): p. 913-21.
59. Wicki, A., et al., *Tumor invasion in the absence of epithelial-mesenchymal transition: podoplanin-mediated remodeling of the actin cytoskeleton.* Cancer Cell, 2006. **9**(4): p. 261-72.
60. Kimura, N. and I. Kimura, *Podoplanin as a marker for mesothelioma*. Pathol Int, 2005. **55**(2): p. 83-6.
61. Ordonez, N.G., *D2-40 and podoplanin are highly specific and sensitive immunohistochemical markers of epithelioid malignant mesothelioma.* Hum Pathol, 2005. **36**(4): p. 372-80.
62. Mishima, K., et al., *Increased expression of podoplanin in malignant astrocytic tumors as a novel molecular marker of malignant progression.* Acta Neuropathol, 2006. **111**(5): p. 483-8.
63. Shibahara, J., et al., *Podoplanin is expressed in subsets of tumors of the central nervous system.* Virchows Arch, 2006. **448**(4): p. 493-9.
64. Lowe, K.L., L. Navarro-Nunez, and S.P. Watson, *Platelet CLEC-2 and podoplanin in cancer metastasis.* Thromb Res, 2012. **129 Suppl 1**: p. S30-7.
65. Kitano, H., et al., *Podoplanin expression in cancerous stroma induces lymphangiogenesis and predicts lymphatic spread and patient survival.* Arch Pathol Lab Med, 2010. **134**(10): p. 1520-7.
66. Yamanashi, T., et al., *Podoplanin expression identified in stromal fibroblasts as a favorable prognostic marker in patients with colorectal carcinoma.* Oncology, 2009. **77**(1): p. 53-62.
67. Noack, M., N. Ndongo-Thiam, and P. Miossec, *Interaction among activated lymphocytes and mesenchymal cells through podoplanin is critical for a high IL-17 secretion.* Arthritis Res Ther, 2016. **18**: p. 148.
68. Weyand, C.M., P.J. Kurtin, and J.J. Goronzy, *Ectopic lymphoid organogenesis: a fast track for autoimmunity.* Am J Pathol, 2001. **159**(3): p. 787-93.
69. Mahtab, E.A., et al., *Podoplanin deficient mice show a RhoA-related hypoplasia of the sinus venosus myocardium including the sinoatrial node.* Dev Dyn, 2009. **238**(1): p. 183-93.
70. Uhrin, P., et al., *Novel function for blood platelets and podoplanin in developmental separation of blood and lymphatic circulation.* Blood, 2010. **115**(19): p. 3997-4005.
71. Douglas, Y.L., et al., *Pulmonary vein, dorsal atrial wall and atrial septum abnormalities in podoplanin knockout mice with disturbed posterior heart field contribution.* Pediatr Res, 2009. **65**(1): p. 27-32.
72. Thiery, J.P., *Epithelial-mesenchymal transitions in tumour progression.* Nat Rev Cancer, 2002. **2**(6): p. 442-54.
73. Zoller, M., *Tetraspanins: push and pull in suppressing and promoting metastasis.* Nat Rev Cancer, 2009. **9**(1): p. 40-55.

74. Nakazawa, Y., et al., *Tetraspanin family member CD9 inhibits Aggrus/podoplanin-induced platelet aggregation and suppresses pulmonary metastasis.* Blood, 2008. **112**(5): p. 1730-9.
75. Colonna, M., J. Samaridis, and L. Angman, *Molecular characterization of two novel C-type lectin-like receptors, one of which is selectively expressed in human dendritic cells.* Eur J Immunol, 2000. **30**(2): p. 697-704.
76. Kaneko, M.K., et al., *Conservation of a platelet activating domain of Aggrus/podoplanin as a platelet aggregation-inducing factor.* Gene, 2006. **378**: p. 52-7.
77. Cueni, L.N. and M. Detmar, *Galectin-8 interacts with podoplanin and modulates lymphatic endothelial cell functions.* Exp Cell Res, 2009. **315**(10): p. 1715-23.
78. Kerjaschki, D., et al., *Lymphatic neoangiogenesis in human kidney transplants is associated with immunologically active lymphocytic infiltrates.* J Am Soc Nephrol, 2004. **15**(3): p. 603-12.
79. Luther, S.A., et al., *Coexpression of the chemokines ELC and SLC by T zone stromal cells and deletion of the ELC gene in the plt/plt mouse.* Proc Natl Acad Sci U S A, 2000. **97**(23): p. 12694-9.
80. Cairns, L.A., et al., *Kit regulatory elements required for expression in developing hematopoietic and germ cell lineages.* Blood, 2003. **102**(12): p. 3954-62.
81. Cavasin, M.A., et al., *Gender differences in cardiac function during early remodeling after acute myocardial infarction in mice.* Life Sci, 2004. **75**(18): p. 2181-92.
82. Gao, X.M., et al., *Mouse model of post-infarct ventricular rupture: time course, strain- and gender-dependency, tensile strength, and histopathology.* Cardiovasc Res, 2005. **65**(2): p. 469-77.
83. Signore, S., et al., *Late Na(+) current and protracted electrical recovery are critical determinants of the aging myopathy.* Nat Commun, 2015. **6**: p. 8803.
84. Pinto, A.R., et al., *Revisiting Cardiac Cellular Composition.* Circ Res, 2016. **118**(3): p. 400-9.
85. Fatima, A., et al., *Foxc1 and Foxc2 deletion causes abnormal lymphangiogenesis and correlates with ERK hyperactivation.* J Clin Invest, 2016. **126**(7): p. 2437-51.
86. Prabhu, S.D. and N.G. Frangogiannis, *The Biological Basis for Cardiac Repair After Myocardial Infarction: From Inflammation to Fibrosis.* Circ Res, 2016. **119**(1): p. 91-112.
87. Ren, G., et al., *Morphological characteristics of the microvasculature in healing myocardial infarcts.* J Histochem Cytochem, 2002. **50**(1): p. 71-9.
88. Oliver, G. and R.S. Srinivasan, *Endothelial cell plasticity: how to become and remain a lymphatic endothelial cell.* Development, 2010. **137**(3): p. 363-72.
89. Zheng, W., A. Aspelund, and K. Alitalo, *Lymphangiogenic factors, mechanisms, and applications.* J Clin Invest, 2014. **124**(3): p. 878-87.
90. Secker, G.A. and N.L. Harvey, *VEGFR signaling during lymphatic vascular development: From progenitor cells to functional vessels.* Dev Dyn, 2015. **244**(3): p. 323-31.
91. Dashkevich, A., et al., *VEGF Pathways in the Lymphatics of Healthy and Diseased Heart.* Microcirculation, 2016. **23**(1): p. 5-14.
92. Kasten, P., et al., *Similarities and differences of human and experimental mouse lymphangiomas.* Dev Dyn, 2007. **236**(10): p. 2952-61.

93. Zhao, W., et al., *Platelet-derived growth factor involvement in myocardial remodeling following infarction.* J Mol Cell Cardiol, 2011. **51**(5): p. 830-8.
94. Iwayama, T., et al., *PDGFRalpha signaling drives adipose tissue fibrosis by targeting progenitor cell plasticity.* Genes Dev, 2015. **29**(11): p. 1106-19.
95. Kramann, R., et al., *Perivascular Gli1+ progenitors are key contributors to injury-induced organ fibrosis.* Cell Stem Cell, 2015. **16**(1): p. 51-66.
96. Klotz, L., et al., *Cardiac lymphatics are heterogeneous in origin and respond to injury.* Nature, 2015. **522**(7554): p. 62-7.
97. Moore-Morris, T., et al., *Resident fibroblast lineages mediate pressure overload-induced cardiac fibrosis.* J Clin Invest, 2014. **124**(7): p. 2921-34.
98. Cooley, L.S., et al., *Reversible transdifferentiation of blood vascular endothelial cells to a lymphatic-like phenotype in vitro.* J Cell Sci, 2010. **123**(Pt 21): p. 3808-16.
99. Chong, J.J., et al., *Progenitor cells identified by PDGFR-alpha expression in the developing and diseased human heart.* Stem Cells Dev, 2013. **22**(13): p. 1932-43.
100. Pessina, P., et al., *Fibrogenic Cell Plasticity Blunts Tissue Regeneration and Aggravates Muscular Dystrophy.* Stem Cell Reports, 2015. **4**(6): p. 1046-60.
101. Lee, S., I. Choi, and Y.K. Hong, *Heterogeneity and plasticity of lymphatic endothelial cells.* Semin Thromb Hemost, 2010. **36**(3): p. 352-61.
102. Petrova, T.V., et al., *Lymphatic endothelial reprogramming of vascular endothelial cells by the Prox-1 homeobox transcription factor.* EMBO J, 2002. **21**(17): p. 4593-9.
103. Alitalo, K., *The lymphatic vasculature in disease.* Nat Med, 2011. **17**(11): p. 1371-80.
104. Kim, H., R.P. Kataru, and G.Y. Koh, *Inflammation-associated lymphangiogenesis: a double-edged sword?* J Clin Invest, 2014. **124**(3): p. 936-42.
105. Braun, N., et al., *The spectrum of podoplanin expression in encapsulating peritoneal sclerosis.* PLoS One, 2012. **7**(12): p. e53382.
106. Harvey, N.L. and E.J. Gordon, *Deciphering the roles of macrophages in developmental and inflammation stimulated lymphangiogenesis.* Vasc Cell, 2012. **4**(1): p. 15.
107. Ran, S. and K.E. Montgomery, *Macrophage-mediated lymphangiogenesis: the emerging role of macrophages as lymphatic endothelial progenitors.* Cancers (Basel), 2012. **4**(3): p. 618-57.
108. Kerjaschki, D., et al., *Lymphatic endothelial progenitor cells contribute to de novo lymphangiogenesis in human renal transplants.* Nat Med, 2006. **12**(2): p. 230-4.
109. Park, C., J.Y. Lee, and Y.S. Yoon, *Role of bone marrow-derived lymphatic endothelial progenitor cells for lymphatic neovascularization.* Trends Cardiovasc Med, 2011. **21**(5): p. 135-40.
110. Lee, J.Y., et al., *Podoplanin-expressing cells derived from bone marrow play a crucial role in postnatal lymphatic neovascularization.* Circulation, 2010. **122**(14): p. 1413-25.
111. Mahtab, E.A., et al., *Cardiac malformations and myocardial abnormalities in podoplanin knockout mouse embryos: Correlation with abnormal epicardial development.* Dev Dyn, 2008. **237**(3): p. 847-57.
112. Maruyama, Y., et al., *The effect of podoplanin inhibition on lymphangiogenesis under pathological conditions.* Invest Ophthalmol Vis Sci, 2014. **55**(8): p. 4813-22.
113. Fiedler, U., et al., *The sialomucin CD34 is a marker of lymphatic endothelial cells in human tumors.* Am J Pathol, 2006. **168**(3): p. 1045-53.

114. Dulauroy, S., et al., *Lineage tracing and genetic ablation of ADAM12(+) perivascular cells identify a major source of profibrotic cells during acute tissue injury.* Nat Med, 2012. **18**(8): p. 1262-70.
115. Nazari, B., et al., *Altered Dermal Fibroblasts in Systemic Sclerosis Display Podoplanin and CD90.* Am J Pathol, 2016. **186**(10): p. 2650-64.
116. Liu, C., et al., *Platelet-derived growth factor blockade on cardiac remodeling following infarction.* Mol Cell Biochem, 2014. **397**(1-2): p. 295-304.
117. Chen, W.S., et al., *Pathological lymphangiogenesis is modulated by galectin-8-dependent crosstalk between podoplanin and integrin-associated VEGFR-3.* Nat Commun, 2016. **7**: p. 11302.
118. Schacht, V., et al., *T1alpha/podoplanin deficiency disrupts normal lymphatic vasculature formation and causes lymphedema.* EMBO J, 2003. **22**(14): p. 3546-56.
119. Sitnik, K.M., et al., *Context-Dependent Development of Lymphoid Stroma from Adult CD34(+) Adventitial Progenitors.* Cell Rep, 2016. **14**(10): p. 2375-88.
120. Bianchi, R., et al., *Postnatal Deletion of Podoplanin in Lymphatic Endothelium Results in Blood Filling of the Lymphatic System and Impairs Dendritic Cell Migration to Lymph Nodes.* Arterioscler Thromb Vasc Biol, 2017. **37**(1): p. 108-117.
121. Yang, Y. and G. Oliver, *Transcriptional control of lymphatic endothelial cell type specification.* Adv Anat Embryol Cell Biol, 2014. **214**: p. 5-22.
122. Hall, K.L., et al., *New model of macrophage acquisition of the lymphatic endothelial phenotype.* PLoS One, 2012. **7**(3): p. e31794.
123. Ubil, E., et al., *Mesenchymal-endothelial transition contributes to cardiac neovascularization.* Nature, 2014. **514**(7524): p. 585-90.
124. Cimini, M., et al., *Phenotypically heterogeneous podoplanin-expressing cell populations are associated with the lymphatic vessel growth and fibrogenic responses in the acutely and chronically infarcted myocardium.* PLoS One, 2017. **12**(3): p. e0173927.

Acknowledgments

I would like to thank Professor Gianandrea Pasquinelli without whom this PhD wouldn't ever been earned; for me, it is a dream came true.

I am also grateful to Dr. Polina Goichberg and Dr. Raj Kishore for their patience and support in overcoming numerous obstacles I have been facing through my PhD.

A very, very big thank you goes to Mom, Dad, Tonia and Francesca; they supported me so much, without them I would fall down; they give me the driving force to peruse my dream.

Last but not the least, I would like to thank my friends for supporting me spiritually throughout all of those years, it has been great to have all of you cheering me.

As Darwin said: "It is not the strongest species that survive, nor the most intelligent, but the ones most responsive to change"; I strongly adapt myself to several changing during my PhD, I have been strong and I can say that somehow I feel evolved.

.